



Universität  
Bremen

**Making nanoporous gold a predictable catalyst:  
From its reliable catalytic activation to a  
quantitative assessment of mass transport  
limitations at the example of CO oxidation**

Dissertation  
zur Erlangung des Doktorgrades  
der Naturwissenschaften  
- Dr. rer. nat. -

Vorgelegt dem Promotionsausschuss  
des Fachbereichs 2 (Chemie/Biologie)  
der Universität Bremen  
von

**Stefan Wild**

Tag der mündlichen Prüfung: 4. Dezember 2023

1. Gutachter: Prof. Dr. Thomas Risse (Freie Universität Berlin)
2. Gutachterin: Prof. Dr. Helena Hagelin-Weaver (University of Florida)

Ort, Datum: Bremen, 23. Oktober 2023

**Versicherung an Eides Statt**

Ich, **Stefan Wild** (wohnhaft: Straßburger Str. 1, 28211 Bremen)

versichere an Eides Statt durch meine Unterschrift, dass ich die vorstehende Arbeit selbständig und ohne fremde Hilfe angefertigt und alle Stellen, die ich wörtlich dem Sinne nach aus Veröffentlichungen entnommen habe, als solche kenntlich gemacht habe, mich auch keiner anderen als der angegebenen Literatur oder sonstiger Hilfsmittel bedient habe. Ich versichere an Eides Statt, dass ich die vorgenannten Angaben nach bestem Wissen und Gewissen gemacht habe und dass die Angaben der Wahrheit entsprechen und ich nichts verschwiegen habe.

Die Strafbarkeit einer falschen eidesstattlichen Versicherung ist mir bekannt, namentlich die Strafandrohung gemäß § 156 StGB bis zu drei Jahren Freiheitsstrafe oder Geldstrafe bei vorsätzlicher Begehung der Tat bzw. gemäß § 161 Abs. 1 StGB bis zu einem Jahr Freiheitsstrafe oder Geldstrafe bei fahrlässiger Begehung.

Bremen, 23.10.2023



(Ort, Datum, Unterschrift)

**This cumulative thesis is based on the following (peer-reviewed) publications, which will be referred to in the following summary of the main results by their Roman numerals:**

**I) Thermal Activation of Nanoporous Gold for Carbon Monoxide Oxidation**

**Stefan Wild**, Thomas Risse and Marcus Bäumer

*The Journal of Physical Chemistry C* **2022**, 126 (4), 1770–1777.

<https://doi.org/10.1021/acs.jpcc.1c08222>

**II) Disentangling catalysis and mass transport: Using diffusion measurements by pulsed field gradient NMR to reveal the microkinetics of CO oxidation over nanoporous gold**

Amineh Baniani\*, **Stefan Wild\***, Evan M. Forman, Thomas Risse, Sergey Vasenkov and Marcus Bäumer

(\* Shared first co-authorship)

*Journal of Catalysis* **2022**, 413, 1123 – 1131.

<https://doi.org/10.1016/j.jcat.2022.08.020>

**III) New perspectives for evaluating the mass transport in porous catalysts and unfolding macro- and microkinetics**

**Stefan Wild**, Christoph Mahr, Andreas Rosenauer, Thomas Risse, Sergey Vasenkov and Marcus Bäumer

*Catalysis Letters* **2022**.

<https://doi.org/10.1007/s10562-022-04218-6>

## Statement regarding my contribution to the published work

All publications mentioned above emerged from work within the *Research Unit 2213* “Nanoporous Gold” funded by the German Science Foundation (DFG) and are based on collaborations with other researchers of this consortium as well as with Prof. Dr. Sergey Vasenkov and his PhD students at the Univ. of Florida at Gainesville. All persons who participated in the work appear as co-authors of the articles. In the following, I elucidate their contributions and detail my own achievements.

### **Publication I:**

I carried out all experimental work and evaluated the data. My supervisor Prof. Bäumer and Prof. Risse participated in the discussion of the results and supported me in outlining the publication. I was eventually responsible for writing the manuscript which was iteratively finalized in joint discussions with both of them.

### **Publication II:**

The publication is based on the combination of data originating from PFG NMR experiments in the group of Prof. Vasenkov and catalytic experiments carried out in Bremen. While the PFG NMR measurements were performed and analyzed by Amineh Baniani and Evan Forman under the supervision of Prof. Vasenkov at the University of Gainesville, I was responsible for the latter, including their evaluation. Furthermore, the conflation of the results, allowing, in the first place, to draw the overarching conclusions of the joint work, belonged to my tasks. I drafted the manuscript, using text modules which were provided by Prof. Vasenkov regarding the PFG NMR experiments, and finalized it with the help of my supervisor Prof. Bäumer and Prof. Risse who both participated in the corresponding scientific discussions.

### **Publication III:**

As far as this article is concerned, I was in charge of consolidating own catalytic data by complementing these with results obtained within the Research Unit (Prof. Rosenauer, Dr. Mahr, Prof. Risse) and together with external collaborators (Prof. Vasenkov). The objective was to develop a general framework for disentangling diffusive mass transport and catalytic conversion in porous heterogeneous catalysts and to derive, on these grounds, perspectives for novel approaches in this field. All coauthors contributed to this effort by scientific discussions. The composition and writing of the manuscript lay in my responsibility. In this process, I was supported by my supervisor.

## Acknowledgements

During my time in academia as a PhD student, I had the great pleasure to work together with a number of inspiring and very supportive people who accompanied me in various ways during this thesis and helped me completing this work successfully. To these belong ...

... my supervisor, **Prof. Dr. Marcus Bäumer**, who enabled this work, motivated and encouraged me continuously, contributed to numerous scientific and personal discussions and showed a steadfast commitment over the whole time;

... my collaborators, **Prof. Dr. Thomas Risse** and **Prof. Dr. Sergey Vasenkov**, to whom I am sincerely grateful for their confidence in me and my scientific development as well as for many intensive discussions, granting me insight in scientific areas I previously was not familiar with;

... **PD Dr. Volkmar Zielasek** who always had an ear for me regarding any scientific or technical question I asked;

... all the **other PhD students** in the working group whom I want to thank for their pleasant company and their unreserved readiness for personal and scientific conversations;

... **the technicians** of the group, i.e., Ms. **Conny Rybasch-Steinke** and **Martin Nowak** for their unrestricted cooperativeness and practical help in numerous cases as well as **Ms. Petra Witte** (Fachbereich 5) for her admirable endurance in so many SEM sessions;

... the **team assistant**, Ms. **Vera Suling** for guiding me through the bureaucratic jungle in so many cases:

... the **master students** who contributed to some of the experimental findings by preparatory work.

## Summary

A long-standing dream in heterogeneous catalysis has always been the predictability of catalytic characteristics on the basis of structural and compositional features, which are synthetically adjustable and optimizable for a given application. Such an endeavour, however, not only poses challenges on the atomic level where the actual surface reaction takes place, but also on the mesoscopic and macroscopic scale. The mesoscopic pore structure, for example, is decisive for the diffusive transport of reactants and products between the interior of a porous catalyst and the surrounding bulk gas atmosphere. But also, the macroscopic form and size of the used catalyst particles co-determine the mass transport. The overall conversion or yield is furthermore dependent on the total surface area exposed in a process, which, for a given reactor volume, scales with the specific surface area. Traditional methods for the preparation of porous catalysts typically neither allow a controlled variation of all relevant characteristics nor do they ensure spatial homogeneity. In contrast, in other technological areas, such as materials science, distinctly more progress has been achieved. Actually, in some instances such materials not only promise interesting catalytic properties, but also stand out due to their well-defined and homogeneous structures, providing sufficiently large surface areas and good conditions for diffusive mass transport. An example of that kind is nanoporous gold (npAu), obtained by controlled oxidative corrosion of a suitable binary Au alloy with a less noble element, mostly Ag (as in this thesis), which is leached out in the process. It was studied in materials science long before its catalytic potential was discovered. While some of its structural features, such as the mean pore and ligament size, can be varied and adjusted during its chemical or electrochemical preparation, others are fixed and characteristic for this material. Nonetheless, two aspects prevented so far to decide whether and to which extent clear-cut structure-property relationships exist for npAu allowing to predict and possibly tune its catalytic performance. On the one hand, noticeable uncertainties existed in the literature before this thesis how to attain a surface state that reliably provides the best-possible catalytic activity. On the other hand, solid knowledge about the mass transport properties of npAu was missing. At the example of low-temperature CO oxidation, both of these open questions could be successfully addressed in the work presented in the following. As far as the catalytic surface state is concerned, previous results revealed that npAu samples, even when prepared in exactly the same way, often show distinct differences regarding their activation behaviour and final activities. If, however, catalysts with the same mean ligament size are subjected to a series of short high-temperature annealing cycles, reproducibly the same high activity level is achievable. The findings point to surface impurities that may remain from the synthesis or accumulate under atmospheric conditions and re- or suppress the catalytic turnover on the surface. After their removal at sufficiently high temperatures, however, an identical and highly active surface state can safely be established, indicating that the well-defined structure of npAu indeed warrants predictable catalytic properties on the atomic scale. To elucidate whether this conclusion also holds on larger scales, PFG NMR experiments were performed in collaboration with the group of Prof. Vasenkov in Gainesville (Florida, USA). The goal was to characterize the diffusion of CO and CO<sub>2</sub> - as reactant and product of CO oxidation - within npAu in comparison to the bulk gas phase. Representing the first successful attempt to study a porous metal with this technique, it was possible to derive effective diffusion coefficients and, on these grounds, to extract the tortuosity of the pore system, being a key structural parameter for the mass transport within the material. Taking advantage of this knowledge, not only could be determined the kinetics of the catalytic surface reaction from experimentally observed macrokinetics for the first time accurately but also measures to minimize mass transport limitations and to thus optimize the catalytic efficiency became predictable.

## Zusammenfassung

Ein grundlegendes und seit langem bestehendem Ziel in der heterogenen Katalyse ist die Entwicklung von Katalysatoren mit Eigenschaften, die auf der Basis ihrer strukturellen Eigenschaften und ihrer Zusammensetzung vorhergesagt und synthetisch variiert bzw. für eine gegebene Anwendung optimiert werden können. Die Schwierigkeit dabei besteht darin, dass zu diesem Zweck die Verfasstheit eines katalytischen Materials sowohl auf der atomaren wie auch auf der mesoskopischen und makroskopischen Ebene betrachtet werden muss. Die mesoskopische Struktur des Porensystems zum Beispiel ist für den diffusen Stofftransport von Edukten und Produkten zwischen katalytisch aktiven Bereichen im Inneren des Katalysators und der umgebenden Gasphase entscheidend. Aber auch die makroskopische Form und die Abmessungen eines Katalysatorteilchens spielen dafür eine Rolle. Der auf dieser Ebene in einer konkreten Anwendung erzielbare Umsatz hängt überdies von der exponierten Gesamtoberfläche und damit - für ein gegebenes Reaktorvolumen - von der spezifischen Oberfläche des Materials ab. Klassische Methoden der Katalysatorherstellung ermöglichen typischerweise weder Kontrolle über die jeden Teilaspekt bestimmenden strukturellen Faktoren noch können sie sicherstellen, dass diese homogen in einer Probe ausgeprägt sind. Hier bieten nanotechnologische Methoden, wie sie beispielsweise in verschiedenen Bereichen der Materialwissenschaften entwickelt wurden, interessante und in dieser Hinsicht überlegene Alternativen an. Auf diese Weise hergestellte poröse Materialien versprechen zum Teil nicht nur hervorragende katalytische Eigenschaften, sondern zeichnen sich auch durch wohldefinierte und homogen ausgeprägte Porenstrukturen mit hoher Oberfläche und guten Voraussetzungen für den diffusiven Stofftransport aus. Ein gutes Beispiel in dieser Hinsicht ist nanoporöses Gold (npAu), das durch korrosive Entlegierung einer Goldlegierung mit einem weniger edlen Metall, wie Silber, auf reproduzierbare Weise hergestellt werden kann und bereits Gegenstand vieler materialwissenschaftlicher wie auch katalytischer Studien in der Vergangenheit war. Während sich einige der katalytischen relevanten Strukturparameter, wie mittlere Poren- und Steggrößen, synthetisch variieren lassen, sind andere durch die charakteristische Porenstruktur des Materials definiert und vorgegeben. Zwei Aspekte jedoch verhinderten trotz dieser guten Voraussetzungen bislang Aussagen darüber zu treffen, ob für npAu klare Struktur-Eigenschaftsbeziehungen möglich sind, auf deren Basis die katalytische Leistungsfähigkeit in einer Anwendung vorausgesagt werden kann. Auf der einen Seite war zu Beginn dieser Arbeit unklar, ob und auf welche Weise sich ein Oberflächenzustand mit reproduzierbar hoher katalytischer Aktivität erreichen lässt. Auf der anderen Seite fehlten Informationen über die Stofftransporteigenschaften des Materials. Am Beispiel der Tieftemperaturoxidation von CO konnten beide Fragen in dieser Arbeit erfolgreich geklärt werden. Im ersten Fall erwiesen sich Zyklen, in denen die Katalysatoren vor der Anwendung kurz auf höhere Temperaturen gebracht werden, als erfolgreich. Im Gegensatz zu früheren Arbeiten, bei denen strukturell nominell gleiche npAu Proben zu zum Teil deutlich verschiedenen Umsätzen nach Aktivierung führten, zeigten so aktivierte Proben ein nahezu identisches Leistungsniveau. Dieses Ergebnis legt nahe, dass Verunreinigungen, die nach der Präparation auf den Stegoberflächen verbleiben oder sich unter atmosphärischen Bedingungen auf diesen anreichern, die Ursache für fehlende oder eingeschränkte katalytische Aktivität sind und erst bei ausreichend hoher Temperatur entfernt werden müssen. Insofern konnte der Beweis erbracht werden, dass die wohldefinierte poröse Struktur von npAu nicht nur auf der mesoskopischen und für den diffusen Stofftransport wichtigen Ebene, sondern auch auf der atomaren Ebene die Voraussetzungen für vorhersagbare katalytische Eigenschaften erfüllt. Um im ersteren Fall die Grundlage für solche zu legen, wurden in Zusammenarbeit mit der Arbeitsgruppe von Prof. Vasenkov in Gainesville (Florida, USA) PFG NMR Messungen an npAu durchgeführt und die

Diffusion von CO, CO<sub>2</sub> und – zu Vergleichszwecken - CH<sub>4</sub> im Porensystem von npAu untersucht. Hierbei handelte es sich um die ersten erfolgreichen Experimente mit einem metallischen porösen Material, auf deren Basis nicht nur die Diffusionskoeffizienten der genannten Gase, sondern auch die Tortuosität von npAu als zentrale, für die quantitative Beschreibung des Stofftransportes wichtige Größe bestimmt werden konnte. Auf dieser Basis und der weiterer Strukturparameter konnte dann auch zum ersten Mal die mikrokinetische Geschwindigkeitskonstante für die von npAu katalysierte CO-Oxidation bei 30 °C exakt bestimmt werden und so das Ausmaß von Stofftransportlimitierungen sowie Maßnahmen zu deren Minimierung vorausgesagt werden.



## Table of Content

I. INTRODUCTION.....	1
II. MATERIAL'S ASPECTS.....	5
II. (A) Porous materials: Requirements for predictable properties.....	5
II. (B) Nanoporous gold: Preparation and structure.....	6
III. CATALYTIC ASPECTS.....	10
III. (A) Heterogeneous catalysts: general requirements for catalytic surface activity.....	10
III. (B) Nanoporous gold: surface structure and catalytic activation.....	12
IV. MASS TRANSPORT ASPECTS.....	15
IV. (A) Diffusion in porous materials: general requirements for avoiding mass transport limitations.....	15
IV. (B) Nanoporous gold: transport properties and their experimental characterization.....	18
V. INTERPLAY OF CATALYTIC SURFACE REACTION AND MASS TRANSPORT.....	19
V. (A) Catalytic effectiveness: general requirements for achieving high catalyst productivities.....	19
V. (B) Nanoporous gold: derivation of microkinetics and optimization of catalytic effectiveness.....	21
VI. CONCLUSIONS.....	25
VII. REFERENCES.....	29

## APPENDICES

### Publication I:

*Thermal Activation of Nanoporous Gold for Carbon Monoxide Oxidation*

### Publication II:

*Disentangling catalysis and mass transport:  
Using diffusion measurements by pulsed field gradient NMR  
to reveal the microkinetics of CO oxidation over nanoporous gold*

### Publication III:

*New perspectives for evaluating the mass transport in porous catalysts  
and unfolding macro- and microkinetics*

---

## I. INTRODUCTION: IMPORTANT FEATURES OF A HETEROGENEOUS CATALYST

Heterogeneously catalysed processes play an eminent role for the global economy. Not only they are involved in the production of commodity and special chemicals, materials and exhaust catalysts, for instance, but also become increasingly important in new areas of technology, such as the renewable energy sector (water electrolysis, fuel cells, power-to-x technologies, etc.). To this end, highly active and selective catalysts are needed, which furthermore need to be durable and ideally recyclable [1].

As far as the performance of a given catalytic material is concerned, three central factors can be distinguished between and need to be optimized, when aiming at a yielding and profitable process [2]:

- (1) A suitable *surface composition and structure* allowing efficient (and, as the case may be, selective) catalytic turnover of the gas phase reactants (after adsorption on the surface).
- (2) An associated *specific surface area* which is sufficiently large enough to achieve reasonably high conversion rates per mass or volume of the catalyst - typically requiring porous materials with pore sizes mainly in the micro- ( $\leq 2\text{nm}$ ) or mesoporous range (2 – 50 nm).
- (3) *Pore characteristics* that do not result in too severe impediments for the diffusive transport of reactants and products so that their supply or removal, respectively, fall below the rate of the catalytic surface reaction, thus limiting the productivity of the catalyst to an unacceptable extent.

When subsuming these figures of merit – abbreviated **FoM** in the following - into an integral picture, it becomes apparent that the latter two points are not independent but inversely related to each other so that a conflicting situation may arise. While diffusive mass transport is facilitated when increasing pore diameters, at the same time the specific surface area decreases, of course. However, good compromises can be found for materials in the mesoporous regime. In case of bulk catalysts, also FoM (1) and (3) may be interrelated, since it is likely that the pore curvatures determine the surface structure of the pore walls - for instance in terms of defect densities, which are typically catalytically important.

Most of the catalysts nowadays used in industry for standard processes and the production of commodity chemicals have been optimized over many years along these FoMs (in addition to economic considerations), thus typically guaranteeing high and profitable conversion levels [1]. Yet, novel upcoming applications (such as in the energy sector, for instance) or new technology fields (such as micro reactors) might pose challenges not yet satisfactorily tackled, thus rendering a continuous development of new catalytic materials indispensable [3].

Unfortunately, however, traditional catalyst preparation techniques (such as impregnation or co-precipitation) typically entail problems when aiming at a targeted and efficient development, because they do not or do only to a limited degree allow controlling those structural and (surface) chemical properties which are relevant for the catalytic function [2]. A remedy in this context may arise from the increasing arsenal of novel synthesis methods for nanostructured materials which have become available in the last 20 and more years through modern materials science and nanotechnological approaches [4]. Two prominent examples in this respect, are, on the one hand, colloidal chemistry for the preparation of well-defined nanoparticles through which, after deposition on a suitable support, supported catalysts with narrow particle size distributions and tailored compositions are assessable [5]. The increasing realm of advanced synthesis and structuring methods for porous matter, on the other hand, opens another field with fascinating new pathways to catalytic materials with adjustable and well-defined pore systems [6].

---

As far as the latter area is concerned, mainly porous oxides, for instance used as support materials, have been in the focus of interest. But also, porous metals belong to this class. Nanoporous gold (npAu), for instance, is a good example in this respect [7, 8]. The preparation of the material by leaching a less noble metal – such as Ag for instance – out of a gold starting alloy has been known since many decades [9] and studied for its interesting mechanical properties [10]. But it took until 2006 to finally enter the field of heterogeneous catalysis [11, 12]. From thereon, increasing interest in and research on npAu revealed a high catalytic potential in particular for aerobic oxidation reactions [8]. Not only total oxidations, such as CO oxidation, but also partial oxidations are selectively catalysed already at room temperature, as demonstrated for methanol and also other alcohols [13].

It is important to mention in this context that the insight of gold not being too “inert” for applications in heterogeneous catalysis, but rather exhibiting interesting catalytic properties - especially for oxidation reactions at low temperature - was not a new one at the time the first results on npAu were published. It was gained a long time before, when Haruta, Hutchings and co-workers reported first on the catalytic activity of small oxide-supported Au nanoparticles (NPs) in the range of a few nm [14, 15]. Nevertheless, the finding that, in form of npAu, another and structurally totally different – one could say “inverted” – Au catalyst entered the arena, evoked some surprise in the catalytic community in the beginning. Not only is missing an oxide component, which, in case of its NP counterparts, plays an essential and crucial role, but also the catalytically active feature sizes - ligament and pore diameters vs. particle sizes – are an order of magnitude larger for npAu.

Although it appeared at the start that the material could be an example of a pure gold catalyst, intensive research, motivated by the unexpected properties, revealed that this notion is not true. Driven by the question how molecular oxygen, which is too weakly bound on Au to get dissociated and to explain npAu’s activity for aerobic oxidation reactions, is activated on the surface, a substantial number of theoretical studies were carried out [8]. In agreement with experimental findings for AuAg nanoparticles, these indicated that residues of the second metal – usually Ag – are not undesired species acting as spectators or even deteriorating the catalytic function, but represent an essential ingredient for this step [16]. Even though not all mechanistic details on how and in which chemical form Ag enables the oxygen activation and ensures its efficient supply on the surface could have been unravelled so far, all hitherto existing observations clearly suggest that all further reaction steps take place on Au [13]. In other words, as far as activity and selectivity issues are concerned, npAu can indeed be considered as a gold catalyst. Without noticeably changing this pattern, the second metal, however, compensates for the inertness of Au surfaces towards oxygen – a role which, in case of oxide supported Au NPs, is ascribed to the support.

Clearly, the lack of the latter brings about the disadvantage of losing the opportunity to boost the catalytic turnover by a proper choice of the support material. In case of deposited Au NPs, for instance, an activity for CO oxidation was reported for some oxide supported systems, with which npAu factually cannot compete [17, 18]. In contrast though, npAu provides the advantage of a well-defined and homogeneous structure, that, in certain ranges, is amenable to systematic and rationally based variations as far as porosity and composition are concerned. Reverting to knowledge gained in material science over the years, ligament and pore sizes, for example, can be varied from a few nm to several microns [19]. Although an alike adjustment of the residual Ag concentration was not in the focus of research originally - as it does not play a significant role for the material bulk properties -, at the time when catalysis applications came up, the underlying chemical and electrochemical dealloying

---

methods were successfully refined and optimized in this respect [20, 21]. In this way also a sufficient control over the Ag surface concentrations could eventually be reached.

In essence, it is nowadays possible to prepare npAu catalysts with homogeneous and well-defined pore structures exhibiting different ligament/pore sizes and defined Ag residual contents. Considering that, in contrast, for supported nanoparticulate Au catalysts a comparable degree of structural definition is usually not achievable, validates what has been stated above: materials such as npAu hold realistic perspectives as catalysts which can be tailored and optimized with respect to their catalytic and transport behaviour or, in other words, as catalysts with widely “predictable” and manipulable properties.

This thesis was devoted to the clarification of two prerequisites which still need to be fulfilled, though, to turn this theoretical option into reality. On the one hand, a defined and catalytically active surface state throughout the material is required which can be reliably established for identically prepared samples. Even though npAu’s homogeneous porosity renders comparable structural conditions on its ligament surfaces likely, this feature represents only a necessary but not sufficient criterion. Precipitates remaining on the surfaces after preparation or impurities adsorbed during storage under atmospheric conditions are typical reasons for unpredictable activity losses or even inactivity. In agreement with that, varying performances of npAu catalysts and inconsistent measures to initiate catalytic turnover have been reported for low-temperature CO oxidation, for instance, in the literature [22, 23].

**Accordingly, the first important goal of this thesis was to clarify if an activation protocol can be developed which allows to reliably and reproducibly achieve such a surface state in case of CO oxidation.**

On the other hand, a pathway must exist to get insight into the structural specifics of the material’s pore structure, being relevant for the diffusive mass transport therein. To this end, a simple microscopic characterization by SEM, for example, does not suffice. Certainly, it can be checked whether the homogeneity of the pore system required to emanate from identical and well-defined transport properties is factually given. Furthermore, pore sizes deciding upon the extent of Knudsen diffusion can be evaluated as well. Information about the pathway elongation associated with the material-specific porosity and its characteristics, however, is not assessable in this way. To predict to which degree transport limitations mitigate the catalytic performance and to be able to reduce or avoid such influences, the so-called tortuosity of the pore system must be known [24].

A method allowing to quantitatively determine this feature by directly measuring gas diffusivities is PFG NMR [24]. While such experiments have been successfully carried out for porous oxide materials already, the applicability of this technique for nanoporous *metals*, however, was unclear at the beginning of this thesis and not tried before. In contrast to oxides, the likelihood for success was questionable as in this case so-called eddy currents induced in the metal during the measurements could impede the acquisition of meaningful data.

**In view of the novel and far-reaching perspectives arising from the possibility to determine tortuosities of porous metals as well, the second goal of the thesis was to provide a corresponding proof of principle in case of npAu.**

Figure 1 schematically shows the overall concept of this dissertation in view of the discussed considerations. All results have been published meanwhile in peer-reviewed scientific journals (see front matter) and will be summarized in the following. Prior to that, the material in the focus, nanoporous gold, will be described in a first chapter - as far as structure and catalytic features are concerned, that were known at the beginning of this thesis.

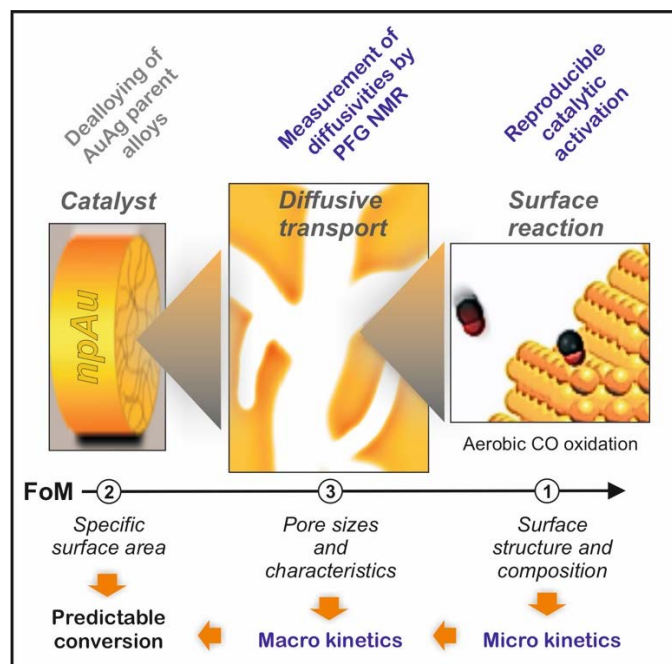


**Figure 1:** Research concept of this dissertation. Central FoMs determining the productivity of a porous heterogeneous catalysts are: (1) the rate of the catalytic surface reaction (called microkinetics), (2) the specific surface area and (3) the efficiency of the mass transport in the pore system. FoM (1) is related to the number of catalytic turnovers which, at maximum, can take place per unit surface area. Typically, however, lower rates, called macrokinetics, are observed. This is the case, when the diffusive transport of reactants and products, determined by FoM (3), cannot compete with the reaction rate. To achieve a high overall conversion in a catalytic process, moreover a sufficiently high specific surface area is required: FoM (2). The first goal of this thesis was to develop a reliable procedure to activate npAu for low-temperature CO oxidation so that catalytically highly active surface conditions, i.e., optimal microkinetics, can be routinely attained. The second goal was to measure and evaluate npAu's diffusive transport properties, thus laying a foundation for quantitatively describing the macrokinetics in this case. Using, in addition, concepts proposed in the literature to calculate the specific surface area for porous catalysts with well-defined porosities, such as npAu, the dissertation overall aimed at demonstrating that on these grounds catalytic performances can be predicted and even optimized with good accuracy. (Colour coding: blue – topics being part of this thesis, grey – topics integrated from literature.)

All chapters are divided in two sections. The first one describes general considerations with respect to the central question raised above:

(A) *What are requirements for porous catalytic materials with predictable properties and how are these related to their structure?*

The second subsection then specifically applies these considerations to nanoporous gold as a catalyst for CO oxidation and answers the question:

(B) *Can npAu be considered as such a catalyst?*

In a last consolidating chapter, final conclusions regarding the latter question will be drawn on the basis of all results of this thesis.

---

## II. MATERIALS' ASPECTS

### II. (A) Porous materials: Requirements for predictable properties

As far as porous materials, including porous heterogeneous catalysts, are concerned, two borderline cases can be differentiated between, in principle. In case of preparation techniques, where the structural evolution of the porosity proceeds under locally varying or uncontrollable conditions as usually given for classical approaches, often spatially inhomogeneous pore systems - in terms of locally varying ligament and pore diameters, porosities or pore shapes - are obtained. In the opposite case, i.e. under conditions where the pore formation proceeds slowly and in a defined kinetic way so that also potential restructuring processes on the emerging strut surfaces may concomitantly take place, the chance that materials result whose porosity is spatially homogeneous from the mesoscopic to the macroscopic scale is clearly higher.

Comprehensibly, not only bears the latter case practical advantages but also opens the way to a uniform structural description of the system. Under such circumstances, namely, the porous network can be envisioned as (or approximated by) an arrangement of identical (or almost identical) unit cells, constituting the overall structure when periodically repeated in space. In other words, it is possible to define a microscopic/mesoscopic volume which represents or contains, respectively, all relevant structural characteristics of the porous structure exhibited by a macroscopic sample of the material [25].

Provided that such an "elementary cell" reflecting the overall porosity is sufficiently small and certain geometric conditions are fulfilled (such that a bi-continuous pore structure is given), this approach allows predicting the specific surface area (being an intensive property) in an astonishingly easy fashion. Interestingly, however, a corresponding concept was only recently proposed in the literature by Detsi et al. [25]. As re-enacted in [publication III](#) (on the basis of a slightly different logical argumentation, though) [26], the specific surface area  $A_m$  ( $m^2/g$ ) accordingly depends inversely on the (mean) ligament diameter  $d_L$ :

$$A_m = \frac{\zeta}{d_L \cdot \rho} \sim \frac{1}{d_L} \quad (eq. 1)$$

Here,  $\rho$  denotes the (bulk) density of the material, the ligaments are consisting of (not of the porous material as a whole!), and  $\zeta$  a material-specific parameter, being characteristic of the geometric details of the given pore system and depending on the shape and connectivity of the pores and ligaments. As demonstrated by Detsi et al. in this context, this constant can vary between  $\sim 0.5$  and  $\sim 6$  for different materials [25].

Typically, the value of  $\zeta$  needs to be experimentally determined once by using, for example, BET gas adsorption to measure  $A_m$  and SEM to derive  $d_L$ . With the known material's density,  $\zeta$  can then be calculated and further on employed for quantitatively predicting the specific surface area on the basis of the (mean) ligament size which is relatively easily assessable by a routine microscopic characterization. Moreover, the fixed relationship between both quantities also implies that, in case the latter ( $d_L$ ) can be tuned by the synthesis process, the same holds true for the former ( $A_m$ ).

As said, for most conventional preparation techniques clear-cut and systematic correlations between synthetic parameters, on the one hand, and the evolving pore structure, on the other hand, are commonly not known or simply do not exist. As stated already in the Introduction, research in other fields such as materials science and nanotechnology, however, has borne techniques which, in some instances, do feasibly allow a tailored fabrication of porous matter, displaying a porosity which is well-defined on the mesoscale and spatially homogeneous on

---

the macroscopic scale [6]. Under such circumstances the above considerations, including eq. 1, are applicable.

Coming, at the end of this subsection, back to the list of FoMs discussed in the Introduction, it becomes evident that in cases where such advanced synthetic approaches can be taken advantage of, the opportunity arises to systematically manipulate and – as the case may be – to optimize **FoM (2)**.

## II. (B) Nanoporous gold: Preparation and structure

The preparation of npAu, in principle, is similar to Raney nickel. In both cases, the synthesis is based on a wet-chemical corrosion process in which a binary alloy is used as a starting material and the less noble component is continuously leached out under suitable oxidative conditions. This process, in the literature often dubbed as dealloying, finally leads to a mesoporous, often called “nanoporous” framework of the more noble metal - in the present case: Au [27].

In this way, (purely) metallic catalysts are obtained, which, in contrast to supported metal catalysts go without a second auxiliary material needed to deposit the catalyst in the latter case. In passing, we note that for the second (and much more usual) class of systems the FoMs (2) and (3) rest with the support, being here the porous component, while for FoM (1) the metal deposits are responsible (unless catalytic contributions of the support or metal-support interactions play a role). In contrast, for porous metal catalysts all FoMs trace back to the same structure and are hence interlinked.

As briefly brought up in the Introduction, these differences existing between the two types of heterogeneous catalysts also become obvious, when comparing npAu with supported Au NPs. Under this perspective, it is by no means clear beforehand whether npAu really brings in the better synthetic preconditions to optimize the catalytic performance along *all* 3 FoMs, when considering that in case of deposited Au catalysts the option to “decouple” these might provide factual advantages. We will come back to this point later, after having shed light on all three areas and the possibilities to predict and control them for npAu.

As starting alloy for its preparation most often the combination with Ag was employed in the literature, even though other less noble metals, such as Cu, for instance, are possible, too [28]. Suitable Au/Ag ratios lie between 40 at%/60 at% and 20 at%/80 at%. When undercutting the lower limit of this window (Au concentrations > 40 at%), called parting limit, passivating Au layers evolve at the surface and early terminate the structure formation. On the contrary, Au concentrations below 20 at% lead to a different problem; here the forming ligament structures are structurally not stable enough [10, 29].

In contrast to Raney nickel, prepared under alkaline conditions, the dealloying process for npAu is carried out under acidic conditions. In principle, two options exist to dissolve the Ag, i.e. to strip the solid phase and transfer Ag to the liquid phase: a purely chemical way, called free corrosion, or an electrochemically assisted way, entailing the advantage that the oxidation potential can be experimentally controlled [20, 21].

In the first case, samples of the parent alloy are submersed in a corrosive acid, such as conc. HNO<sub>3</sub>, known to be able to oxidize metallic Ag to Ag<sup>+</sup>(aq). In the second case either the applied electrochemical potential (potentiostatically controlled dealloying: PCD) or the resulting current (density) is fixed (galvanostatically controlled dealloying: GCD) so that a continuous and directed removal of Ag from the alloy is achieved either way. To this end, the latter is employed as the working electrode in a classical three-electrode setup, furthermore containing a chemically inert counter electrode and a suitable reference electrode. In all cases, the process ends, when the Ag bulk content falls below ~ 1 at%. The remaining porous Au structure then exhibits porosities  $\phi = V_{pores}/V_{total}$ , as predetermined by the initial alloy com-

---

position (see above), between 0.6 (60 %) and 0.8 (80 %). To reach this point, typically several hours up to a few days are needed [7].

While the electrochemical methods generally implicate more options and a higher flexibility to direct and monitor the corrosion progress, the first variant, i.e., the free corrosion, has the advantage of being experimentally much easier to realize. Furthermore, it allows fabricating larger sample batches at a time, rendering this route insofar much more attractive for practical applications. For these reasons, it was in the focus of this work. It could be demonstrated in the course of the project that, by a careful adjustment of all experimental parameters, npAu materials with defined structural features are here reproducibly obtainable as well (see below) [22].

The corrosion process reliably leading to the same, characteristic type of porous network (largely independently of the synthesis method) was the topic of many studies in the past and meanwhile is mechanistically well-understood. Apart from the details found in the original publications, the fundamentals are well described in various reviews and, hence, will not be dealt with here [10, 30]. For the following, it is only important to note that the underlying dissolution and reorganization steps, taking place at the surface, fulfil the conditions of a slow and kinetically controlled process, addressed in the previous subsection (A) to be requisite for an ordered structural evolution process. In agreement with that, the resulting pore structures of npAu were consistently found to be well-defined and spatially homogeneous in numerous studies [31, 32]. As illustrated by the SEM micrograph in Fig. 2 (inset), these consist of interconnected and intertwined gold ligaments with diameters in the range of a few 10 nm and pores of basically the same size. (In certain instances, it was reported in the literature that ligament and pore sizes close to the outer surface were smaller than in the interior, but such discrepancies were not observed in this work in agreement with many other studies where free corrosion was utilized [20].)

As opposed to Raney nickel, the material does not break up during the dealloying so that monolithic samples possessing the shape of the initial alloy specimen are obtained as final products. In many catalytic studies on npAu, disc-shaped specimen with diameters  $d$  in the range of several mm and thicknesses  $h$  in the range of a few 100 microns were employed - in analogy to the present work ( $d = 5$  mm,  $h = 200$   $\mu$ m).

The standard protocol applied here and in several other studies to prepare such kind of npAu samples typically comprised the following steps [33]:

- (1) Preparation of the starting alloy by melting the two metals in the desired ratio, using a crucible and a suitable furnace or by reverting to an arc melting setup. In the work, described here and in the following, the crucible method and a composition of 70 at% Ag / 30 at% Au was chosen.
- (2) Subsequent tempering of the obtained alloy ingots for several days under an inert gas atmosphere at a temperature closely below the melting point to achieve best-possible homogenisation.
- (3) Step-wise mechanical cold-rolling of the ingots to thin alloy sheets with the desired thickness with intermittent thermal treatments, applied for strain relief and healing of the grain structure.
- (4) Fabrication of the final alloy specimen by punching discs with respective diameters out of the white gold sheets produced in (3).
- (5) Dealloying by free corrosion at room temperature using conc. HNO<sub>3</sub> for several hours. (Alternatively: electrochemical methods (PCD, GCD).)
- (6) Cleaning of the npAu discs by submersing them several times in ultra-pure water.
- (7) Drying in air or, as done in this work, in an exicator with a drying agent (here: P<sub>2</sub>O<sub>5</sub>).



---

(The exact values of all experimental parameters applied in this work for the sample preparation can be taken from the experimental sections of [publication I and II](#) [22, 23].)

Aiming at high precision and reproducibility, significant experimental effort has been undertaken in this thesis to standardize and improve this protocol. To this end, for example, boron nitride instead of carbon crucibles, as used in many previous studies, were tried for the first time. In this way, carbon impurities which, as a matter of fact, have a good solubility in Au and corresponding alloys could be avoided. Furthermore, the cold rolling procedure was optimized, ensuring the fabrication of discs with reproducible dimensions and weights.

A particularly interesting feature of npAu or of its preparation by dealloying, respectively, is the possibility to tune the size of the ligaments and pores as well as the residual Ag content in certain ranges by varying experimental parameters. This statement, in particular holds, true for the electrochemical methods. For GCD (galvanostatic control), for example, it was proven that ligament sizes in the range between 25 and 30 nm and Ag residual bulk concentrations between 1 and 10 at% can be adjusted quite precisely and, perhaps even more importantly, independently from each other [21]. As already mentioned in the Introduction, the latter aspect, not really being considered in materials science studies of the past, is of high relevance for catalytic studies, taking into account that Ag plays a crucial role as a co-catalytically active partner of Au at the surface. Since this context affects FoM (1) which will be dealt with in the next chapter, we come back to it there.

Focussing here on structural aspects, is worth mentioning that the opportunity exists to extend the range of ligament and pore sizes assessable by dealloying alone by combining it with a subsequent thermal treatment. As reported in various studies on this topic, in this way a controlled coarsening of the porous network can be achieved when applying temperatures  $> 100$  °C. A feature of npAu being as unique as also important in this context is the observation that the underlying restructuring processes let the feature sizes grow but do not change the structural layout of the pore system. In other words, self-similar geometries with identical pore and ligament shapes and an unaltered connectivity are obtained. This additional option for targeted structural manipulations underpins the broad realm of preparative possibilities existing for npAu [19, 34].

In essence, the information summarized here clearly reveals that, thanks to npAu's homogeneous porosity, in principle only a few arbitrarily chosen mesoscopic areas of a given sample need to be microscopically analysed (e.g. by SEM) for its characterization. As long as the chosen areas do not undercut the size of the porous "elementary cell" as introduced in (A), they can be considered representative for the whole porous structure in the material. This conclusion, in fact, also agrees with the practical experience. Even though not really knowing how large such an "elementary cell" in case of npAu's pore system factually is, it certainly can be assumed that SEM micrographs acquired with a magnification of 100 K, for instance, and imaging areas of several 100 nm are not too small in this respect. At the same time, the resolution suffices to size the ligaments and to determine their mean value  $d_L$  with sufficient accuracy.

On these grounds, the specific surface area can be directly derived then, reverting to eq. 1. The material-specific constant  $\zeta$ , needed to this end, has been determined previously in the literature and turned out to be close to a single gyroid pore structure (cf. inset of Fig. 2) [25]. Fig. 2 provides an overview how  $A_m$  varies as a function of the mean ligament size, revealing that for ligament diameters between 20 nm and 50 nm, i.e., typical sizes as obtained by all dealloying techniques (without further treatments), the specific surface areas lie in the range between  $\sim 4$  m<sup>2</sup>/g and  $\sim 10$  m<sup>2</sup>/g. As compared to supported catalysts where the values often are an order of magnitude larger, these values appear relatively low. It has to be taken into

account, though, that in case of a porous metal catalyst potentially the whole exposed surface area is catalytically active, whereas in the former case only that fraction of the surface associated with the deposited metal particles is supposed to contribute.

For larger ligament sizes which, as mentioned, are in principle assessable by subsequent thermal treatments,  $A_m$  declines further and, at  $d_L = 100$  nm, reaches  $\sim 2$  m<sup>2</sup>/g. A potential reason for increasing ligament and pore sizes was stated in the Introduction: FoM (2) and (3) are interrelated and larger pores could encompass a concomitant improvement of the diffusive transport, possibly outweighing the loss of surface area. As will become obvious in chapter V, however, this is not the case.

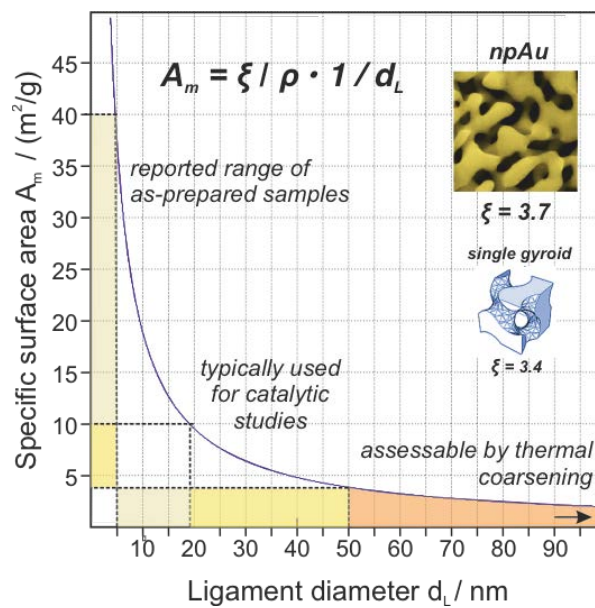


**Figure 2:** Specific surface area  $A_m$  provided by npAu as a function of the mean ligament diameter, calculated on the basis of eq. 1.; for (mean) ligament diameters  $d_L$  between 20 nm and 50 nm, i.e., within the window of sizes assessable by dealloying (regardless of the specific method), surface areas between  $\sim 4$  m<sup>2</sup>/g and  $\sim 10$  m<sup>2</sup>/g are expected; larger ligament sizes as achievable by subsequent thermal coarsening lead to values below 4 m<sup>2</sup>/g and become increasingly uninteresting for catalytic applications; in contrast,  $A_m$  can in principle also be increased up to 40 m<sup>2</sup>/g by decreasing  $d_L$  down to a value of 5 nm; in some instances, such small ligament sizes were indeed reported in the lit., but only for dealloyed gold leaves with thicknesses of  $\sim 100$  nm [35], furthermore they quickly coarsen at higher temperatures [36] so that this regime does not come into consideration either; the constant  $\zeta$  determined for npAu (see inset with SEM image: 3.7) resembles that of a single gyroid structure (see inset: 3.4), suggesting a certain comparability of the pore arrangements. (Fig. reproduced from [publication III.](#))

In the present thesis, only npAu materials with a fixed ligament size (and fixed residual Ag content) were investigated since the experimental focus (cf. Fig. 1) was on aspects for which such variations played no role. Specifically, the mean ligament size of all samples used here amounted to  $d_L \sim 20$  nm, corresponding to a specific surface area  $A_m$  of  $\sim 10$  m<sup>2</sup>/g. As described in [publication I](#), this value of  $d_L$  was derived on the basis of a FFT (fast Fourier transform) analysis (going in some details beyond a corresponding approach of Ch. Mahr, described in his dissertation [37]) of suitable SEM images acquired to this end [22]. This evaluation also provided access to the mean pore diameter  $d_P$  which was shown to be basically identical with  $d_L$  – a finding often observed for npAu and also being in line with the structural similarity of the ligament and pore system in the single gyroid structure (see Fig. 2) [38].

---

### III. CATALYTIC ASPECTS (PUBLICATION I)

#### III. (A) Heterogeneous catalysts: general requirements for catalytic surface activity

Ever since catalysis moved out of the arena of alchemy into the area of science, one central question occupied researchers: what are structural and chemical features enabling a catalyst to open more favourable kinetic pathways for a reaction to run at higher rate (or at all)? In case of heterogeneous catalysis, this question refers to the surface of the catalytic material where, after adsorption, the conversion of the reactants can take place more facilely than e.g., in the gas phase [39, 40]. Studies aiming at providing corresponding answers for practically employed catalysts, however, are often impossible to perform due to their high structural complexity. In case of supported metal catalysts, for instance, many features, such as particle size and particle size distribution, particle distances, as well as the type of support and resulting metal/support interactions at the interface can influence the catalytic function.

This problem could – at least partially – be solved with the advent of UHV technology in the 1960's and the possibility to investigate suitable model surfaces under well-defined conditions, excluding surrounding gas atmospheres and unwanted adsorbates [41]. In certain instances – such as the famous example of ammonia synthesis studied by G. Ertl and honoured with the Nobel prize in 2007 [42] – a detailed mechanistic understanding could be achieved in this way. In most other practically relevant cases, though, only limited insight into structure-property relationships exists and general predictions commonly fail in view of the many factors playing a role and being intertwined.

A rule which universally applies is the Sabatier principle, though: the reactants (and intermediates) of a reaction must be bound strongly enough on the surface to ensure sufficiently high transient surface coverages but also weakly enough to prevent too long residence times, eventually leading to a blocking and even poisoning of the active sites. In this context, often defect sites at the surface, i.e., under-coordinated surface atoms (as compared to regular ones) exposed at step or kink sites, for instance, play a role and provide suitable (i.e., the “right”) adsorption energies in this respect.

In case of molecular adsorbates, such as O<sub>2</sub> for example, whose dissociation into atoms is typically required for subsequent oxidation steps to happen on the surface, the electronic binding situation at the surface needs to be concomitantly connected with a weakening of the intermolecular bond. For the consecutive reaction steps, it may furthermore be important which kind of surface oxygen species eventually forms on the surface (oxygen atoms, surface oxide phases, subsurface species or oxide clusters, for example) since they may differ quite substantially with respect to their reactivity [43]. In case of the oxidation chemistry running on Au surfaces, single O<sub>ad</sub> atoms are known to exhibit Brønsted basicity, enabling them to hydrogen abstraction reactions which play a central role for the selective oxidation of alcohols, for instance. Other species, such as 2D (surface oxide) structures observed by STM on single crystal Au surfaces, are rather Lewis basic and supposedly responsible for total oxidation reactions, like CO oxidation [8].

But even when having some knowledge about key structural features or species driving a certain surface reaction (e.g. from UHV studies or theory), such insight is of low value unless this can be deliberately dissected during the synthesis or during catalyst activation. Taking the large number of potentially influencing parameters in case of supported catalysts and their very limited controllability by classical preparation techniques into account, it becomes clear what has been mentioned already: traditional catalysts only entail a limited potential for predictability.

---

So, the question arises whether what has been deduced in the previous chapter with respect to FoM (2), applies for FoM (1) as well: can advanced nanotechnological methods also provide a remedy in this direction, being, of course, closer to the centre of heterogeneous catalysis: the catalytic surface reaction? Before trying to answer this question, it is important to note that most of the considerations and conclusions in the following must stay at the level of plausibility arguments. The problem is that, without knowing the catalytically active state of the surface under working conditions, its dependence on structural and compositional features, as shaped or, as the case may be, tuned during the synthesis, usually are difficult or impossible to derive. Even though research based on operando techniques is continuously growing, possibilities to characterize the working state of a catalyst are still not standard due to the high experimental effort [3].

Catalysts such as nanoporous Au, whose uniform composition promises identical or similar surface conditions throughout the material, however, render some hypotheses likely. Since, in case of porous bulk catalysts, the catalytic action takes place on the surfaces of the ligaments, their size (diameter) and shape can be assumed to have an impact on the catalytic properties - taking into account that the resulting mesoscopic curvature must be accommodated on the microscopic level. At sufficiently high temperatures, crystallographic facets according to the Wulff shape (low total surface energy) will be formed, while at temperatures, which are too low to reach the thermodynamically most stable state, the compensation via (atomic) steps, including step bunching, prevails. As mentioned above, such defects represent under-coordinated surface sites, which typically govern the catalytic surface events. Since their number is expected to increase with increasing curvature, a decrease of the (mean) ligament size is likely to lead to higher catalytic activity (per area). Preparation techniques, such as dealloying, in fact synthetically allow such structural variations.

As far as the chemical composition of the surface and the question how this is related to the composition of the material in the bulk is concerned, analogous conclusions are less easily drawn. From fundamental surface science, however, it is known that in case of alloys, for instance, surface and bulk concentrations are typically not identical [44]. The driving force for such inhomogeneities are differences between the surface energies of the metal components involved, preferencing those at the surface which exhibit the lower values. In case the surface is not exposed to the vacuum, the composition of the surrounding gas atmosphere plays an additional role. For metals, it is easily comprehensible that in this context oxygen is of particular interest. Less noble metals with a higher affinity to oxygen are thus expected to be drawn to the surface under oxidative conditions. The question, however, to which degree such segregation processes take place also depends on kinetic factors and in particular on the temperature. Although this complex situation typically prevents predictions, an interdependence between the bulk and surface composition often exists so that the latter can at least empirically be optimized, when having control over the former during the synthesis.

In any event, it has to be taken into account that the as-prepared situation may not yet provide catalytic activity or represents the best-possible surface state in this respect – a problem which is quite typical in heterogeneous catalysis [45]. The reasons for low activity or even inactivity of a freshly prepared catalyst can be manifold, including, among others, deposition of various surface impurities during the preparation or accumulated during storage under atmospheric conditions. Often, such species act as catalytic poisons either because they physically block catalytically active surface area or, in more severe cases, lead to changes of the geometrical or electronic structure. A typical measure in heterogeneous catalysis to remove such species and “free” the surface are thermal treatments at elevated temperatures usually under

---

oxidative conditions (calcinations). In this way, species, such as nitrates or carbonates e.g., are decomposed and others, such as carbon or sulphur deposits, removed as gaseous species [2]. For catalysts prepared along classical impregnation or precipitation routes such issues often play a large role and rather “drastic” measures, including longer annealing steps up to several 100 °C, must be taken to activate them, i.e., to transfer the surfaces into a sufficiently active state. In contrast, preparative routes stemming from materials science and other fields in some instances provide cleaner conditions so that the resulting surfaces are less loaded with detrimental deposits. The fabrication of npAu by corrosive dealloying is a good example in this context. Nonetheless and as detailed in the next subsection, also here attention must be paid to a proper activation of the materials.

Coming finally back to **FoM (1)**, it can be said, however, that in cases, such as npAu, there is a reasonable chance to access features at the atomic level which are key for the catalytic surface reactions, simply by adjusting mesoscopic features (such as the ligament size) during the synthesis. When being able to remove adventitious surface species blocking active sites or areas before catalytic use, predictable and tunable properties also according to FoM (1) can, in principle, be expected. This will be elucidated in the next subsection.

### III. (B) Nanoporous gold: surface structure and catalytic activation

The example reaction chosen in this thesis to explore the question whether npAu factually entails the advantages of a material whose catalytic properties are largely structurally pre-determined and as such reproducibly attainable, was low-temperature CO oxidation (30 °C). Together with methanol oxidation, this reaction not only was most intensively investigated under catalytic working conditions, but also subject of many UHV (ultrahigh vacuum) model studies, using suitable Au single crystal surfaces to this end [8].

Without going into details here, two central conclusions, drawn with respect to the question which surface features are most decisive for this reaction to be efficiently catalysed, shall be highlighted here:

- (a) As far as **CO** is concerned, there is ample evidence that only low-coordinated Au surface sites as available at atomic steps and – if these do not run in low-indexed crystallographic directions – kinks can bind the molecule sufficiently strong. On regularly coordinated Au sites (i.e., terrace sites), it is bound too weakly. Accordingly, a sufficiently high density of such defects is required [46].
- (b) In case of **O<sub>2</sub>**, as the other reactant, it is clear that its interaction neither with regular nor with defect Au surface sites is strong enough to allow for a transient residence time on the surface being long enough so that subsequent dissociation can take place. To unravel why npAu nevertheless is catalytically active for aerobic oxidation reactions, a large number of theoretical studies was carried out. Even though the decisive or prevailing mechanistic pathway among various conceivable possibilities could not yet have been unambiguously identified, the bulk of the results suggests that the second metal, i.e., Ag in the present case, is responsible for the activation of oxygen on the surface of npAu [8].

Regarding point (a), detailed TEM investigations indeed revealed a high density of atomic steps of about 20 % for pristine as well as for spent catalysts [47]. Even though not explicitly investigated, it can be assumed on the basis of the considerations in subsection (a) that the abundance of such defect sites and the ligament sizes are directly interlinked. Interestingly, the found share of low-coordinated surface sites is in the same range than that of catalytically active Au NPs. This analogy hence discloses why both systems, though differing in the dimensions of their structural features by one order of magnitude, likewise catalyse this reaction.

---

As far as point (b) is concerned, the insight that Ag is crucial for the turnover on the oxygen side implicates that the parameter relevant here is its surface concentration. In agreement with that, it indeed was found experimentally that the higher the residual content in the material the higher the conversion level observed [48]. Nonetheless, the derivation of a quantitative relationship, was hampered so far by issues already discussed in the preceding subsection (A). Ag segregates to the surface where it can enrich up to a factor of 10 as compared to the bulk [49]. This process depends on the temperature as well as on the gas environment and, here and foremost, on the oxygen partial pressure. Under conditions, where the relationship between bulk and surface concentration is thermodynamically controlled (equilibrium), this enrichment is of course predictable, also meaning that control over the Ag bulk content, as provided, in particular, by electrochemical dealloying techniques (see chapter II), represents at least an indirect synthetic measure to optimize FoM (1) with respect to the surface composition.

Notwithstanding these advantageous prerequisites, a critical review of the literature dealing with low-temperature CO oxidation over npAu and published prior to this thesis revealed no conclusive picture regarding its catalytic potential (FoM (1)) - neither in absolute terms nor in relation to supported Au catalysts [23]. On the one hand, quite diverging observations regarding npAu's initial activity were reported, ranging from high activities detected directly from the start to cases where the catalysts were initially totally inactive and showed onsetting activity only over time. On the other hand, and perhaps even more irritating, the rates or TOFs reported for conversion under steady state conditions showed a surprisingly large scatter.

Following the considerations of the preceding subsection (A), it was assumed that the most probable explanation for these deviations were impurities, remaining on the surfaces after the wet chemical preparation or deposited before use under atmospheric conditions. For instance, AgNO<sub>3</sub> precipitates are likely to form on the ligament surfaces when drying the samples, since a complete removal of soluble synthesis residues during the washing steps is supposedly difficult to achieve in the extended pore system. But also, silver carbonates, hydroxide or oxide species are possible candidates for blocking or poisoning the surfaces and thus repressing catalytic turnover.

An obvious strategy to remove such deposits is to decompose, oxidize and desorb them at sufficiently high temperatures. Interestingly, such an option had never been taken into account before this thesis for npAu - most probably because it was known that npAu's pore structure is quite sensitive to thermally induced coarsening when applying temperatures above 100 °C [36]. It had been simply overlooked in this context, however, that this fact does not necessarily exclude high temperature annealing steps which are short enough to not deteriorate the pore structure but still may suffice to efficiently clean its surfaces and catalytically activate the material. Supposedly, such fallacies based on seemingly reasonable but in the end crude judgements are understandable.

To check out the feasibility of such a strategy and its potential to activate npAu in a more reliable and reproducible way than before, different annealing temperatures and times were tested based on the following considerations:

- (a) In view of the desorption or decomposition temperatures of possible surface impurities, such as AgNO<sub>3</sub>, Ag carbonates and hydroxide species, it was concluded that a minimum **annealing temperature** of 300 °C is needed, on the one hand [22]. To minimize the risk of thermal coarsening, on the other hand, 400 °C was chosen as an upper bound for the activation experiments.
- (b) As opposed to studies in literature where thermally induced coarsening was observed, distinctly shorter **annealing times** in the range of just a few minutes were applied, on the

other hand. Assuming that only the final temperature is relevant for cleaning the surface from impurities and slow heating or cooling rates only increase the chance for coarsening processes, the experimental setup used in this thesis was optimized so that the npAu catalysts could be subjected to almost instantaneous temperature jumps.

The experiments carried out in this way revealed that, indeed, the classical concept for catalyst activation also works for npAu, when observing the following points:

- (a) As temperature, **300 °C** is sufficient and should not be exceeded.
- (b) Annealing times in the range of **just a minute** at this temperature do not cause noticeable coarsening; for longer times it cannot be excluded.
- (c) The activation should be performed **in the reaction mixture** (CO + O<sub>2</sub> in excess).
- (d) Typically, one short-term annealing step of this kind does not suffice to guarantee full catalytic steady state activity in all cases; in contrast, **a series of about 5 steps** – even if carried out quickly in a row – was found to be a reliable means to obtain the same high conversion level reproducibly for samples identically prepared.

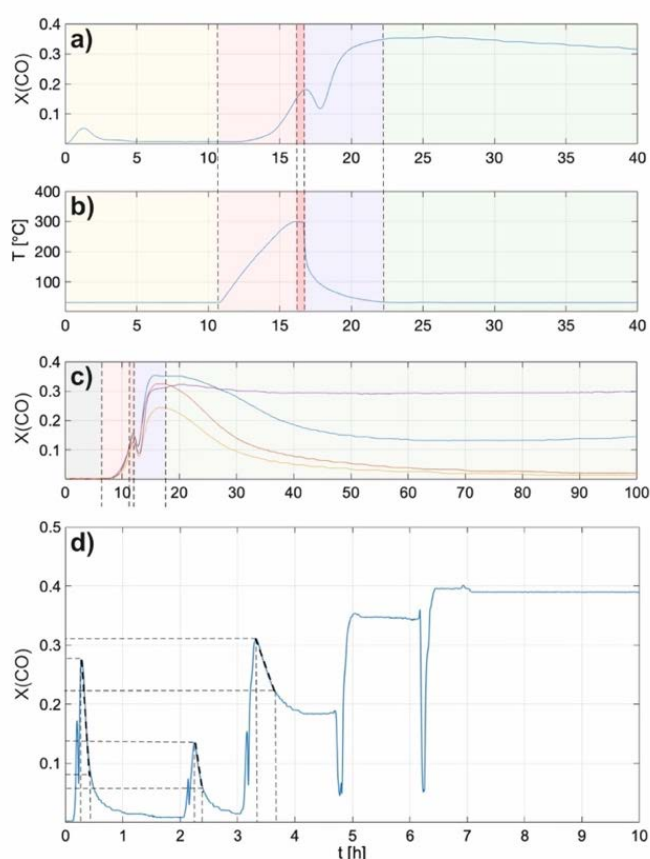


**Figure 3:** Catalytic activation of npAu for low-temperature CO oxidation (30 °C) – summary of the experimental results reported in [publication 1](#). a) & b): Temperature profile of a short annealing step applied to a pristine sample in the reaction mixture and concurrent evolution of catalytic activity (ratio of CO in the feed converted: X) as a function of time. Yellow shaded area: initial activity - the CO<sub>2</sub> formation seen in the beginning is only transient and not sustainable; during the heat-up phase (light red), carried out with a high heating rate of about ~1 K/min, a continuously rising conversion is detected; even after reaching the target temperature of 300 °C, kept constant for 1 min, this increase continues; only in the cooling phase (violet) performed similarly fast than the heating phase the conversion declines first but shortly after rises again; after reaching 30 °C again, a high conversion of around 40 % (under the applied reaction conditions) is achieved. c): Evolution of the conversion for 5 different but identically prepared samples after applying a single activation step, revealing a range of different behaviours including a total decrease of activity over time in some cases. D) Application of 5 successive annealing steps, showing that afterwards a constant and sustainable steady-state conversion is achieved.

---

Even though it was not possible to derive mechanistic explanations for the success of this approach on the basis of the experimental results, a likely scenario is the following. Due to the noble character of Au and the temperature being high enough to decompose potential Ag compounds, a restoration of metallic surfaces can be expected at 300 °C. It is not unreasonable to assume that during the subsequent cooling phase in the oxygen-rich reaction mixture, the catalytically active oxygen or (surface) oxide species can directly form on these pristine surfaces. As a result, a highly active surface state is created homogeneously and throughout the material ensuring an efficient catalytic turnover under steady state conditions, when finally reaching 30 °C again.

The fact that, for methanol oxidation, a way to reliably activate npAu by ozone treatment was comparatively quickly found [50], while it took almost 15 years in case of CO oxidation where such an activation approach does not work, illustrates that this seemingly simpler reaction factually depends on a more complex surface chemistry - in line with conclusions drawn from experimental as well as theoretical studies [8]. Nevertheless, the finding that, in spite of this complexity, npAu's catalytic activity can be reproducibly and straightforwardly evoked with a recipe still being relatively simple indicates a decent command of FoM (1).

## IV. MASS TRANSPORT ASPECTS (PUBLICATION II)

### IV. (A) Diffusion in porous materials: general requirements for avoiding mass transport limitations

Diffusion in porous matter is slowed down for several reasons as compared to the bulk gas phase [24]. These are connected with different structural features of the material which limit the diffusive transport and will be summarized in the following:

- (a) **Pore diameter:** In the bulk gas phase the propagation of molecules in space – called molecular diffusion - is determined and limited by the mean free path between intermolecular collisions. It decreases with the pressure  $p$  and so does the corresponding diffusion coefficient  $D_M$ . If the spatial dimensions of the surrounding, as in a narrow pore, fall below this mean free path, however, collisions with the walls become more likely than those among the diffusing molecules. Under such conditions, called **Knudsen regime**, the corresponding diffusion coefficient  $D_K$  no longer depends on the pressure but on the spatially limiting dimension – in his case, on the pore diameter  $d_p$ . The transition between both regimes, depicted in Fig. 4 for CO at 25 °C and 1 bar (chosen here as an example in view of the reaction, low-temperature CO oxidation, studied in this thesis) is not abrupt but continuous and can be described by  $D_T$  according to the *Bonsquet* equation:

$$D_T = \left( \frac{1}{D_M} + \frac{1}{D_K} \right)^{-1} \quad (\text{eq. 2})$$

- (b) **Pore shape:** If the pores in a porous material are not strictly cylindrical – a situation hardly encountered in reality –, the diffusing molecules will experience varying pore cross sections along their pathway. As a consequence, “bottle necks” may be created at those positions where these, i.e., the pore diameters are minimal, slowing down the diffusive flux and hence representing a further impediment for the mass transport in the Knudsen regime.



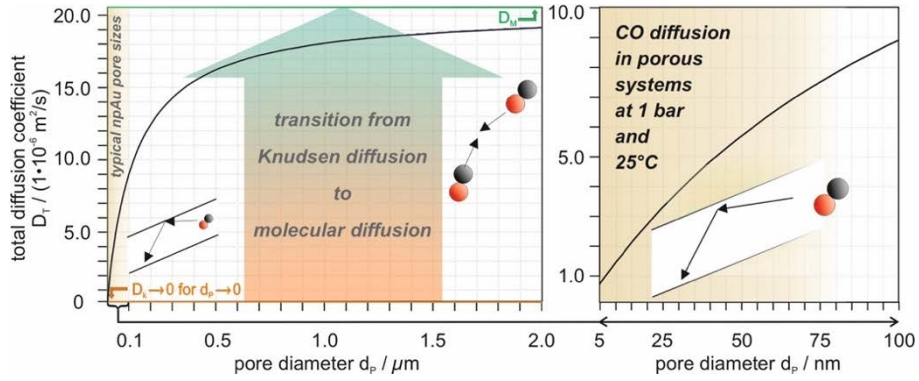


**Figure 4:** Dependence of the total diffusion coefficient  $D_T$ , comprising the contributions of molecular and Knudsen diffusion in a porous material, on the (mean) pore diameter. As an example, CO at 25 °C and 1 bar was chosen. On the right hand-side, the range below 100 nm, being relevant for npAu, has been enlarged. Reproduced from [publication III](#).

Even though this kind of influence was often neglected or, at least, less explicitly discussed in the literature, it is straightforwardly comprehensible that this aspect will contribute the more the more pronounced such pore size variations are. To take the resulting deceleration properly into account, a quantity, called **constrictivity**  $\delta$ , was introduced in the literature, ranging between 0 and 1 and simply representing the factor by which the mass transport in the material is reduced due this effect. An accurate quantitative assessment of  $\delta$  on the basis of the structural details of a given pore system is difficult, but for an estimation a formula, derived by Petersen already a long time ago, may be used [51]. To this end, only the maximum and minimum pore cross sections  $A_p$  or the corresponding pore diameters  $d_p$ , respectively, must be known:

$$\delta \approx 1 - 0.21 \cdot \ln\left(\frac{A_{p,max}}{A_{p,min}}\right) = 1 - 0.21 \cdot \ln\left(\frac{d_{p,max}^2}{d_{p,min}^2}\right) = 1 - 0.42 \cdot \ln\left(\frac{d_{p,max}}{d_{p,min}}\right) \quad (eq. 3)$$

As the latter are not sharply defined for a continuous, for instance, gaussian pore size distribution, of course, the values at the lower and upper end of its standard deviation may be used instead, as e.g., obtained by a statistical evaluation of SEM images.

- (c) **Pore length:** Within a porous material exhibiting non-straight pores the gas molecules have to travel longer diffusion pathways as compared to the bulk gas phase. Clearly, the retarding impact on the mass transport in the material will be the more pronounced, the stronger the pores are curved. A structural parameter introduced to consider this effect is the so-called **tortuosity**  $\tau$  ( $\tau \geq 1$ ), quantifying the factor by which the porous pathways are on average longer as compared to straight trajectories. In principle,  $\tau$  can be evaluated microscopically as well. In contrast to  $\delta$ , though, a characterization by SEM alone is not sufficient here, as this technique does not provide enough depth of field to judge the (third) dimension perpendicular to the imaged surface. An alternative, being factually able to provide the necessary information about the full three-dimensional structure of a mesoporous material, is STEM tomography. It has to be considered, however, that, in addition to the high experimental effort which is necessary for such studies, only comparatively small volumes with edge lengths in the range of a few 10 nm can be investigated in this way. To derive the tortuosity from such data, in a second step all pathways a diffusing molecule could possibly take in the imaged pore system need to be numerically evaluated. But even in case of materials with a spatially homogeneous

porosity whose “elementary cell” (see chapter II) is smaller than the imaged volume and thus representative for the whole material, the results are not free of ambiguities [26]. These result from the possibility to base the analysis on different assumptions. For interconnected pores – as given in most cases –, for instance either only the shortest possible options existing for the diffusing molecules or all pathways alternatives branching off at a crossing point may be considered. The mean value in the first case is called *geometric tortuosity*  $\tau_{\text{geo}}$  and obviously is smaller than the *branch tortuosity*  $\tau_{\text{branch}}$  as derived in the second case. A priori it is not clear which of the two values reflects the situation under real experimental conditions better. In this context, the constrictivity comes into play, rendering longer pathways the less likely the smaller  $\delta$ , because these are associated with a higher chance of impeding bottle necks. As a consequence, preference is then given to the shortest pathway, resulting in an effective tortuosity  $\tau$  approaching  $\tau_{\text{geo}}$ , while for  $\delta \sim 1$ ,  $\tau$  is supposed to rather reflect  $\tau_{\text{branch}}$ . Such uncertainties illustrate why methods providing direct insight into the diffusion processes are indispensable. A technique that, although limited in use by the availability of suitable instruments, proved unprecedented capabilities in this respect is PFG NMR [24]. While it was already successfully applied to porous oxides and zeolites in the past, porous metals had not been studied at the beginning of this thesis.

- (d) **Pore volume:** The diffusive flow under mass transport conditions is related to area, which, in a porous material, is reduced proportional to the volume occupied by the solid phase. This effect can be easily considered by means of the **porosity**  $\phi$ , representing the share of the pore volume  $V_{\text{pores}}$  in a given volume  $V_{\text{total}}$  of the material.

The impact such factors on the gas diffusion in a porous material is accounted for in an efficient diffusion constant  $D_E$  used to describe the mass transport within its pore system. The extent to which each of the 4 points discussed above contributes to the net deceleration, depends on the related structural parameters in a comprehensible and predictable manner:

$$D_E = \frac{\phi \cdot \delta}{\tau} \cdot D_T \quad (\text{eq. 4})$$

On the side of the porous material, i.e., the **transport medium**, the tortuosity  $\tau$ , on the one hand, takes impediments into account which the molecules encounter *along* their diffusive pathway in the pore system.<sup>1</sup> Obstacles *perpendicular* to their pathway, on the other hand, are subsumed in  $\delta$ , the constrictivity. A further reduction of the mass transport results from the porosity  $\phi$  of the material, reflecting, however, not mesoscopic specificities of the material but the (trivial) aspect that just the material-filled volume is available for the diffusive mass transport. On the side of the gases, i.e., the **transported species**, it is a change from molecular diffusion to Knudsen diffusion that decelerates the mass transport. Since, however, this transition depends on the (mean) pore diameter  $d_p$ , also this contribution is structure dependent in the end.

Notably, two borderline cases may be distinguished between. Either  $\tau$ ,  $\delta$ ,  $\phi$  and  $d_p$ , apply only locally or these quantities describe the porous material as a whole so that they can be considered as material-specific and – as the case may be - synthetically adjustable features. It is obvious that only in the latter case,  $D_E$  as calculated on the basis of eq. 4 will describe a pore

<sup>1</sup> Instead of eq. 4, in the literature sometimes an equation is found, where the tortuosity of the pore system is considered by a factor  $\tau'$  which enters in a squared form:  $D_E \sim 1/\tau'^2$ . The reasons for this alternative concept are discussed in [publication III](#) [26]. Without going into details here, it shall be mentioned that  $\tau'$  and  $\tau$  are related by:  $\tau' = \sqrt{\tau}$ .

---

system globally. As mentioned already in the Introduction, the structural homogeneity and isotropy, which needs to be given to this end, often cannot be reached for traditionally prepared heterogeneous catalysts. This circumstance explains to a good deal why the vision of “rationally designed catalysts” – although always sought in research – has, if at all, only come true in selected cases. In contrast to that, novel nanotechnological approaches have demonstrated in many instances their potential to provide access to porous materials with spatially uniform and well-defined properties. Provided that even synthetic options exist to systematically vary some or all of the discussed parameters, not only can be predicted mass transport properties but also optimized according to **FoM (3)**.

#### IV. (B) Nanoporous gold: transport properties and their experimental characterization

In chapter II it has already become clear that, thanks to its kinetically controlled formation mechanism during dealloying, npAu exhibits a well-defined and homogeneous porosity providing identical conditions for diffusive transport throughout the material.

Among the structural features, which are determinant here according to the discussion in the previous section, the porosity belongs to those parameters which, to some degree, can be synthetically varied. It can be adjusted between 60 % and 80 %, simply by choosing a corresponding composition of the master alloy. Smaller or larger values cannot be prepared due to the fundamental limits set by the dealloying process. This restriction, however, usually is not crucial for catalytic applications, since high porosities as achievable within this window are sought not only but also in view of an optimal mass transport ( $D_E \sim \phi$ ).

Relying, in particular, on advanced electrochemical dealloying approaches, furthermore ligament and pore sizes can be controlled and adjusted in ranges between a few and a few 100 nm, as discussed in chapter II. In this way, the contribution of Knudsen diffusion to  $D_T$  can be influenced and, in principle, reduced. By increasing npAu’s pore diameters from 5 nm to 50 nm, i.e., by a factor of 10, an increase of the (total) diffusion coefficient by almost also an order of magnitude is hypothetically achievable, as can be inferred from Fig. 4. It has to be taken into account though that, in parallel, the specific surface area decreases by an order of magnitude (see Fig. 2) as well, suggesting, at first sight, that both trends cancel each other. It will become apparent only in the next chapter, however, that such simple considerations are misleading. This is due to the fact that not absolute  $D_E$  values are decisive in the end, but their relation to the microkinetics of the surface reaction under consideration. In other words, it is the interplay between catalytic reaction and diffusive mass transport which factually determines the achievable productivity and the occurrence of mass transport limitations.

As far as the constrictivity and tortuosity as further relevant parameters are concerned, it is clear that, in case of npAu, these features are not subject to preparative manipulation but are predetermined by its characteristic pore structure. This aspect, however, not necessarily represents a drawback. The fact that these quantities are material-specifically fixed, bears the advantage that they, once known, are universally applicable and do not need to be laboriously evaluated for each sample batch prepared. Using the approach of Petersen (eq. 3), the constrictivity of npAu, in particular, can be rather straightforwardly assessed on the basis of its well-known pore size distribution, the relative halfwidth or standard deviation, respectively, of which was shown in the literature to be independent of the mean pore diameter [19]. The low value of  $\delta \approx 0.5$  derived in this way indicates that the broad range of pore sizes characteristic of npAu exerts a quite substantial impact on the diffusive mass transport within the material slowing it down by 50% as compared to the bulk gas phase.

As detailed in subsection (A), an accurate evaluation of the tortuosity, in contrast, is significantly more difficult and was accomplished for the first time within the framework of this

---

thesis. To this end, PFG NMR has been drawn on in a collaboration with the group of Prof. Sergey Vasenkov at the University of Florida at Gainesville where NMR instruments, suitable for such measurements, are available. As detailed in [publication II](#) [23], the acquisition of NMR attenuation curves for different diffusion times allowed to determine the self-diffusion coefficients of CO, CO<sub>2</sub> and CH<sub>4</sub> at 15 bar and room temperature inside and outside of npAu. Applying elevated pressure conditions provided the advantage that Knudsen diffusion could be largely repressed and  $D_T \approx D_M$  assumed. Under such conditions, eq. 4 predicts that the ratio  $D_E/D_T \approx D_E/D_M$  corresponds to  $\delta/\tau$ , when additionally taking into account that, in case of self-diffusion as studied here, the porosity  $\phi$  does not play a role and hence drops out of the equation.

The experimental finding that  $D_E/D_M \approx 0.5$  in combination with the estimated value of  $\delta \approx 0.5$  reveals for  $\tau$  a value being close to 1, suggesting that, in contrast to pore size variations, impediments for the diffusive transport due to elongated pathways are almost negligible for npAu. In this context, it is instructive to factor the results of STEM tomography experiments into the discussion which were carried out to evaluate the tortuosity of the pore system also microscopically [52].<sup>2</sup> The geometric tortuosity  $\tau_{\text{geo}}$  determined on these grounds was close to 1, in agreement with the outcome of the PFG NMR measurements, while the branch tortuosity turned out to be by a factor of about 2 larger. According to the previous subsection, the equivalence of  $\tau$  and  $\tau_{\text{geo}}$  indirectly corroborates the dominating influence of the constrictivity for slowing down the mass transport within npAu. As explained there,  $\tau$  is expected to approach  $\tau_{\text{geo}}$ , when  $\delta$  assumes values distinctly smaller than 1.

As detailed in [publication II](#), the knowledge of  $\delta$  and  $\tau$  or, more precisely, of  $\delta/\tau$  allowed calculating (eq. 4) the effective diffusing coefficients  $D_E$  of all gases in the reaction mixture used in catalytic lab experiments on low-temperature CO oxidation over npAu under ambient pressure conditions and at 30 °C. Additional information needed to this end - such as molecular or Knudsen diffusion coefficients - were taken from the literature or could be calculated on the basis of kinetic gas theory. This data was key to not only determine microkinetic rate constants for this reaction accurately for the first time but also to reliably predict how mass transport limitations can be minimized for this catalyst [23]. This topic will be dealt with in the following chapter.

## V. INTERPLAY OF CATALYTIC SURFACE REACTION AND MASS TRANSPORT (PUBLICATION III)

### V. (A) The interplay of catalytic surface reaction and mass transport: general requirements for achieving high catalyst productivities

For a working porous catalyst in every volume element catalytic turnover at the ligament surfaces (i.e., at the pore walls) and diffusive transport driven by the resulting concentration gradients take place at the same time and, hence, are interlinked (as long as the concentrations of the reactants do not drop to zero). To evaluate the resulting net catalytic conversion, when using catalyst particles of a specific form and shape in a process, 1939 W. Thiele introduced a concept which ever since has been key in chemical engineering to quantitatively predict the impact of the interplay between catalytic reaction and mass transport on the overall performance [53].

---

<sup>2</sup> To this end, npAu nanoparticles were used which, though prepared in a different way, are supposedly structurally largely equivalent to npAu monoliths as studied in this thesis.

It is obvious in this context that the maximum conversion rate that can be reached is limited by the catalytic surface reaction. Yet, as reactants have to be delivered and resupplied – in the same way as products have to be transported back to the outer surface of the catalyst particles – by diffusive transport, the actually observed conversion rate may be smaller [54]. This is the case when gas diffusion in the pore system cannot cope with the catalytic turnover on the inner surfaces of the catalyst. The resulting loss of productivity, caused by such mass transport limitations, is expressed in form of an **effectiveness factor**  $\eta$ , which is defined as the ratio of the actually observed rate and the maximum rate of catalytic turnover on the surface. The more this number deviates from one, the more influential are mass transport limitations. Under such circumstances, steeply falling concentration profiles within a catalyst particle may result so that, in extreme cases, inner parts of a catalyst particle, where the reactant concentrations drop to zero, cannot contribute and are thus lost for the catalytic conversion. The central quantity determining a catalyst effectiveness is the so-called **Thiele modulus** which, in turn, depends on the ratio of the kinetic rate constant of the catalytic surface reaction and the effective diffusion coefficients of the reactants in the material. Apart from these material-related quantities, also the actual geometry of the catalytic particles, used in an application, plays a role. Their shape and their dimensions enter the Thiele modulus in form of a length  $\ell$ , called characteristic length, representing the mean distance the diffusing molecules have to travel in the particles if projected onto a 1D situation. The full mathematical expression of the Thiele modulus differs for different kinetic rate laws and can be comparatively complex. An exception is given for a rate law of first order:

$$r_{micro} = k \cdot c_{Reactant} \quad (eq.5)$$

( $k$ : rate constant,  $c_{Reactant}$ : molar conc. of the rate-determining reactant) which will be considered in the following, as the Thiele modulus  $\varphi$  takes a particularly simple form here [54]:

$$\varphi = \sqrt{\frac{k \cdot \ell^2}{D_E}} = \ell \cdot \sqrt{\frac{k}{D_E}} \quad (eq.6)$$

On the basis of  $\varphi$  the effectiveness factor  $\eta$  can then be directly calculated according to [54]:

$$\eta = \frac{\tanh(\varphi)}{\varphi} \quad (eq.7)$$

So, as long as the kinetics of the surface reaction, called microkinetics, and the effective diffusion coefficient of the rate determining reactant are known, the Thiele modulus formalism allows predicting the effectiveness of a catalyst applied in form of particles with defined shapes and dimensions. As a rule of thumb,  $\eta$  approaches 1 for Thiele moduli  $\varphi < 0.3$ , meaning that, under such conditions, mass transport limitations are negligible. For  $\varphi > 3$ , their influence reduces the effectiveness to  $\sim 1/\varphi$ , i.e., to a significant extent [54].

As far as the **microkinetics** are concerned, it is important to note that  $k$  (defined in line with standard chemical kinetics and exhibiting the unit [ $s^{-1}$ ]) is related to  $k_s$ , the rate constant per area catalyst (being the more appropriate quantity in het. cat., unit: [ $m/s$ ]), in the following way:

$$k = k_s \cdot \frac{A_{pore\ walls}}{V_{pores}} = k_s \cdot \frac{A_{ligaments}}{V_{pores}} = k_s \cdot \frac{(1 - \phi)}{\phi} \cdot \frac{\zeta}{d_L} \quad (eq.8)$$

It is  $k_s$ , which quantifies the catalytic surface activity (as given by its composition and structure (see chapter II)) and, as such, stands for FoM (1), while  $k$  is volume related and not only depends on the latter, but also on the surface area exposed in a certain pore volume. This

---

ratio  $A_{ligaments}/V_{pores}$  can be derived from  $A_m$  and the ratio of ligament and pore volume (see [publication II](#) for details), explaining why the porosity  $\phi$  as well as the pore size  $d_L$  and  $\xi$  (see chapter II) appear in eq. 8 [23].

In order to repress or even avoid transport limitations and to optimize the catalytic process in this way, either the ratio of  $k$  and  $D_E$  and/or the characteristic length of the used catalyst particles need to be decreased. As far as the microkinetics are concerned, high rates and thus large rate constants,  $k$  or  $k_s$ , respectively, are always desirable of course. To achieve this, the catalyst needs to be suitably activated as discussed in chapter III. For mass transport limitations to be minimal, the effective gas diffusion coefficient (of the rate-determining reactant) must then be sufficiently large in relation to  $k$ . Aiming at increasing  $D_E$ , the influencing structural factors, as discussed in chapter IV, may be adjusted – provided of course that the preparation of the catalyst allows deliberately varying them. In contrast to such preparation related options, improvements of the catalyst effectiveness by reducing the characteristic length of the applied particles (smaller dimensions, changing to other shapes) are often easier to realize or are achieved with lesser effort.

In any event, the Thiele formalism allows predicting the practically achievable conversion rate, i.e., the **macrokinetics**, when using a certain mass of a given catalyst  $m_{cat}$  and a concentration  $C_{Reactant}$  of the (rate determining) reactant in the feed:

$$r_{macro} = m_{cat} \cdot A_m \cdot \eta \cdot k_s \cdot C_{Reactant} \quad (eq. 9)$$

This equation (for a reaction of 1<sup>st</sup> order) instructively demonstrates in which way the figures of merit (**FoMs**) introduced in the Introduction as central determinants for the performance of a heterogeneous catalyst contribute to its productivity:

- **FoM (1)** determines the area-related microkinetic rate constant  $k_s$ ;
- **FoM (2)** comes into play via the specific surface area  $A_m$ ;
- **FoM (3)** is comprised in the effectiveness factor  $\eta$  which, however, also depends on the microkinetics, i.e., on **FoM (1)**.

Yet, the Thiele formalism, in principle, not only allows predicting macrokinetics from known microkinetics [55], but also extracting microkinetics from experimentally observed macrokinetics. The latter opportunity is particularly interesting for fundamental studies (as opposed to technical applications) where the problem exists that mass transport limitations cannot easily be avoided experimentally when characterizing the intrinsic activity of a newly developed catalytic material, for instance [56]. Even though eq. 9 does not allow an analytical solution in this case, numerical or graphical ones are possible, as detailed in [publication II](#) [23].

## V. (B) Nanoporous gold: derivation of microkinetics and optimization of catalytic effectiveness

In view of its well-defined structural features, the broad range of steady state catalytic activities, reported in the literature for npAu catalysts (exhibiting comparable ligament sizes) for low-temperature CO oxidation (30 °C) and derived under seemingly similar conditions (atmospheric pressure, oxygen excess), appears somewhat surprising, not to say, irritating [23]. In case of oxide supported Au catalysts, intensive research over the years revealed that deviations in the catalytic activity can be traced back to the support playing an essential role for the activation and the supply of oxygen on the surface (see Introduction) [57, 58]. As discussed in chapter III, in case of npAu, this function is ascribed to Ag species remaining in the material after dealloying and segregating to the surface under oxidative conditions. Even though it is tempting on these grounds to ascribe the observed scatter to differences in the Ag surface concentration - resulting, for example, from difficulties to reliably establish the

---

same surface composition under nominally identical reaction conditions -, such explanations appear unlikely. Kinetic studies for this reaction revealed a reaction order close to zero for O<sub>2</sub>, indicating that the supply of oxygen is not critically limiting the reaction and, hence, that this aspect is not of foremost importance [59].

There are two alternative explanations that appear more likely on these grounds. Since npAu was typically studied in form of large monoliths with, in part, differing dimensions, it firstly cannot be excluded that mass transport limitations were effective to a different and unknown extent in the respective studies. Secondly, it remains an open question whether all corresponding experiments actually emanated from the same level of activation, i.e., refer to the same catalytic surface state. In view of the wealth of varying activation procedures applied, the opposite seems more probable (see chapter III).

To overcome these ambiguities, npAu samples reliably activated for CO oxidation on the basis of the protocol, described in chapter III and in [publication I](#), were catalytically investigated. Even though it remains unproven that the attained surface state represents the optimal one and yields the highest possible turnover, the high reproducibility found corroborates such an assumption [22]. To evaluate its catalytic capability (FoM (1)), i.e. to extract microkinetic data from experimentally observed conversions, the Thiele modulus formalism was employed, as described in the preceding subsection. The analysis was facilitated by the fact that the kinetic studies mentioned above suggested in case of CO a reaction order close to 1, i.e., a rate law of first order (in CO) for the surface reaction (see eq. 5) [59]. In this way,  $k$  (eq. 5),  $k_s$  (eq. 8) and also the TOF for the reaction could be determined without ambiguities arising from an unknown extent of mass transport limitations (see [publication II](#)) [23]. The results are summarized in Fig. 5.

In a second step, the obtained data were employed to evaluate the catalytic effectiveness of the used thin disc-shaped npAu catalysts, representing that type of specimen which was most frequently investigated in other studies as well. This analysis revealed a Thiele modulus of  $\varphi \sim 1.2$  indicating a noticeable influence of mass transport limitations. Quantitatively, this value predicts that only an effectiveness of 70 % can be reached under these conditions. As mentioned above, Thiele moduli in the range of 0.3 or below are needed to achieve an effectiveness close to 100%, meaning in the present case that  $\varphi$  needs to be decreased by a factor of  $\sim 4$  to largely eliminate mass transport limitations and to exploit the full catalytic potential of the material. In accord with the discussion in the preceding section, two options, in principle, exist to achieve this goal:

- (a) **Decrease of  $k/D_E$**  by either improving the constrictivity and/or tortuosity of the pore system or by increasing the pore diameters to repress Knudsen diffusion:

As far as the first two structural parameters are concerned, the results discussed in chapter IV revealed that not the tortuosity but rather the low constrictivity is decisive for impeding the diffusive transport. Since the pore size distribution determining the constrictivity is a characteristic feature of npAu that is even conserved when thermally coarsening its pore system, no preparative pathway is available to vary it [19]. In contrast, such a coarsening would feasibly allow increasing npAu's pore diameters in a controlled fashion to diminish Knudsen diffusion which, as a matter of fact, dominates at 1 bar, i.e., at the pressure where the catalytic experiments were carried out.

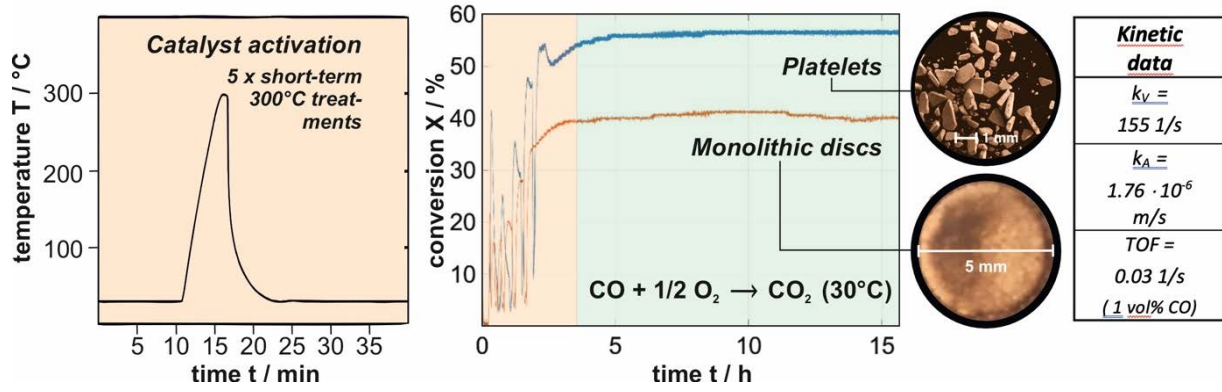


**Figure 5:** Summary of experiments carried out in this thesis to derive the microkinetics of CO oxidation over npAu at 30 °C. Monolithic npAu discs (diameter: 5 mm, thickness: 200 microns), catalytically activated according to the protocol developed in [publication I](#) showed under the applied reaction conditions ( $p_{Total} = 1$  bar,  $p(CO) = 10$  mbar,  $p(O_2) = 100$  mbar, balanced with He as carrier gas) a conversion of ~ 40 %. Taking advantage of the results of [publication II](#) enabling the calculation of the effective diffusion coefficient of CO for this pressure and gas composition, the microkinetic data compiled on the right hand-side could be extracted. In addition to the monolithic samples, also npAu platelets (diameter: a few 100 microns, thickness: 200 microns) were investigated which were obtained by mechanical breakup of the 5 mm monoliths. In this way, the conversion could be increased to 60 %. Reproduced from [publication III](#).

Assuming on these grounds that  $D_E \sim D_T \sim D_K \sim d_p$  and furthermore considering that, according to eq. 8,  $k$  is proportional to  $1/d_L = 1/d_p$ , for the Thiele modulus overall follows (eq. 6):  $\phi \sim 1/d_p$ . Hence, a reduction of  $\phi$  by about a factor of ~ 4 would require an increase of the pore diameter  $d_p$  by the same factor. Since for npAu pore and ligament diameter are similar and the specific surface area is inversely dependent on the latter, such a coarsening of the pore system, however, would concomitantly entail a loss of surface area to the same extent, while the elimination of transport limitations “just” leads to an improvement by a factor of ~ 1.5 (70% -> 100%). So, overall, this strategy is counter-productive (eq. 9).

- (b) **Decrease of the characteristic length** by reducing the dimensions or changing the shape of the used npAu samples:

Taking into account that  $\phi$  is directly proportional to the characteristic length  $l$  of the catalyst particles actually used (eq. 6), any lowering of the latter reduces the Thiele modulus to the same extent. In chemical engineering, the characteristic length is commonly defined as the ratio of the volume of a catalyst particle and its outer surface [45]. Within this thesis, however, a more general expression for this quantity could be derived, based on the dimensions  $x$ ,  $y$  and  $z$  of a given particle shape along the 3 cartesian coordinates [26]:

$$\ell = \frac{1}{2 \cdot \left( \frac{1}{x} + \frac{1}{y} + \frac{1}{z} \right)} \quad (eq. 10)$$

In case of spheres and cubes, all 3 dimensions are identical and refer to the diameter or edge length, respectively. For a cylindric shape  $x$  and  $y$  are given by the diameter and  $z$  by the height, meaning that for discs, whose diameter  $d$  is significantly larger than the thickness  $h$ , the latter or – in quantitative terms – half of its value determines  $l$ . As this is the case for the disc-shaped npAu samples used in this thesis, it can be concluded that their thickness of 200 microns correlates with a characteristic length of 100 microns. An



obvious possibility to reduce this parameter is a change to npAu particles/platelets with smaller dimensions or diameters, respectively.

In view of the preparative advantages connected with the fabrication of larger monoliths – in particular under electrochemical conditions which are preferable when aiming at a higher degree of structural control –, their subsequent transformation into smaller entities comprehensibly is more attractive than dealloying smaller specimen directly. Within this thesis a corresponding approach was therefore explored, based on the idea that grain boundaries are prone to fracture under mechanical stress. In agreement with that, the monolithic discs were intensively shaken in a vial, indeed resulting in a breakup into smaller platelets [23]. These exhibited the same thickness than the original discs but diameters in the range of just a few 100 microns - in general agreement with the grain sizes in the npAu monoliths.

Carrying out CO oxidation under otherwise exactly the same conditions with these npAu platelets resulted in an increase of  $\eta$  to almost 1, in line with a reduction of the characteristic length to 1/3 of the original value and an equivalent diminution of the Thiele modulus. In Fig. 6, the effectiveness factor  $\eta$  is plotted as a function of the characteristic length underpinning that, indeed, the variation of the particle size represents an efficient and comparatively easy measure to adjust FoM (3) and to optimize the conversion achievable under practical conditions in this way. Notably, such a strategy was not considered and systematically explored for npAu in the literature before. The overall approach taken in this thesis to describe the interplay of reaction and diffusive mass transport within materials like npAu featuring a well-defined porosity is discussed in detail in [publication III](#) [26].

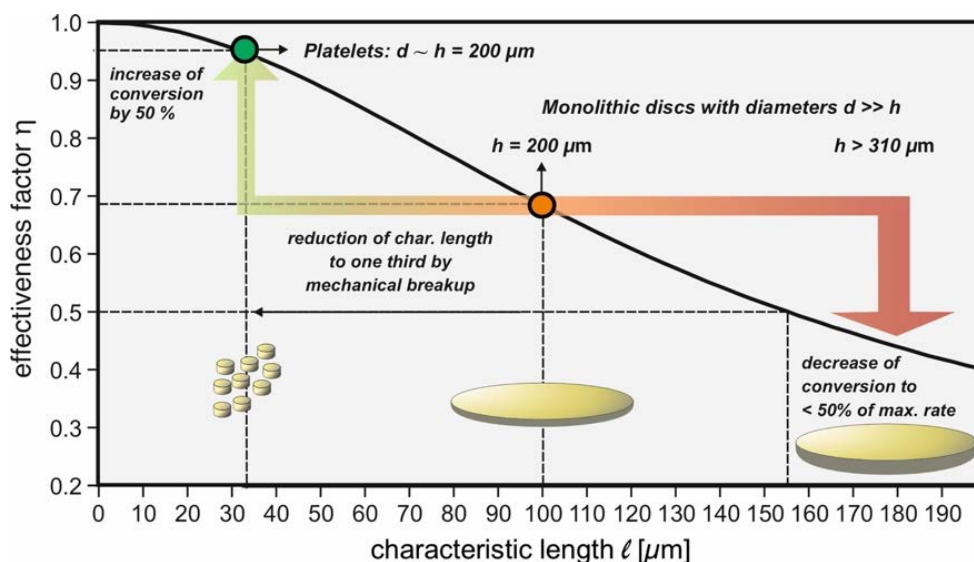


**Figure 6:** Dependence of the catalytic effectiveness factor  $\eta$  on the characteristic length according to eq. 6 and 7, revealing that for cylindrical catalyst particles with a given height  $h$  of 200 microns, a reduction of the diameter from  $d \gg h$  to  $d \sim h$  involves an increase of  $\eta$  from  $\sim 0.7$  to  $\sim 1$ . Reproduced from [publication III](#).

---

## VI. CONCLUSIONS

A long-standing dream in heterogeneous catalysis has always been the development of catalytic materials with predictable properties that can be synthetically tuned and optimized along all **3 FoMs** specified in the Introduction. Traditional preparation techniques, although still very common in practice, are typically based on processes which can neither thermodynamically nor kinetically controlled to a sufficient extent.<sup>3</sup> At the example of nanoporous gold, this thesis was devoted to the question whether the realization of this goal can advance into the realm of possibilities, when taking advantage of more sophisticated synthesis methods developed in materials science and nanotechnology.

In the Introduction, the question was raised:

***What are requirements for porous bulk catalysts with predictable properties and how are these related to their structure?***

The considerations presented in the first subsections (A) of the preceding chapters revealed that well-defined and isotropic characteristics, such as ...

- (a) ... surface structures and compositions at the atomic level, being relevant for the **microkinetics** and thus for **FoM (1)** (see chapter III) as well as
- (b) ... pore sizes, shapes and connectivities, governing **gas diffusivities** in the material and thus impacting **FoM (3)** (see chapter IV) and
- (c) ... ligament arrangements and sizes, determining the exposed surface areas and thus **FoM (2)** (see chapter II)

are important in this context. Under these conditions, it can be assumed that the quantities, governing each FoM, i.e., ...

- (a) ... the area-related catalytic activity ( $k_s$ ),
- (b) ... effective gas diffusion coefficients in the material ( $D_E$ ), and
- (c) ... the available surface area per mass unit catalyst ( $A_m$ ),

apply globally and not just locally within a macroscopic sample and, as such, are dependent on a (common) set of uniform structural parameters which are either material-specifically fixed or variable in a controlled fashion during the synthesis. In case of a porous bulk catalyst to these belong the mean pore and ligament size, the tortuosity of the pore system and the broadness of the pore size distribution, determining its constrictivity. On this basis, the catalytic performance, i.e., the macrokinetics, achieved in an application under given reaction conditions as well as measures to optimize it may be predicted (see chapter V). It is important to note, however, that only for (b) and (c) quantitative structure-property relationships can be realistically derived, while in case of (a) these often must stay at the level of qualitative considerations – based on the assumption, for example, that the density of catalytically relevant surface sites, such as under-coordinated atoms located at steps or kinks, is related to the curvature, i.e., the diameter of the ligaments/struts.

In the opposite case, i.e., when structural and compositional characteristics vary spatially and possibly statistically within a macroscopic catalyst particle, an individual examination of the three FoMs is typically not possible as their interplay is locally intertwined. Average values,

---

<sup>3</sup> Taking the preparation of supported metal catalysts by wet-chemical impregnation, calcination and reduction as an example, catalytically relevant structural features, such as particle sizes finally obtained can depend on a complex interplay of thermodynamic and kinetic factors, determining the processes. For Ostwald ripening, for example, increasing particle sizes during the preparation or also later in the catalytic application, the optimization of surface energies is the driving force on the thermodynamic side, while on the kinetic site the rate of involved surface diffusion and aggregation processes plays a role [64].

---

even if they are under synthetic control, are then of limited value when aiming at forecasting the performance of a catalytic material along single FoMs or with respect to the overall productivity.

The second subsections (B) of the chapter II - V, dealt with the question:

***Can npAu be considered as such a catalyst?***

In essence, the discussion has suggested that this is largely the case. The potential of the material as a mesoporous bulk catalyst in particular for aerobic oxidation reactions at low temperatures was well enough demonstrated in the literature before this thesis. Its preparation by dealloying, developed and refined in materials science, was shown to reliably lead to a characteristic bi-continuous porous structure that is homogeneously exhibited throughout a macroscopic catalyst particle/sample. Proving that such alternative synthesis techniques for catalytic materials indeed often provide more structural control, some structural features, such as pore and ligament sizes or the porosity can be synthetically varied (in certain ranges), while others, such as the tortuosity and constrictivity of the pore system, are fixed and as such reproducibly attainable.

A factor (influencing FoM(1)), being, admittedly, more difficult to control, is the surface composition. Since residues of the less noble metal remaining in the material after dealloying – in this thesis as well as in most other studies in the literature: Ag – are co-catalytically involved, their surface concentration plays an important role. As mentioned in chapter II, sophisticated electrochemical preparation recipes have been developed after realizing this point which allow tuning the Ag bulk concentration independently of the structure. As discussed in chapter III, bulk and surface concentrations, however, differ and their relationship, moreover, is subject to dynamical changes, depending on the temperature and the surrounding gas atmosphere. Practical experience nevertheless suggests that, for a given set of reaction conditions, one can emanate from similar surface compositions for samples with identical residual Ag concentrations. Accordingly, even if the surface concentrations are unknown and cannot be directly controlled, they at least can be indirectly assessed via controlling the Ag bulk content [60].

Table 1 summarizes the structure-property relationships derived in the subsections (A) of chapters II – V and the conclusions drawn in sections (B) regarding the question how these apply to npAu. The overview suggests that npAu catalysts with similar features (2<sup>nd</sup> column) or characteristic parameters (3<sup>rd</sup> column) should show comparable catalytic performances (under identical reaction conditions). The literature available for low-temperature CO oxidation at the beginning of this thesis, however, seemingly contradicted this hypothesis. In spite of the quite remarkable scatter of reported conversion rates or TOFs, neither these discrepancies nor the possibility of persistent surface contaminations case-specifically remaining after preparation or formed under ambient conditions to different extents was taken into account or systematically discussed. This consideration led to the first objective of this thesis, aiming to ...

**...clarify if an activation protocol can be developed in case of CO oxidation (at 30 °C) which allows reliably and reproducibly achieving the same catalytically active surface state.**

<b>FoMs and associated physical quantities</b>	<b>Relevant structural features</b>	<b>Related mat. parameters and their relation to FoM determining quantities</b>	<b>Controllable in synthesis of npAu?</b>
<b>(1) Catalytic surface activity: <math>k_s</math></b> (microkinetic rate constant)	<b>Defect density</b> , exposed crystallographic surfaces and strain,  <b>Surface composition</b>	<b>Ligament diameter <math>d_L</math></b>  <b>Residual Ag content</b> , oxygen partial pressure	✓  (✓)
<b>(2) Specific surface area: <math>A_m</math></b>	<b>Ligament sizes</b> , layout of pore system	<b>Ligament diameter <math>d_L</math></b> , <b>structural constant <math>\xi</math></b>  $A_m \sim \xi / d_L$	✓ x
<b>(3) Mass transport properties: <math>D_E</math></b> (effective diffusion constant in the pore system)	<b>Pore sizes</b>  <b>Pore curvatures and their connectivity</b> Local “bottle necks” along the pores  <b>Pore volume</b>	<b>Pore diameter <math>d_p</math></b> $D_E \sim D_K \sim d_p$ (for Knudsen regime)  <b>Tortuosity <math>\tau</math></b>  <b>Constrictivity <math>\delta</math></b> = f (width of pore size distribution);  <b>Porosity <math>\phi</math></b>  $D_E \sim \phi \cdot \delta / \tau^2$	✓  x x  ✓
<b>Resulting catalyst features</b>	<b>Relevant FoMs and further determinants</b>	<b>Associated quantities</b>	<b>Assessable for npAu?</b>
<b>Catalyst effectiveness: <math>\eta</math></b>	FoM (1): <b>microkinetics</b> FoM (3): <b>diff. transport</b> <b>Dimensions and shape of catalyst particles</b>	$k = f(k_s, \phi, \xi, d_L)$ $D_E$ <b>characteristic length <math>\ell</math></b> $\ell = (2 \cdot (x^{-1} + y^{-1} + z^{-1}))^{-1}$  $\eta = \tanh(\phi) / \phi$ with (for a rate law of 1 <sup>st</sup> order):  $\phi = \ell \cdot k^{1/2} / D_E^{1/2}$	✓
<b>Macrokinetics:</b> $r_{macro}$ or <b>X</b> (conversion)	FoM (1): <b>microkinetics</b> FoM (2): <b>surface area</b> <b>Catalyst effectiveness</b>	$k_s$ $A_m$ $\eta$ For rate law of 1 <sup>st</sup> order:  $r_{macro} = m_{cat} \cdot A_m \cdot \eta \cdot k_s \cdot c_{Reactant}$	

**Table 1:** Overview over all FoMs and resulting operational features which govern the performance/productivity of a porous bulk catalyst along with the quantities (bold) determining them (1<sup>st</sup> column). In the second column all influential structural (and compositional) factors are summarized, which, if the material exhibits a well-defined and isotropic pore structure, are homogeneously exposed throughout a macroscopic sample. In the third column associated parameters are listed which, under this condition, characterize the structure as a whole and, as the case may be, material-specifically and furthermore allow assessing (qualitatively or even quantitatively) not only individual FoMs but also the resulting catalyst effectiveness and the macrokinetics for a given application. The corresponding quantitative structure-property relationships (equations) have been highlighted (grey-shaded). In the last column, those parameters which are subject to synthetical control for npAu are marked with “✓”, while those which are invariant but material-specifically well-defined are marked with “x”.

---

In accord with commonly applied approaches to activate freshly-prepared catalysts, high temperature treatments were tested to efficiently remove such impurities for the first time. Taking into account that npAu is prone to thermally induced coarsening of its pore structure already at moderate temperatures, only short annealing steps were applied. In accord with the decomposition temperature of likely species, poisoning or blocking the surface, a temperature of 300 °C turned out to be sufficient. In this way, samples identically prepared but originally showing a quite different and erratic catalytic behaviour indeed could be reliably activated so that they afterwards showed basically identical catalytic activities for CO oxidation. With these results published in [publication I](#), the first goal of this thesis could be achieved and demonstrated that npAu's well-defined porosity indeed is likely to lay the foundation for predictable catalytic properties according to **FoM (1)**.

As far as the transport properties are concerned, Table 1 shows that to this end information about the constrictivity and tortuosity of the pore system is needed. While it was demonstrated in this thesis that for npAu the former can be estimated on the basis of the characteristic pore size distribution and its halfwidth, the latter was unknown. Therefore, PFG NMR, allowing to directly measure diffusion processes not only in the bulk gas phase but also in confined pore systems, was used in collaboration with an external partner to evaluate...

[... whether PFG NMR can be applied to npAu to evaluate the tortuosity of its pore system.](#)

The results, published in [publication II](#), indeed revealed that also porous metals, not studied before, can be characterized with this technique. Achieving in this way the second goal of this thesis, the tortuosity of npAu was successfully determined and the diffusive mass transport quantitatively described, showing that predictions also along **FoM (3)** can be made for this material.

In conjunction with the specific surface area (**FoM (1)**) which, thanks to its homogeneous porosity, can be easily calculated for npAu from structural data as well, in essence, it could be demonstrated that, indeed, all three catalytically relevant FoMs are assessable and that, on this basis, the obtainable catalytic conversion under given reaction conditions can be forecasted and optimized [26].

From a more general perspective, this thesis illustrated at the example of a nanoporous material that preparation techniques discovered or developed in other areas than heterogeneous catalysis indeed can open novel and potent pathways to catalysts with predictable properties. In case of nanoparticles, representing, so to speak, the structurally inverse situation and playing an important applied role in form of supported catalysts, an analogous strategy can be followed by taking advantage of colloidal chemistry (see Introduction). Within the working group, the present work was performed in, such an approach was successfully applied in case of CO oxidation over Pt NPs deposited on alumina - just to name one example [61].

In any event, practical drawbacks of such non-classical preparation techniques are the typically much higher experimental effort and the limitation to relatively small sample batches. For small-scale applications, such as micro reactors or catalytic membranes, actuators and sensors, for instance (see ref. [7, 62, 63] or corresponding applications in case of npAu), for which only small amounts are factually needed, these restrictions, however, might not represent a problem so that the advantage of advanced structuring options preponderates. If furthermore embracing the capabilities of novel instrumental methods, in particular PFG NMR, to study the diffusive mass transport properties within porous matter – a subject that virtually was not assessable experimentally in the past – truly new perspectives emerge in the area of heterogeneous catalysis. Some of these have been highlighted in [publication III](#). Foremost and as sketched in the concluding figure 7, in this way a description of catalytic

processes within an integrated picture becomes possible, linking all relevant scales - from the atomic to the macroscopic level.

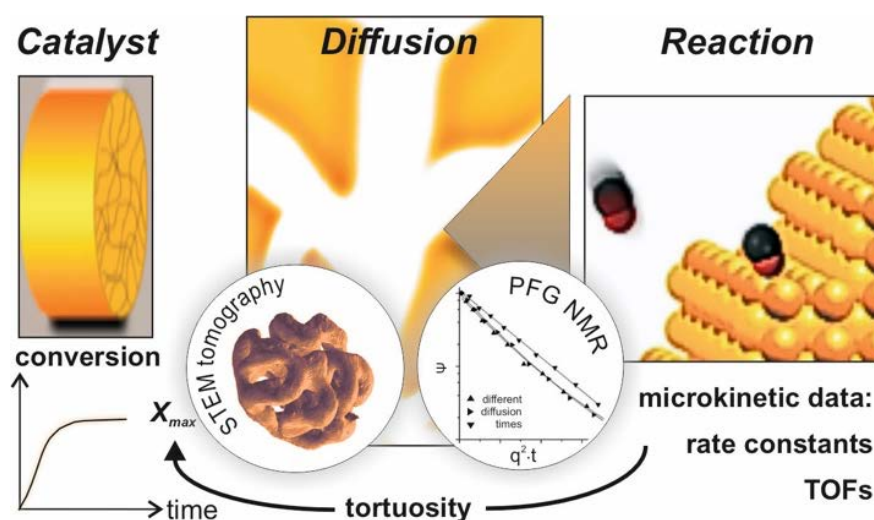


**Figure 7:** Making npAu a predictable catalyst: the well-defined and uniform pore structure of the material reflected on all length scales allows describing and linking the performance of the catalytically relevant processes which take place on the micro- (reaction), meso- (diffusion) and macroscopic (conversion) level. A central quantity needed to this end is the tortuosity of the pore system, which can be determined by PFG NMR (and verified by STEM tomography). On these grounds, the mass transport properties of npAu were quantitatively assessable so that, in a first step, the microkinetic rate constant for low-temperature CO oxidation could be accurately evaluated. Having quantitative knowledge about reaction and diffusion, it was possible in a second step to make predictions about the conversion achievable under practical conditions within the self-contained scheme sketched here. Figure reproduced from [publication III](#).

## VII. References

1. Deutschmann O, Knözinger H, Kochloefl K, Turek T (2009) Heterogeneous Catalysis and Solid Catalysts. In: Ullmann's Encyclopedia of Industrial Chemistry
2. Ertl G, Knözinger H, Weitkamp J (2008) Handbook of Heterogeneous Catalysis. Wiley-VCH Verlag GmbH
3. Kalz KF, Kraehnert R, Dvoyashkin M, et al (2017) Future Challenges in Heterogeneous Catalysis: Understanding Catalysts under Dynamic Reaction Conditions. ChemCatChem 9:17–29. <https://doi.org/10.1002/cctc.201600996>
4. Chowdhury AH, Salam N, Debnath R, et al (2019) Design and fabrication of porous nanostructures and their applications
5. Sonström P, Bäumer M (2011) Supported colloidal nanoparticles in heterogeneous gas phase catalysis: On the way to tailored catalysts. Phys Chem Chem Phys 13:19270–19284. <https://doi.org/10.1039/c1cp22048a>
6. Wu L, Li Y, Fu Z, Su BL (2020) Hierarchically structured porous materials: Synthesis strategies and applications in energy storage. Natl Sci Rev 7:1667–1701. <https://doi.org/10.1093/nsr/nwaa183>
7. Wittstock A, Biener J, Bäumer M (2010) Nanoporous gold: a new material for catalytic and sensor applications. Phys Chem Chem Phys 12:12919–12930. <https://doi.org/10.1039/c0cp00757a>
8. Wittstock G, Bäumer M, Dononelli W, et al (2023) Nanoporous Gold: From Structure

- 
- Evolution to Functional Properties in Catalysis and Electrochemistry. *Chem Rev* 123:6716–6792. <https://doi.org/10.1021/acs.chemrev.2c00751>
9. A.J.Forty (1979) Corrosion micromorphology of noble metal alloys and depletion gilding. *Nature* 282:597–598
  10. Wittstock A, Biener J, Erlebacher J, Bäumer M (2012) Nanoporous Gold: From an Ancient Technology to a High-Tech Material. Royal Society of Chemistry, Cambridge
  11. Zielasek V, Jürgens B, Schulz C, et al (2006) Gold catalysts: Nanoporous gold foams. *Angew Chemie - Int Ed* 45:8241–8244. <https://doi.org/10.1002/anie.200602484>
  12. Xu C, Su J, Xu X, et al (2007) Low temperature CO oxidation over unsupported nanoporous gold. *J Am Chem Soc* 129:42–43. <https://doi.org/10.1021/ja0675503>
  13. Lee JD, Miller JB, Shneidman A V., et al (2021) Dilute Alloys Based on Au, Ag, or Cu for Efficient Catalysis: From Synthesis to Active Sites. *Chem Rev*. <https://doi.org/10.1021/acs.chemrev.1c00967>
  14. Hutchings GJ (1985) Vapor phase hydrochlorination of acetylene: Correlation of catalytic activity of supported metal chloride catalysts. *J Catal* 96:292–295. [https://doi.org/10.1016/0021-9517\(85\)90383-5](https://doi.org/10.1016/0021-9517(85)90383-5)
  15. Haruta M, Kobayashi T, Sano H, Yamada N (1987) Novel Gold Catalysts for the Oxidation of Carbon Monoxide at a Temperature far Below 0 °C. *Chem Lett* 16:405–408. <https://doi.org/10.1246/cl.1987.405>
  16. Jürgens B, Kübel C, Schulz C, et al (2007) New gold and silver-gold catalysts in the shape of sponges and sieves. *Gold Bull* 40:142–149. <https://doi.org/10.1007/BF03215571>
  17. Lai SY, Qiu Y, Wang S (2006) Effects of the structure of ceria on the activity of gold/ceria catalysts for the oxidation of carbon monoxide and benzene. *J Catal* 237:303–313. <https://doi.org/10.1016/j.jcat.2005.11.020>
  18. Comotti M, Li WC, Spliethoff B, Schuth F (2006) Support effect in high activity gold catalysts for CO oxidation. *J Am Chem Soc* 128:917–924. <https://doi.org/10.1021/ja0561441>
  19. Jeon H, Kang NR, Gwak EJ, et al (2017) Self-similarity in the structure of coarsened nanoporous gold. *Scr Mater* 137:46–49. <https://doi.org/10.1016/j.scriptamat.2017.05.009>
  20. Graf M, Roschning B, Weissmüller J (2017) Nanoporous Gold by Alloy Corrosion: Method-Structure-Property Relationships. *J Electrochem Soc* 164:C194–C200. <https://doi.org/10.1149/2.1681704jes>
  21. Lackmann A, Bäumer M, Wittstock G, Wittstock A (2018) Independent control over residual silver content of nanoporous gold by galvanodynamically controlled dealloying. *Nanoscale* 10:17166–17173. <https://doi.org/10.1039/c8nr03699c>
  22. Wild S, Bäumer M, Risse T (2022) Thermal Activation of Nanoporous Gold for Carbon Monoxide Oxidation. *J Phys Chem C* 126:1770–1777. <https://doi.org/10.1021/acs.jpcc.1c08222>
  23. Baniani A, Wild S, Forman EM, et al (2022) Disentangling catalysis and mass transport: Using diffusion measurements by pulsed field gradient NMR to reveal the microkinetics of CO oxidation over nanoporous gold. *J Catal* 413:1123–1131. <https://doi.org/10.1016/j.jcat.2022.08.020>
  24. Kärger J, Ruthven DM, Theodorou DN (2012) Diffusion in Nanoporous Materials. Wiley-VCH Verlag GmbH & Co. KGaA., Weinheim
  25. Detsi E, De Jong E, Zinchenko A, et al (2011) On the specific surface area of nanoporous materials. *Acta Mater* 59:7488–7497.

- 
- <https://doi.org/10.1016/j.actamat.2011.08.025>
26. Wild S, Mahr C, Rosenauer A, et al (2022) New Perspectives for Evaluating the Mass Transport in Porous Catalysts and Unfolding Macro- and Microkinetics. *Catal Letters*. <https://doi.org/10.1007/s10562-022-04218-6>
  27. Adkins H, Billica HR (1948) The Preparation of Raney Nickel Catalysts and their Use Under Conditions Comparable with Those for Platinum and Palladium Catalysts. *J Am Chem Soc* 70:695–698. <https://doi.org/10.1021/ja01182a080>
  28. Tse AY, Karasz EK, Sieradzki K (2020) Dealloying and morphology evolution of ordered and disordered Cu<sub>3</sub>Au. *Scr Mater* 176:112–116. <https://doi.org/10.1016/j.scriptamat.2019.09.008>
  29. Martínez LL, Segarra M, Fernández M, Espiell F (1993) Kinetics of the dissolution of pure silver and silver-gold alloys in nitric acid solution. *Metall Trans B* 24:827–837. <https://doi.org/10.1007/BF02663143>
  30. Erlebacher J, Aziz MJ, Karma A, et al (2001) Evolution of nanoporosity in dealloying. *Nature* 410:450–453. <https://doi.org/10.1038/35068529>
  31. McCue I, Stuckner J, Murayama M, Demkowicz MJ (2018) Gaining new insights into nanoporous gold by mining and analysis of published images. *Sci Rep* 8:1–11. <https://doi.org/10.1038/s41598-018-25122-3>
  32. Li Z, Zhuo S, Li H, et al (2009) Determination of ligament size distribution of nanoporous gold by scanning electron microscopy and image analysis. *J Nanosci Nanotechnol* 9:1651–1654. <https://doi.org/10.1166/jnn.2009.C224>
  33. Wittstock A, Wichmann A, Bäumer M (2012) Nanoporous gold as a platform for a building block catalyst. *ACS Catal* 2:2199–2215. <https://doi.org/10.1021/cs300231u>
  34. Chen-Wiegart YCK, Wang S, Chu YS, et al (2012) Structural evolution of nanoporous gold during thermal coarsening. *Acta Mater* 60:4972–4981. <https://doi.org/10.1016/j.actamat.2012.05.012>
  35. Xu C, Su J, Xu X, et al (2007) Low temperature CO oxidation over unsupported nanoporous gold. *J Am Chem Soc* 129:42–43. <https://doi.org/10.1021/ja0675503>
  36. Viswanath RN, Chirayath VA, Rajaraman R, et al (2013) Ligament coarsening in nanoporous gold: Insights from positron annihilation study. *Appl Phys Lett* 102:. <https://doi.org/10.1063/1.4812290>
  37. Mahr C (2018) Charakterisierungen der Struktur und der chemischen Zusammensetzung von nanoporösem Gold mittels Transmissionselektronenmikroskopie. *Mensch & Buch*
  38. Hodge AM, Biener J, Hayes JR, et al (2007) Scaling equation for yield strength of nanoporous open-cell foams. *Acta Mater* 55:1343–1349. <https://doi.org/10.1016/j.actamat.2006.09.038>
  39. Chorkendorff I, Niemantsverdriet JW (2003) Concepts of Modern Catalysis and Kinetics. Wiley-VCH Verlag GmbH & Co. KGaA
  40. Dumesic JA, Huber GW, Boudart M (2008) Principles of Heterogeneous Catalysis. *Handb Heterog Catal*. <https://doi.org/10.1002/9783527610044.hetcat0001>
  41. Bäumer M, Freund HJ (1999) Metal deposits on well-ordered oxide films. *Prog Surf Sci* 61:127–198. [https://doi.org/10.1016/S0079-6816\(99\)00012-X](https://doi.org/10.1016/S0079-6816(99)00012-X)
  42. Ertl G (2008) Reactions at surfaces: From atoms to complexity (nobel lecture). *Angew Chemie - Int Ed* 47:3524–3535. <https://doi.org/10.1002/anie.200800480>
  43. Jones TE, Wyrwich R, Böcklein S, et al (2018) The Selective Species in Ethylene Epoxidation on Silver. *ACS Catal* 8:3844–3852. <https://doi.org/10.1021/acscatal.8b00660>



- 
44. Ruban A V., Skriver HL, Nørskov JK (1999) Surface segregation energies in transition-metal alloys. *Phys Rev B - Condens Matter Mater Phys* 59:15990–16000. <https://doi.org/10.1103/PhysRevB.59.15990>
  45. Thomas JM, Thomas WJ (2014) *Principles and Practice of Heterogeneous Catalysis*. Wiley-VCH, Weinheim
  46. Yim WL, Nowitzki T, Necke M, et al (2007) Universal phenomena of CO adsorption on gold surfaces with low-coordinated sites. *J Phys Chem C* 111:445–451. <https://doi.org/10.1021/jp0665729>
  47. Lackmann A, Mahr C, Schowalter M, et al (2017) A comparative study of alcohol oxidation over nanoporous gold in gas and liquid phase. *J Catal* 353:99–106. <https://doi.org/10.1016/j.jcat.2017.07.008>
  48. Wittstock A, Wichmann A, Biener J, Bäumer M (2011) Nanoporous gold: a new gold catalyst with tunable properties. *Faraday Discuss* 152:87–98. <https://doi.org/10.1039/c1fd00022e>
  49. Schaefer A, Ragazzon D, Wittstock A, et al (2012) Toward controlled modification of nanoporous gold. A detailed surface science study on cleaning and oxidation. *J Phys Chem C* 116:4564–4571. <https://doi.org/10.1021/jp207638t>
  50. Personick ML, Zugic B, Biener MM, et al (2015) Ozone-Activated Nanoporous Gold: A Stable and Storable Material for Catalytic Oxidation. *ACS Catal* 5:4237–4241. <https://doi.org/10.1021/acscatal.5b00330>
  51. Petersen EE (1958) Diffusion in a pore of varying cross section. *AIChE J* 4:343–345. <https://doi.org/10.1002/aic.690040322>
  52. Mahr C, Dworzak A, Schowalter M, et al (2021) Quantitative 3D Characterization of Nanoporous Gold Nanoparticles by Transmission Electron Microscopy. *Microsc Microanal* 27:678–686. <https://doi.org/10.1017/S1431927621000519>
  53. Thiele EW (1939) Relation between Catalytic Activity and Size of Particle. *Ind Eng Chem* 31:916–920. <https://doi.org/10.1021/ie50355a027>
  54. Fogler HS (2021) *Elements of Chemical Reaction Engineering*. Ser Phys Chem Eng Sci 719–766
  55. Campbell CT (1994) Future Directions and Industrial Perspectives Micro- and macro-kinetics: Their relationship in heterogeneous catalysis. *Top Catal* 1:353–366. <https://doi.org/10.1007/BF01492288>
  56. Mears DE (1971) Tests for Transport Limitations in Experimental Catalytic Reactors. *Ind Eng Chem Process Des Dev* 10:541–547. <https://doi.org/10.1021/i260040a020>
  57. Thompson D (1998) New advances in gold catalysis part I. *Gold Bull* 31:111–118. <https://doi.org/10.1007/BF03214775>
  58. Grisel R, Weststrate KJ, Gluhoi A, Nieuwenhuys BE (2002) Catalysis by gold nanoparticles. *Gold Bull* 35:39–45. <https://doi.org/10.1007/BF03214836>
  59. Wittstock A, Neumann B, Schaefer A, et al (2009) Nanoporous Au: An unsupported pure gold catalyst? *J Phys Chem C* 113:5593–5600. <https://doi.org/10.1021/jp808185v>
  60. Wittstock A, Zielasek V, Biener J, et al (2010) Nanoporous gold catalysts for selective gas-phase oxidative coupling of methanol at low temperature. *Science (80- )* 327:319–322. <https://doi.org/10.1126/science.1183591>
  61. Neumann S, Gutmann T, Buntkowsky G, et al (2019) Insights into the reaction mechanism and particle size effects of CO oxidation over supported Pt nanoparticle catalysts. *J Catal* 377:662–672. <https://doi.org/10.1016/j.jcat.2019.07.049>
  62. Biener J, Wittstock A, Zepeda-Ruiz LA, et al (2009) Surface-chemistry-driven actuation in nanoporous gold. *Nat Mater* 8:47–51. <https://doi.org/10.1038/nmat2335>

- 
63. Ruffino F, Grimaldi MG (2020) Nanoporous gold-based sensing. *Coatings* 10:.  
<https://doi.org/10.3390/COATINGS10090899>
  64. Marqusee JA, Ross J (1983) Kinetics of phase transitions: Theory of Ostwald ripening. *J Chem Phys* 79:373–378. <https://doi.org/10.1063/1.445532>

## **PUBLICATION I**

**Thermal Activation of Nanoporous Gold for Carbon Monoxide Oxidation**

**Stefan Wild**, Thomas Risse and Marcus Bäumer

*The Journal of Physical Chemistry C* **2022**, *126* (4), 1770–1777.

<https://doi.org/10.1021/acs.jpcc.1c08222>

## **PUBLICATION II**

**Disentangling catalysis and mass transport:  
Using diffusion measurements by pulsed field gradient NMR  
to reveal the microkinetics of CO oxidation over nanoporous gold**

Amineh Baniani\*, **Stefan Wild\***, Evan M. Forman,  
Thomas Risse, Sergey Vasenkov and Marcus Bäumer

(\* Shared first co-authorship)

*Journal of Catalysis* **2022**, *413*, 1123 – 1131.

<https://doi.org/10.1016/j.jcat.2022.08.020>



# Disentangling catalysis and mass transport: Using diffusion measurements by pulsed field gradient NMR to reveal the microkinetics of CO oxidation over nanoporous gold



Amineh Baniani<sup>a,1</sup>, Stefan Wild<sup>b,c,1</sup>, Evan M. Forman<sup>a</sup>, Thomas Risse<sup>d</sup>, Sergey Vasenkov<sup>a</sup>, Marcus Bäumer<sup>b,c,\*</sup>

<sup>a</sup> Department of Chemical Engineering, University of Florida, Gainesville, FL 32611, USA

<sup>b</sup> Institute for Applied and Physical Chemistry, University of Bremen, 28359 Bremen, Germany

<sup>c</sup> MAPEX Center of Materials and Processes, University of Bremen, 28359 Bremen, Germany

<sup>d</sup> Institute of Chemistry and Biochemistry, Free University Berlin, 14195 Berlin, Germany

## ARTICLE INFO

### Article history:

Received 24 June 2022

Revised 12 August 2022

Accepted 16 August 2022

Available online 19 August 2022

### Keywords:

Nanoporous metals

Au catalysts

Diffusive mass transport

Low temperature CO oxidation

Macrokinetics

Microkinetics

PFG NMR

## ABSTRACT

Since the first studies reporting on its surprising catalytic properties, nanoporous gold (npAu) has emerged as a novel and ever since intensively investigated type of Au based catalyst. To judge its genuine catalytic potential and to be able to optimize its use in applications, it is mandatory, however, to quantify the influence of mass transport in the porous structure on the observed catalytic rates, i.e., to study the interplay between diffusion and reaction. To this end, we used pulsed field gradient (PFG) NMR for the first time to directly determine the diffusivities of reaction gases in a nanoporous metal – in this case for CO and CO<sub>2</sub> as species involved in low temperature CO oxidation efficiently catalyzed by npAu. By comparing the diffusion coefficients within the 20 nm pores of the material with the values in the bulk gas phase, the tortuosity of npAu's pore system was assessable as the central geometrical parameter describing the extent to which diffusive transport in the pore system is slowed down. This knowledge allowed us in the following to disentangle the contributions of mass transport and the kinetics of the surface reaction (microkinetics). In particular, we were able to determine the rate constant and turnover frequency for low-temperature CO oxidation without previous ambiguities arising from potential transport limitations and to compare the results with other reported values. Based on the results, it was furthermore possible to predict optimized dimensions of the catalyst, resulting in minimized or even suppressed diffusion limitations. These predictions could be successfully verified, using np-Au platelets with lateral dimensions in the range of a few hundred microns. In this way, the catalytic conversion could be ramped up by 50 % and an activity level advanced which reflected the microkinetic potential of np-Au.

© 2022 The Authors. Published by Elsevier Inc. This is an open access article under the CC BY-NC-ND license (<http://creativecommons.org/licenses/by-nc-nd/4.0/>).

## 1. Introduction

Nanoporous gold emerged in 2006 as a new type of Au catalyst not known before and being structurally distinct from supported Au catalysts which had been in the focus of research before [1,2]. The material, representing, like Raney nickel, a skeletal metal catalyst, is obtained as the result of a corrosive dealloying process, during which a less noble sacrificial metal – usually silver – is leached out of an alloy with Au chemically or electrochemically [3]. Already in the first studies dealing with the oxidation of CO, npAu had been found to efficiently catalyze aerobic oxidation reactions

at room temperature and even below [1,2]. Later, also npAu's ability to catalyze partial oxidation reactions with high selectivity was exemplified for methanol oxidation to methylformate [4].

In the case of Au nanoparticles (NP), typically only a narrow range of particle sizes around a few nm shows catalytic activity for which also the type of oxide used as a support plays a decisive role [5]. In contrast, npAu exhibits pores and ligaments, i.e., structural features, which are about an order of magnitude larger (typically 20–50 nm) than their nanoparticulate counterparts [6]. The high activity and selectivity of this seemingly pure Au catalyst attracted considerable attention and led to many research activities which ever since have documented npAu's catalytic potential for a variety of reactions in gas as well as in liquid phase [3,7,8]. Even though it meanwhile turned out that the notion of npAu being a pure Au catalyst is wrong and residues of the sacrificial

\* Corresponding author.

E-mail address: [mbaeumer@uni-bremen.de](mailto:mbaeumer@uni-bremen.de) (M. Bäumer).

<sup>1</sup> These authors contributed equally to the work.

metal (such as Ag) have been identified to play an important part as well [9,10], the material holds great promises in particular as an oxidation catalyst, performing already at temperatures where Pt and other established metals not yet work.

Two factors, though, hampered a concluding judgement of npAu's catalytic potential – also in view of technical applications – and a well-founded comparison with other types of Au catalysts so far. The first one relates to its activation. Taking CO oxidation as an example of a frequently studied reaction in the area of Au catalysis, the synopsis of previous work suggests that npAu not always displays activity directly after preparation, but rather evolves it slowly over time [11–13]. For this total oxidation reaction, we recently found that short-term annealing treatments to 300 °C in the reaction gas mixture provide a reliable means to reach high catalytic activity quickly and reproducibly, while retaining the surface area of the porous structure [14]. Yet, for the wealth of reactions catalyzed by npAu the microscopic details of the underlying active surface states still are a matter of intense research and thus are robust procedures of evoking them [8]. The other factor not sufficiently clarified up to now relates to the quantitative assessment of mass transport limitations, resulting from npAu's pore structure. Such knowledge not only is necessary for an unambiguous evaluation of npAu's intrinsic catalytic capabilities (in terms of TOFs, i.e., turnover frequencies, for instance), but also constitutes a prerequisite for reducing such contributions and thus optimizing the catalytic productivity in any kind of application.

It was early speculated that npAu's ubiquitous mesoporosity could indeed pose a serious impediment for exploiting the full catalytic potential of npAu [12]. In particular, in case of larger monoliths, being the typical kind of specimen obtained by established protocols for preparing npAu by dealloying, the lack of larger macropores, which have an ability of facilitating the mass transport into deeper sections of the material, could render major parts of the material catalytically unused. In fact, preliminary studies on low temperature CO oxidation suggested that under unfavorable conditions as far as the tortuosity and the connection of the pores is concerned a severe productivity cut-off is not unlikely, which would make large scale applications unattractive in view of Au's high market prices [12,15]. Precise assessments, however, were baffled due to lacking precise quantitative knowledge about npAu's transport properties.

Dealing with mass transport in porous matter where molecular confinement plays a decisive role, two factors have to be taken into account, altering and limiting the diffusive transport as compared to the bulk gas phase [16]. On the one hand, molecular diffusion turns into Knudsen diffusion when the mean free path of the molecules exceeds the pore diameters so that collisions with their walls become more likely than intermolecular collisions. This aspect is less of a problem, as diffusion constants in the Knudsen regime can be derived on the basis of (mean) pore diameters as obtainable e.g. from SEM micrographs [17]. Even when both mechanisms – Knudsen and molecular – contribute, the resulting transition regime can be accounted for by reverting to the so-called Bosanquet equation ( $1/D_T = 1/D_{\text{molecular}} + 1/D_{\text{Knudsen}} = 1/D_M + 1/D_K$ ) [17]. The second factor, however, is material specific and not assessable on the basis of general principles. It results from the elongation of the diffusive pathways enforced by the particular pore system under consideration [18]. A parameter that was introduced to integrally characterize this structurally caused impact is the so-called tortuosity factor  $\tau$  [16]. It needs to be experimentally determined either on the basis of structural information or measurements of the gas diffusivities within the material [19,20].

Embarking on the latter strategy, we took advantage of pulsed field gradient (PFG) NMR and its far-reaching capabilities to study diffusion of gases not only in the bulk phase but also in porous materials to get quantitative insight into the transport properties

of npAu [21]. In case of micro- and mesoporous oxides the method has already contributed tremendously to our understanding of diffusive transport in porous matter [16,18]. Notably, PFG NMR and NMR relaxometry have also been applied successfully to study diffusion and dynamics in supported metal and also supported gold catalysts [22–24]. Porous metals, such as npAu, however, have not been the subject of corresponding experiments so far – perhaps because of concerns that eddy currents induced in the metallic framework could prevent meaningful experiments by PFG NMR. Herein, we show the applicability of the technique also for this class of systems by determining the diffusivities of CO and CO<sub>2</sub>, i.e., the educt and the product of CO oxidation, in the pore system of npAu.

Deriving diffusivities from such data of course requires short contact times of the investigated molecules with the pore walls. In other words, the corresponding residence times on the surface have to be sufficiently short as compared to the time scale of the experiment to assure that the results not only cover a fraction of the diffusing gas ensemble [20,24]. Since CO oxidation is known to follow a Langmuir-Hinshelwood mechanism [25], the educts and products, however, must be trapped on the surface at least for some time so that this question clearly is of relevance in the present case and needs to be addressed beforehand. In this context, experimental knowledge about the adsorption properties of the involved gases on Au surfaces provides a basis to dispel corresponding concerns.

In case of CO, for example, temperature programmed desorption (TPD) experiments carried out under UHV conditions revealed desorption temperatures, ranging from 120 K to ~220 K for npAu [26]. These values indicate binding energies between ~0.4 and 0.6 eV (assuming a typical preexponential factor of  $10^{13} \text{ s}^{-1}$ ) – in contrast to flat defect-free Au(111) surfaces, where the molecule is known to be much weaker bound (~0.3 eV) [27]. It was thus concluded and also corroborated by theoretical calculations that the higher binding energies belong to defect sites, which were found to make up a share of 20 % of npAu's surface atoms [28] and to act as primary adsorption (and probably reaction) sites for CO on this catalyst [29]. In spite of this comparatively high number, only chemisorption on those surface sites exhibiting the highest binding energies will lead to residence times that come close to the studied diffusion times (6–30 ms). Their fraction, however, is low enough to ensure that the number of CO molecules trapped there on their diffusive pathway inside the material is sufficiently small. In accord, for CH<sub>4</sub>, included in our study as an inert molecule which neither chemisorbs nor reacts on Au surfaces, very similar results were obtained by PFG NMR.

CO<sub>2</sub> as the product, is known to exhibit low binding energies on Au as well [30] so that it desorbs from the surface once it is formed. Accordingly, its diffusive transport out of the pores into the bulk gas phase is not likely to mitigate the catalytic conversion. This conclusion also holds true for O<sub>2</sub>, i.e., the other reactant of CO oxidation. Here, previous kinetic studies revealed reaction orders close to zero [12,31], implying that, in contrast to CO, where reaction orders close to 1 were typically found, the supply of oxygen at the surface represents no limiting factor for the kinetics and thus for the mass transport in case of CO oxidation over npAu.

Based on the PFG NMR results obtained for the studied gases, we were therefore in the position to determine the tortuosity factor of npAu's pore structure for the first time experimentally, revealing that the resistance posed for diffusive transport is less pronounced than previously assumed [12]. This knowledge allowed in a second step to determine the effective diffusion coefficient of CO within the material, as the kinetically governing reactant for its catalytic conversion to CO<sub>2</sub> at 30 °C and under ambient pressure. By employing the Thiele modulus concept as an established formalism in chemical engineering to evaluate catalyst effi-

ciencies (macrokinetics) [32], resulting from the interplay of catalytic turnover at the surface (microkinetics) and diffusive mass transport, it was possible to disentangle the macro- and microkinetics for this reaction. To make sure that the data revealed in this way reflect the catalytically most active state of the surface, we took advantage of an activation procedure, for which we recently showed that it ensures achieving maximal CO conversion levels for npAu [14].

The quantitative knowledge about the transport properties, on the one hand, and the microkinetics of the surface reaction under consideration, on the other hand, lays the foundation for strategies aiming at optimizing the productivity in any kind of catalytic application. When the structure of the pore system itself cannot easily be adjusted to minimize mass transport limitations, changing the shape and size of the catalyst can provide an alternative option in this respect. In a first attempt to exemplify this approach, we compared larger monolithic npAu discs - as a sample type often employed in the past - with smaller platelets which exhibited the same thickness (200  $\mu\text{m}$ ) but diameters that were an order of magnitude smaller (a few 100  $\mu\text{m}$  as compared to a few mm). The conversion gain achieved in this way quantitatively reflected the prediction made on the basis of npAu's experimentally determined tortuosity and the microkinetics, thus confirming the consistency of the data set.

## 2. Experimental

### 2.1. Preparation of npAu samples

Nanoporous gold was prepared by leaching silver out of an AgAu alloy in conc.  $\text{HNO}_3$  - a dealloying process called "free corrosion". The AgAu starting alloy was fabricated by alloying gold (Chempur, 99.999 %) and silver (Chempur, 99.99 %) in a ratio of  $30.00 \pm 0.03$  at% Au and  $70.00 \pm 0.03$  at% Ag at 1100  $^\circ\text{C}$  for 30 min (initial heating rate: 0.2  $^\circ\text{C}/\text{s}$ ) in a boron nitride crucible (Situs, purity: 99.9 %). The resulting alloy was subsequently cooled down to room temperature (0.2  $^\circ\text{C}/\text{s}$ ) and traces of boric acid deposited on the surface of the obtained ingots were removed with 1 M citric acid (Sigma-Aldrich, 99.5 %) at 50  $^\circ\text{C}$  for 30 min. Before further processing, the material was homogenized at 875  $^\circ\text{C}$  in a tube furnace under an argon atmosphere (Linde, 99.999 %, flow: 20 sccm) for 120 h.

To obtain suitable specimen for the PFG NMR and the catalytic experiments, thin sheets of the starting alloy were prepared by using an adjustable roller and applying several cold rolling steps. In each step the reduction of thickness was limited to 20 % to minimize the associated mechanical stress which was subsequently dissipated by annealing the material in a furnace at 400  $^\circ\text{C}$  for 15 min. After 5–6 passes, alloy sheets with a nominal thickness of  $\sim 200$   $\mu\text{m}$  were finally obtained. For the PFG NMR measurements discs of about 3 mm were punched out of such sheets, whereas the disc diameters amounted to 5 mm in case of the catalytic investigations.

For dealloying, the samples were put on a porous (250–500  $\mu\text{m}$ ) borosilicate disc, which, in turn, was placed in a 100 ml beaker. Subsequently, the specimen were immersed in 50.0 ml conc.  $\text{HNO}_3$  (Merck,  $\geq 65\%$ , p.a.) for 18–24 h and then washed three consecutive times for 1 min with 100 ml deionised water. Overall, the preparation followed established protocols, as for example described in Ref. [14], yielding a mean ligament diameter of  $\langle d_l \rangle = 18 \text{ nm} \pm 4.2 \text{ nm}$  in the present case (as determined by a careful Fourier analysis of acquired SEM micrographs).

To break up the monolithic npAu discs into entities with smaller lateral dimensions, we developed a mechanical method based on shaking them in a closed glass vial for several min. To this end,

we took advantage of the grain microstructure of the polycrystalline material and its propensity to show predominant fracture at associated grain boundaries. The platelets obtained in this way exhibited a thickness identical with the former discs (200  $\mu\text{m}$ ) but were broken down to lateral dimensions being an order of magnitude smaller than the previous disc diameters (a few 100  $\mu\text{m}$  vs. a few mm). Since the grain structure and thus particle sizes assessable by this strategy are determined by the cold rolling process and the intermittent annealing steps, they are susceptible to manipulation, bearing the opportunity to tune their mean size and to optimize the size distribution. Exploring this potential, however, was beyond the scope of the present study. In any event, it entails the advantage of not damaging the porosity - in contrast to previously described methods in the literature that were based, e.g., on piercing and disrupting samples with a needle or a pincer [33].

### 2.2. PFG NMR measurements

The npAu gold discs prepared for the NMR measurements were stacked on top of each other inside a 5 mm (medium walled) NMR tube (Wilma Labglass, Inc.), reaching a height of  $28 \pm 3$  mm. The tube was attached to a custom-made vacuum system and exposed to high vacuum at room temperature overnight, enabling the removal of any sorbates present in the sample. Subsequently, sorbate loadings were performed. The sorbates used for this study were  $^{13}\text{C}$ -enriched carbon monoxide (CO) exhibiting 99 % isotopic purity (Sigma-Aldrich),  $^{13}\text{C}$ -enriched methane ( $\text{CH}_4$ ) with 99 % isotopic purity (Sigma-Aldrich), and  $^{13}\text{C}$ -enriched carbon dioxide ( $\text{CO}_2$ ) with 99 % isotopic purity (Sigma-Aldrich). A known mass of the  $^{13}\text{C}$ -labelled sorbate was transferred cryogenically into the NMR tubes containing the nanoporous gold particles. Upon the sorbate loadings were accomplished, the tubes were flame-sealed. The sorbate loadings in each sample were checked in the same way as discussed in Ref. [34]. In all cases a pressure of 15 bar corresponding to gas loadings of  $0.11 \pm 0.02$  mmol/g(npAu) was used. For  $\text{CO}_2$ , in addition, a lower loading was prepared and measured to confirm that the tortuosity factor of npAu derived from the PFG NMR data does not depend on the sorbate concentration (see SI).

PFG NMR diffusion measurements and NMR relaxation measurements were subsequently performed with a 17.6 T Avance III HD spectrometer (Bruker Biospin), operating at a resonance frequency of 188.6 MHz for  $^{13}\text{C}$ . For methane, additional PFG NMR diffusion measurements and NMR relaxation measurements were carried out at a proton resonance frequency of 750 MHz, using the same spectrometer. Sine-shaped, bipolar magnetic field gradients with an effective duration of 0.15 ms and amplitudes up to 5 T/m were generated, using a DIFF50 diffusion probe (Bruker BioSpin). For the diffusion measurements, the 13-interval PFG NMR pulse sequence with bipolar gradients was employed [35], modified by the addition of a longitudinal eddy current delay of about 5 ms. Longitudinal ( $T_1$ ) and transverse ( $T_2$ ) relaxation times were measured, using standard inversion recovery and Carr-Purcell-Meiboom-Gill (CPMG) pulse sequences, respectively. The delay time in the CPMG sequence was equal to 100  $\mu\text{s}$ . All NMR measurements reported in this work were performed at 23  $^\circ\text{C}$ .

Gas diffusivities were obtained from the measured PFG NMR attenuation curves, i.e., dependences of the PFG NMR signal intensity on the effective magnetic field gradient strength, with all other pulse sequence parameters held fixed. The PFG NMR signal intensities were derived by integration of the corresponding NMR spectra (see SI). Under our measurement conditions, the  $^{13}\text{C}$  NMR spectra of CO,  $\text{CH}_4$ , and  $\text{CO}_2$  consisted of just a single line at around 184,  $-10.6$ , and 126 ppm, respectively, and the  $^1\text{H}$  NMR spectra recorded for  $\text{CH}_4$  of a single line at around 2.6 ppm. In more detail, the data evaluation is described in the SI.

### 2.3. Catalytic measurements

The npAu discs employed in the catalytic measurements were placed in a quartz tube reactor (8 mm inner diameter) by sandwiching them in the middle of the tube between 4 cm quartz sand (Roth, grain size: 700–800  $\mu\text{m}$ , calcined at 1000  $^{\circ}\text{C}$  for 10 h) which, in turn, was held in place by quartz wool plugs (Roth, pure). The reactor was inserted in a tube furnace controlled by a Eurotherm PID device for heating. As detailed elsewhere, the reactor could be cooled down quickly on demand by injecting compressed air into the space between the reactor tube and the furnace [14].

The catalytic CO oxidation experiments were carried out, using a reaction mixture of 89.0 vol% Helium (5.0 Linde, 99.999 %), 1.0 vol% carbon monoxide (5.0 Linde, 99.999 %) and 10.0 vol% oxygen (5.0 Linde, 99.999 %), i.e., in an excess of oxygen. The composition was adjusted by mass flow controllers (GE50A, MKS instruments, back-pressure: 3.5 bar) and allowed to stabilize in a reactor bypass, before admitting it to the reactor. The total gas flow used for all experiments amounted to  $Q_{\text{T}}^{\circ} = 40$  ml/min. (Note that the gas flows regulated by the mass flow controllers and thus also the total flow refer to standard conditions: 0  $^{\circ}\text{C}$  and 1000 mbar.)

The npAu samples were catalytically activated, using an optimised version of a recently published activation protocol for CO oxidation. In this way, the reliable and reproducible achievement of high and sustainable conversion levels at 30  $^{\circ}\text{C}$  could be ensured within one hour or less [14]. To this end, the samples were quickly heated (heating ramp:  $\sim 1$   $^{\circ}\text{C}/\text{s}$ ) five consecutive times to 300  $^{\circ}\text{C}$ , holding this temperature for 90 s and subsequently cooling the reactor down to 30  $^{\circ}\text{C}$  again (cooling rate:  $\sim 0.7$   $^{\circ}\text{C}/\text{s}$ ). It was previously shown that this procedure does not affect the pore structure.

The effluent gas mixture leaving the reactor was continuously analysed by a mass spectrometer (HPR-20 QIC, Hiden Analytical) and, in parallel, by an infrared gas analyser (10E, Hartman and Braun). The MS data was quantitatively analysed, using the supplied software of the manufacturer (QGA Professional, Version 1.42i). The conversion curves measured in this way were Fourier filtered (Butterworth, normalised cut-off frequency:  $10^{-6}$ , power: 60) to reduce their noise figure. It was checked and verified that relevant details, such as temporal trends and conversion levels, were not compromised in any way.

## 3. Results & discussion

### 3.1. Evaluation of the PFG NMR diffusion measurements

PFG NMR was used to measure the diffusivities of CO and CO<sub>2</sub> in npAu, being the relevant components for the oxidation of the former to the latter ( $\text{CO} + \frac{1}{2} \text{O}_2 \rightarrow \text{CO}_2$ ) - a prototypical example of a reaction efficiently catalyzed by this material already at room temperature and below. In addition to these gases, CH<sub>4</sub> was included in the study for reference purposes. CH<sub>4</sub> molecules have a similar size than CO and CO<sub>2</sub> but, as far as adsorption and reaction on Au surfaces are concerned, CH<sub>4</sub> is expected to behave as an inert gas (see Introduction).

In a first step, the diffusivities of the bulk gases - i.e., in the absence of any npAu material in the NMR tube - were measured at a pressure of 15 bar. To this end, attenuation curves of the respective PFG NMR signals were recorded for all three gases, using diffusion times of 6 ms, 10 ms and 30 ms. As detailed in the supporting information (SI), on these grounds the molecular self-diffusion coefficients, compiled in Table 1, could be derived. Their comparison with reported experimental values obtained with other techniques under similar conditions as well as with theoretical values calculated on the basis of a refined ideal gas law description and the Chapman's and Enskog's approach reveals very

good agreement in all cases, thus confirming the necessary sensitivity and precision of our PFG NMR measurements.

To determine the diffusivities within npAu's pore system, a sufficient number of npAu samples (see Experimental) was placed in the NMR tubes so that the measurement volume was filled to the maximum possible extent. Subsequently, the tubes were filled with CO, CO<sub>2</sub> or CH<sub>4</sub>, respectively, at a pressure of 15 bar (in analogy to the experiments with the bulk gases) and then sealed. The results of the PFG NMR measurements obtained in the presence of the catalyst are presented in Fig. 1.

Except for long diffusion times (30 ms), in all cases - i.e., for all three gases - the attenuation curves recorded under these conditions clearly showed deviations from a mono-exponential decay as observed in the absence of npAu. Rather, the data could only be fitted, assuming a bi-exponential decay behavior (Eq. S3), in accord with two diffusing gas ensembles - one within the pores of the npAu specimen and one in the surrounding gas phase. The diffusivities derived for both ensembles are presented in Table 2. Within statistical uncertainty, the larger values ( $D_2$ ) reflect the diffusion coefficients measured for the bulk gases (see above) and can thus be attributed to the molecules diffusing outside the material. As the other one ( $D_1$ ) is smaller, it apparently must belong to the gas fraction diffusing inside npAu. The comparison of both values indicates that the transport within the pore system is only about half as fast as in the gas phase under identical conditions (pressure and temperature).

In the absence of strong gas-pore wall interactions (see Introduction) two factors contributing to the slower gas transport could play a role. The first one refers to onsetting Knudsen diffusion when applying pressures where the pore sizes are smaller than the mean free path of the diffusing gas molecules in the bulk gas phase. The second one results from the longer diffusion trajectories enforced by the pore system of the material specifically under consideration. For a pressure of 15 bar where the PFG NMR experiments were carried out, a calculation of the mean free path on the basis of kinetic gas theory reveals values below 10 nm for the molecules studied, i.e., values which are smaller than the typical mean pore diameters of npAu (18 nm  $\pm$  4.2 nm in case of the present study). Accordingly, a significant influence of Knudsen diffusion can be largely excluded under the applied experimental conditions, meaning that  $D_1$  is expected to mostly reflect the second factor. Under these circumstances, the determined ratio  $D_2/D_1$  directly corresponds to the tortuosity factor  $\tau$ , introduced in the literature to quantify the diffusion resistance of a material as set by the shape and curvature as well as the lengths and connectivity of its pores.

In accordance with the similar size and weight of the molecules, alike values for the ratio of both diffusion constants were obtained for all three gases investigated (cf. Table 3). This finding corroborates the assumption of short surface residence times in case of CO and CO<sub>2</sub> (see Introduction) which, as reactants involved in the surface reaction studied, need to be accommodated on npAu's surface at least transiently, in contrast to CH<sub>4</sub>. To furthermore verify the pressure independence of the results, additional experiments at 10 bars (where contributions from Knudsen diffusion should still be minor) were performed for CO<sub>2</sub> (see SI). Also, these measurements revealed, within statistical uncertainty, identical values  $D_2/D_1$ , thus assuring that the mean value of the ratio derived on the basis of the whole data set and amounting to  $2.0 \pm 0.2$  indeed equals the (gas independent) tortuosity factor of npAu.

Aiming at a more differentiated understanding of the structural features influencing the diffusion of gases in porous materials, concepts have been proposed in the literature to split up  $\tau$ , only integrally describing and quantifying this contribution to the decelerated mass transport, into two independent factors [38,39]:



**Table 1**

Self-diffusion coefficients of CO, CO<sub>2</sub> and CH<sub>4</sub> in the bulk gas phase, as derived from our PFG NMR measurements at 15 bar and 23 °C - in comparison to other experimental values reported in the literature for similar pressures and theoretical values, calculated according to Chapman and Enskog (incl. statistical uncertainties).

Gas	This study		Other exp. Data <sup>1</sup>	Calculated <sup>2</sup>	
	D <sub>M,exp</sub> (·10 <sup>-6</sup> ) [m <sup>2</sup> /s]	ΔD <sub>M,exp</sub> (·10 <sup>-6</sup> ) [m <sup>2</sup> /s] (Cl <sub>95</sub> )		D <sub>M,lit</sub> (·10 <sup>-6</sup> ) [m <sup>2</sup> /s]	D <sub>M,calc</sub> (·10 <sup>-6</sup> ) [m <sup>2</sup> /s]
CO	1.36	0.10	no data	1.41	0.04
CO <sub>2</sub>	0.73	0.07	0.74[36]	0.78	0.04
CH <sub>4</sub>	1.40	0.10	1.56[37]	1.56	0.03

<sup>1</sup> Data refers to 25 °C and 14.7 bar.

<sup>2</sup> Calculated on the basis of Chapman's and Enskog's theory with an expected validity for pressures up to 300 bar.

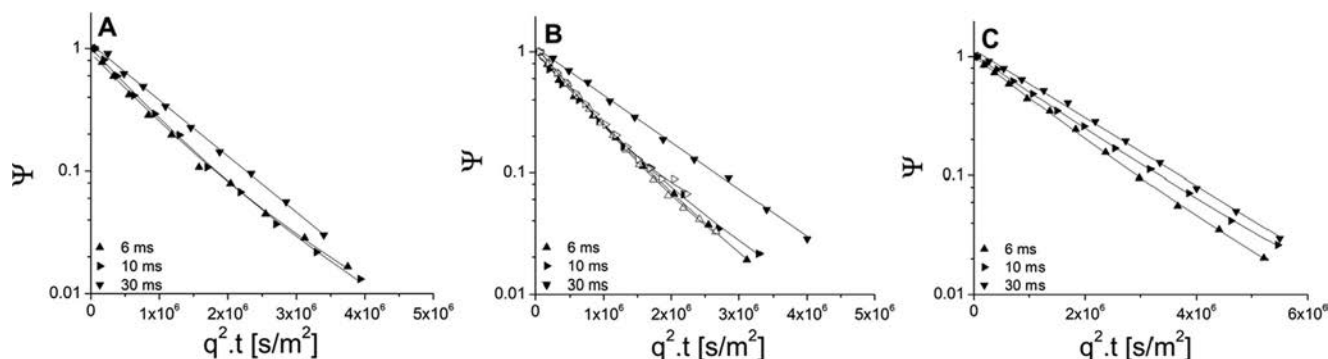


**Fig. 1.** <sup>13</sup>C PFG NMR attenuation curves measured for different diffusion times of CO (A), CH<sub>4</sub> (B), and CO<sub>2</sub> (C) at 23 °C and 15 bar in presence of the npAu samples. The corresponding data obtained for CH<sub>4</sub> diffusion by using <sup>1</sup>H PFG NMR (open symbols) are shown for comparison. The solid lines represent the results of the least-square fits based on a bi-exponential decay behavior (see SI for further details).

**Table 2**

Results of the least-square fitting of the data shown in Fig. 1, summarizing the root mean square displacements (RMSD) experienced by CO, CO<sub>2</sub> and CH<sub>4</sub> when diffusing inside (subscript: 1) and outside (subscript: 2) of the npAu material within the applied measurement time as well as the diffusion coefficients D<sub>1</sub> and D<sub>2</sub> derived on this basis. The last column shows their ratio D<sub>2</sub>/D<sub>1</sub>, representing the tortuosity factor τ.

t <sub>D</sub> [ms]	Gas	RMSD <sub>1</sub> [μm]	RMSD <sub>2</sub> [μm]	D <sub>1</sub> (·10 <sup>-7</sup> ) [m <sup>2</sup> /s]	D <sub>2</sub> (·10 <sup>-7</sup> ) [m <sup>2</sup> /s]	D <sub>2</sub> /D <sub>1</sub>
6	CO	149 ± 15	218 ± 15	7.0 ± 1.4	15 ± 2	2.1 ± 0.5
10	CO	201 ± 20	290 ± 20	7.2 ± 1.4	15 ± 2	2.1 ± 0.4
30	CO	430 ± 20		10.5 ± 1		–
6	CH <sub>4</sub>	167 ± 18	225 ± 15	8.8 ± 1.8	16 ± 2	1.8 ± 0.4
6*	CH <sub>4</sub>	152 ± 16	228 ± 14	7.5 ± 1.5	17 ± 2	2.3 ± 0.5
10	CH <sub>4</sub>	202 ± 22	299 ± 19	7.3 ± 1.5	16 ± 2	2.2 ± 0.5
10*	CH <sub>4</sub>	193 ± 20	302 ± 19	6.8 ± 1.4	17 ± 2	2.5 ± 0.6
30	CH <sub>4</sub>	397 ± 20		9.0 ± 0.9		–
6	CO <sub>2</sub>	124 ± 13	167 ± 7	4.8 ± 1	8.75 ± 0.8	1.8 ± 0.4
10	CO <sub>2</sub>	157 ± 17	208 ± 10	4.4 ± 0.9	7.8 ± 0.8	1.8 ± 0.4
30	CO <sub>2</sub>	340 ± 19		6.6 ± 0.7		–

\* Measurements done using <sup>1</sup>H PFG NMR.

**Table 3**

Average tortuosity factors of npAu derived from the ratio of the diffusivities of CO, CO<sub>2</sub> and CH<sub>4</sub> outside and inside npAu on the basis of the data shown in Table 2.

Sorbate	Pressure/bar	Average tortuosity factor τ
CO	15	2.1 ± 0.4
CH <sub>4</sub>	15	2.2 ± 0.3
CO <sub>2</sub>	15	1.8 ± 0.3
CO <sub>2</sub>	10	1.8 ± 0.4

- impediments due to varying pore diameters, possibly resulting in “bottle necks” for the diffusing molecules;
- elongation of the diffusive pathways due to non-straight but meandering pores.

As a measure for the first contribution, a parameter called *constrictivity* δ was introduced in the literature, whereas contributions

of the latter kind were subsumed in a quantity, (unfortunately) also called *tortuosity* and, for the sake of clarity, denoted τ' in the following. The integral tortuosity τ, as determined by PGF NMR and dealt with above, is then related to δ and τ' in the following way [38,39]:

$$\tau = \frac{\tau'^2}{\delta} \quad (1)$$

The constrictivity δ of a pore system can usually comparatively easily assessed on the basis of a microscopic evaluation of the pore diameters (via SEM or TEM, for instance) [39]. For npAu such an analysis based on the width of its pore size distribution, which was shown to be independent of the mean diameter if normalized to it, yields a value of δ = 0.54, as detailed in section 3 of the SI. Using this value and the value for τ (2.0) derived from the PFG NMR measurements, Eq. (1) indicates that τ' is close to 1 (1.1),

implying comparatively small contributions due to pathway elongations enforced by npAu's pore system. Rather, the main effect seems to result from pore diameter variations in case of this material.

### 3.2. Determination of diffusivities under catalytic conditions

Knowing npAu's tortuosity  $\tau$  as the material specific parameter governing the diffusive mass transport within its porous system enables quantitatively assessing its influence on the conversion levels achievable under the catalytic reaction conditions applied. In this context, it has to be considered, however, that CO oxidation over npAu was typically studied under significantly lower pressures (1 bar) than those employed for the PFG NMR experiments and that gas mixtures (and not pure gases) are present under catalytic conditions. To this end, the molecular diffusion coefficients  $D_M$  of the reactants first need to be rescaled to 1 bar. On this basis, the corresponding values in the applied gas mixture  $D_{M,mix}$  can be calculated. To include potential contributions of Knudsen diffusion ( $D_K$ , see eq. S9 in the SI), which are likely to play a significant role for mesoporous materials, such as npAu, around 1 bar, finally the total diffusion coefficient  $D_{T,mix}$  has to be determined (eq. S8 in the SI). For CO, CO<sub>2</sub>, O<sub>2</sub> and He (carrier gas), i.e., the gases comprising the feed for the catalytic experiments described in the next subsection, the corresponding values are compiled in Table 4. (All details necessary for their assessment can be found in section 4 of the SI.) Comparing  $D_{T,mix}$  and  $D_K$ , it becomes apparent that they are very similar in all cases. This equality underpins that, indeed, Knudsen diffusion dominates the mass transport in npAu at 1 bar – meaning that its pore diameters are distinctly smaller than the mean free path of the molecules in the bulk gas phase under these conditions.

Under these circumstances, it can be safely assumed that transport and self-diffusion coefficients are identical and that effective diffusivities  $D_E$  relevant for the diffusive mass transport in the pore system under reaction conditions can be calculated according to [16,24,40]:

$$D_{E,i} = \frac{\phi}{\tau} \cdot D_{T,mix,i} \quad (2)$$

Here, not only the determined tortuosity factor  $\tau$  but also the known porosity  $\phi$  of npAu (0.7) has to be taken into account. As expected, very similar values are obtained in this way for all gases – except for He as a distinctly lighter gas (yet, as the carrier gas, not involved in the reaction):  $0.83\text{--}1.03 \cdot 10^{-6} \text{ m}^2/\text{s}^2$ .

### 3.3. CO oxidation over npAu and determination of the microkinetics

It was already mentioned in the Introduction that previous work on low-temperature CO oxidation over npAu suggested that it is the supply of CO that controls and limits its catalytic turnover on the surface so that a rate law of first order can be applied to describe its microkinetics [12]:

$$r_{int} = k \cdot c_{CO} = k \cdot \frac{p_{CO}}{R \cdot T} \quad (3)$$

$c_{CO}$ : CO concentration;  $p_{CO}$ : CO partial pressure.

For a porous catalyst, the level of conversion actually observed usually is diminished as a consequence of a retarded supply of the reactants to its inner sections by diffusive mass transport. The effectiveness factor of the catalytic process  $\eta$  is then defined as the ratio of the macroscopically observed rate  $r_{obs}$  and the microkinetic rate  $r_{int}$ :

$$\eta = \frac{r_{obs}}{r_{int}} \iff r_{obs} = \eta \cdot r_{int} \quad (4)$$

On one hand,  $\eta$  is dependent on the macroscopic shape and size of the catalyst particles, pellets, or monoliths used. On the other hand, the relationship between the microkinetic rate and the diffusive flux through the catalyst's pores is decisive. All these quantities can be merged into a single one, called Thiele Modulus, constituting the parameter which determines the effectiveness factor  $\eta$  achievable under the applied process conditions. For a microkinetic rate law of 1<sup>st</sup> order the Thiele Modulus  $\varphi$  has the following form [43]:

$$\varphi = \sqrt{\frac{k \cdot l^2}{D_E}} \quad (5)$$

and is connected to  $\eta$  as follows:

$$\eta = \frac{\tanh(\varphi)}{\varphi} \quad (6)$$

Here,  $D_E$  refers to the effective diffusivity of the kinetically relevant reactant within the pore system, i.e., in our case to CO (see Table 4:  $D_E = 1.03 \cdot 10^{-6} \text{ m}^2/\text{s}$ ) and  $l$  to the so-called characteristic length, representing a 1D measure for the distances to be overcome by diffusion within the applied catalyst particles. As detailed in the SI, this quantity can be calculated on the basis of their shape and size and equals in case of thin, disc-shaped specimen as given for the npAu monoliths (diameter: 5 mm, thickness: 200  $\mu\text{m}$ ) employed in this study to half of their thickness (100  $\mu\text{m}$ ).

A representative progression of the conversion of CO to CO<sub>2</sub> as achieved with such monolithic samples at 30 °C after applying an activation protocol which was previously reported to ensure maximal catalytic turnover is shown in Fig. 2 (lower trace). As inferred from the figure, the maximum conversion eventually reached amounts to  $X = \sim 40\%$  which, if transformed into a CO<sub>2</sub> formation rate ( $r_{obs}$ ), corresponds to the macrokinetics under the given conditions. As elucidated in more detail in the SI, on this basis and the experimentally determined transport properties of npAu the microkinetic rate constants  $k$  (referred to the volume) and  $k_A$  (referred to the catalyst surface area) as well as the corresponding turnover frequency (TOF: number of CO molecules reacted to CO<sub>2</sub> per surface atom and second) can be straightforwardly calculated. The results are summarized in Table 5.

When comparing the TOF derived in this way with values previously reported in the literature, it is important to note that, in contrast to  $k$  and  $k_A$ , this measure for the catalytic activity is proportional to the CO concentration or partial pressure, respectively, because it corresponds to a rate (expressed in microscopic terms) and not to a rate constant. As shown in Ref. [12], the CO<sub>2</sub> formation rate increases, under conditions of O<sub>2</sub> excess, linearly up to several 10 vol% (in line with a rate law of 1<sup>st</sup> order) so that at higher CO partial pressures significantly higher TOFs can be reached. In Table S2 a synopsis of kinetic results that have been published on low-temperature CO oxidation over npAu since 2006 is presented. When considering the CO concentrations applied there and relating the reported TOFs to 1 vol% CO for example, (as used here) it turns out that, by trend, the values are smaller than the one determined in this study. This finding, however, is not unexpected. While a varying and unknown degree of mass transport limitations is one likely reason for the scatter, also an incomplete activation of the npAu catalysts might be another one.

Having access to the diffusive transport properties of npAu and being able to seize best-possible conversion levels reproducibly, such ambiguities, however, can be overcome. Furthermore, predictions regarding an optimized catalyst shape can be made. On the basis of the Thiele Modulus for the npAu discs a catalyst effectiveness factor  $\eta = 0.68$  is calculated, indicating that in this case mass transport still plays a major role, which limits the catalytic activity

**Table 4**

Molecular ( $D_M$ ) and calculated Knudsen ( $D_K$ ) diffusion coefficients as well as the molecular ( $D_{M,mix}$ ) and resulting total diffusion coefficients ( $D_{T,mix}$ ) in the reaction mixture for all gases used for studying CO oxidation over npAu at 1 bar and 30 °C. On the basis of  $D_{T,mix}$  and the tortuosity determined for npAu by PFG NMR, effective diffusion coefficients  $D_E$  relevant for the mass transport within the pore system were calculated and are given in the last column.

Gas	$D_M$ ( $\cdot 10^{-6}$ ) [m <sup>2</sup> /s]	$D_{M,Mix}$ ( $\cdot 10^{-6}$ ) [m <sup>2</sup> /s]	$D_K$ ( $\cdot 10^{-6}$ ) [m <sup>2</sup> /s] <sup>2</sup>	$D_{T,Mix}$ ( $\cdot 10^{-6}$ ) [m <sup>2</sup> /s]	$D_E$ ( $\cdot 10^{-6}$ ) [m <sup>2</sup> /s]
CO	20.4	83.84	3.19	3.07	1.03
O <sub>2</sub>	22.12 <sup>1</sup>	106.91	2.99	2.90	0.97
CO <sub>2</sub>	11.0	70.03	2.55	2.46	0.83
He*	176.38 <sup>1</sup>	109.27	8.44	7.84	2.63

<sup>1</sup> Calculated on the basis of Chapman and Enskog's theory [17,41,42].

<sup>2</sup> Calculated on the basis of kinetic gas theory: see SI.

\* Carrier gas.

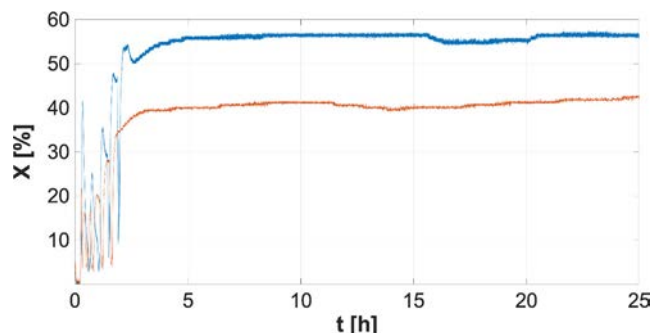


**Fig. 2.** Evolution of catalytic conversion  $X$  of CO to CO<sub>2</sub> as observed for different types of npAu catalysts at 30 °C after activating them on the basis of a protocol reported previously (resulting in the oscillatory behavior recorded between 0 and 2.5 h). Lower trace: monolithic npAu discs (5 mm diameter and 200 μm thickness); upper trace: npAu platelets exhibiting the same thickness but diameters in the range of just a few 100 μm.

to about 2/3 as compared to npAu's full potential. As inferred from Fig. 3, a reduction of the characteristic length  $l$  to already a third (i.e., to < 33 μm) should lead to an increase of  $\eta$  to 0.95 or even higher. As detailed in the SI, such a situation is reached, when decreasing the disc diameter to the dimension of the disc height (200 μm), turning  $l$  from  $h/2$  to  $h/6$ .

To verify this prediction, we developed a simple method of breaking up the monolithic npAu samples into smaller pieces, without compromising the accessibility of the pore system (see Experimental). In this way, we could successfully transform the discs into platelets with diameters in the range of just a few 100 μm (even though exhibiting a broad size range). Repeating the catalytic experiments with this form of the catalyst (under otherwise identical reaction conditions), an increase of the conversion level by ~45–50% (corresponding to absolute conversions of 55–60% under the given experimental conditions) could indeed be achieved (see Fig. 2, upper trace). Based on the microkinetic rate constant  $k$ , this corresponds to a catalyst effectiveness factor  $\eta$  larger than 95%, in agreement with the expectation based on the smaller particles size.

**Table 5**

Micro- and macrokinetics of low-temperature CO oxidation over nanoporous gold: rate constant per volume ( $k$ ) and per area catalyst ( $k_A$ ), turnover frequency (TOF) as well as catalyst effectiveness factor  $\eta$  for large monolithic npAu discs with a thickness of 200 μm and a diameter of 5 mm as well as for smaller npAu platelets where both, thickness and lateral dimensions, were in the range of 200 μm.

Microkinetics and macrokinetics of CO oxidation over npAu at 30 °C and 1 bar				
Microkinetics			Macrokinetics: catalyst effectiveness factor $\eta$	
			npAu discs ( $h = 200$ μm, $d = 5$ mm → $l = 100$ μm)	npAu platelets ( $h = 200$ μm, $d = 200$ μm → $l = 33.3$ μm)
$k$ (1/s)	$k_A$ (m/s)	TOF (1/s)	0.68 ( $\varphi = 1.23$ )	0.97 = $1.43 \cdot \eta_{discs}$ ( $\varphi = 0.34$ )
155	$1.76 \cdot 10^{-6}$	0.03		

## 4. Conclusions

For the first time, we succeeded to measure diffusivities of gas molecules in a porous metallic material by PFG NMR. The system we investigated, nanoporous gold, represents an interesting heterogeneous catalyst which has been found to efficiently catalyze total and partial aerobic oxidation reactions with high activities and selectivities already at room temperature. Taking CO oxidation as an example for which the diffusion of the reactants CO and CO<sub>2</sub> can be straightforwardly studied by <sup>13</sup>C PFG NMR, we were able to experimentally assess the impediment set by the pore system of npAu for their diffusive transport. By including CH<sub>4</sub> as an inert molecule in the experiments, showing the same tortuosity as the two other gases, it was assured that chemisorption of the reactants on the pore walls – being the necessary condition for catalytic conversion – does not influence the data. On grounds of the PFG NMR results, the tortuosity of npAu's pore system could be determined, revealing that mass transport in the material is slowed down by a factor of ~2 as compared to the bulk gas phase. This value is in general agreement with theoretical predictions for porous systems exhibiting high porosities [44,45].

Owing to the independent characterization of the transport properties, we were able to disentangle the macrokinetics, i.e., the observed CO<sub>2</sub> formation rate, and the microkinetics, characterizing the genuine catalytic potential of npAu with respect to this reaction. The turnover frequency determined partly excels previously reported values in the literature, suggesting influences of diffusive transport limitations in former studies. For thin monolithic npAu discs, for instance, typically employed for catalytic investigations in the past, diameters of several mm and a thickness of 200 μm already reduce the catalytic effectiveness by about a third.

Having experimentally determined the microkinetics, this knowledge allowed us making predictions for more efficient shapes of the catalyst where transport limitations are minimized. Making a first attempt into this direction, we broke up larger npAu discs into smaller platelets. The reduction of the catalyst lateral size to values in the range of a few 100 μm resulted in an increase of the catalytic conversion of CO to CO<sub>2</sub> by about 50 % which, in

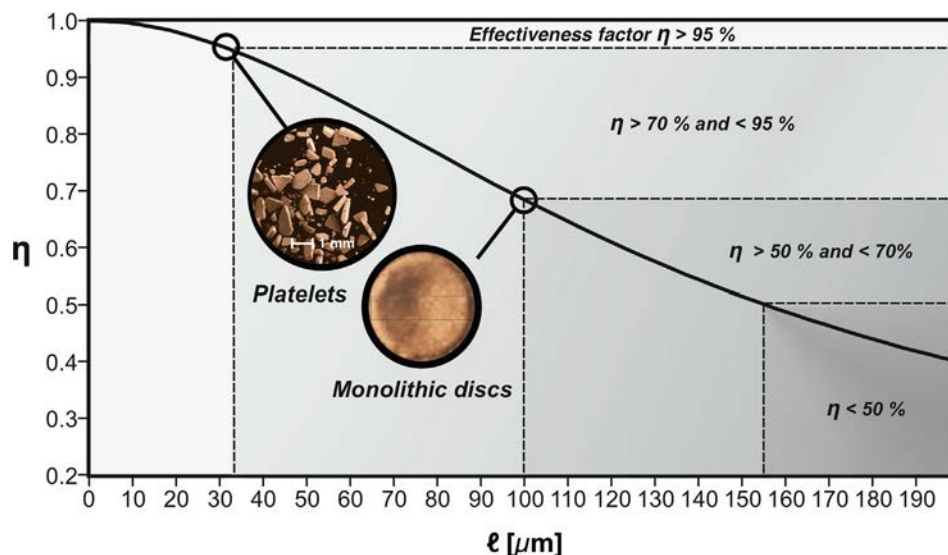


Fig. 3. Effectiveness factor  $\eta$  of npAu catalysts exhibiting different shapes and characteristic lengths.

agreement with predictions, corresponds to an improvement of the effectiveness factor  $\eta$  to almost 100%.

An option for a more controlled fabrication of size-selected npAu particles by breaking up larger npAu monoliths is given by tailoring its gain structure during preparation, since fracture predominantly occurs at grain boundaries. On the one hand, it has been shown that the grain sizes of the starting alloy are conserved during the dealloying process [46]. On the other hand, it is well-established metallurgic knowledge how grain sizes of cold rolled metals change and can be influenced by intermittent annealing steps [47,48]. Thus, optimizing the protocols for thinning and treating the starting alloy used for the dealloying is expected to represent a viable way for preparing npAu catalysts which are optimized with respect to their diffusive transport properties so that their catalytic potential can be fully exploited. An alternative, requiring, however, much more sophisticated fabrication approaches, are hieratically designed nanoporous structures, additionally providing macroporous transport capabilities as have also been suggested in the literature [8,15].

#### Data availability

Data will be made available on request.

#### Acknowledgements

M.B. and T.R. acknowledge gratefully funding of the work provided by the German Research Foundation (DFG) within the framework of the Research Unit 2213 “Nanoporous Gold” (grand no.: BA 1710/29-2 and RI 1025/3-2). A portion of this work was carried out in the McKnight Brain Institute at the National High Magnetic Field Laboratory’s AMRIS Facility, which is supported by National Science Foundation Cooperative Agreement No. DMR-1157490 and the State of Florida. This work was supported in part by an NIH award, S10RR031637, for magnetic resonance instrumentation.

#### Appendix A. Supplementary material

Supplementary data to this article can be found online at <https://doi.org/10.1016/j.jcat.2022.08.020>.

#### References

- [1] C. Xu, J. Su, X. Xu, P. Liu, H. Zhao, F. Tian, Y. Ding, Low temperature CO oxidation over unsupported nanoporous gold, *J. Am. Chem. Soc.* 129 (2007) 42–43, <https://doi.org/10.1021/ja0675503>.
- [2] V. Zielasek, B. Jürgens, C. Schulz, J. Biener, M.M. Biener, A.V. Hamza, M. Bäumer, Gold catalysts: nanoporous gold foams, *Angew. Chem. – Int. Ed.* 45 (2006) 8241–8244, <https://doi.org/10.1002/anie.200602484>.
- [3] A. Wittstock, J. Biener, J. Erlebacher, M. Bäumer, *Nanoporous Gold: From an Ancient Technology to a High-tech Material*, Royal Society of Chemistry (RSC Nanoscience & Nanotechnology, vol. 22), Cambridge, 2012, ISBN 978-1-84973-374-8. <<https://doi.org/10.1039/9781849735285>>.
- [4] A. Wittstock, V. Zielasek, J. Biener, C.M. Friend, M. Bäumer, Nanoporous gold catalysts for selective methanol at low temperature, *Science* 327 (2008) 319–323.
- [5] M. Haruta, Novel catalysis of gold deposited on metal oxides, *CATTECH* 6 (2002) 102–115, <https://doi.org/10.1023/A:1020181423055>.
- [6] I. McCue, J. Stuckner, M. Murayama, M.J. Demkowicz, Gaining new insights into nanoporous gold by mining and analysis of published images, *Sci. Rep.* 8 (2018) 1–11, <https://doi.org/10.1038/s41598-018-25122-3>.
- [7] A. Wittstock, J. Biener, M. Bäumer, Nanoporous gold: a new material for catalytic and sensor applications, *Phys. Chem. Chem. Phys.* 12 (2010) 12919–12930, <https://doi.org/10.1039/c0cp00757a>.
- [8] J.D. Lee, J.B. Miller, A.V. Shneidman, L. Sun, J.F. Weaver, J. Aizenberg, J. Biener, J. A. Boscoboinik, A.C. Foucher, A.I. Frenkel, J.E.S. van der Hoeven, B. Kozinsky, N. Marcella, M.M. Montemore, H.T. Ngan, C.R. O’Connor, C.J. Owen, D.J. Stacchiola, E.A. Stach, R.J. Madix, P. Sautet, C.M. Friend, Dilute alloys based on Au, Ag, or Cu for efficient catalysis: from synthesis to active sites, *Chem. Rev.* 122 (9) (2022) 8758–8808.
- [9] L.V. Moskaleva, S. Röhe, A. Wittstock, V. Zielasek, T. Klüner, K.M. Neyman, M. Bäumer, Silver residues as a possible key to a remarkable oxidative catalytic activity of nanoporous gold, *Phys. Chem. Chem. Phys.* 13 (2011) 4529–4539, <https://doi.org/10.1039/c0cp02372h>.
- [10] W. Dononelli, G. Tomaschun, T. Klüner, L.V. Moskaleva, Understanding oxygen activation on nanoporous gold, *ACS Catal.* 9 (2019) 5204–5216, <https://doi.org/10.1021/acscatal.9b00682>.
- [11] G. Pia, E. Sogne, A. Falqui, F. Delogu, Ag surface segregation in nanoporous Au catalysts during CO oxidation, *Sci. Rep.* 8 (2018) 1–9, <https://doi.org/10.1038/s41598-018-33631-4>.
- [12] A. Wittstock, B. Neumann, A. Schaefer, K. Dumbuya, C. Kübel, M.M. Biener, V. Zielasek, H.P. Steinrück, J.M. Gottfried, J. Biener, A. Hamza, M. Bäumer, Nanoporous Au: an unsupported pure gold catalyst?, *J. Phys. Chem. C* 113 (2009) 5593–5600, <https://doi.org/10.1021/jp808185v>.
- [13] L.C. Wang, Y. Zhong, D. Widmann, J. Weissmüller, R.J. Behm, On the role of residual Ag in nanoporous Au catalysts for CO oxidation: a combined microreactor and TAP reactor study, *ChemCatChem* 4 (2012) 251–259, <https://doi.org/10.1002/cctc.201100297>.
- [14] S. Wild, M. Bäumer, T. Risse, Thermal activation of nanoporous gold for carbon monoxide oxidation, *J. Phys. Chem. C* 126 (2022) 1770–1777, <https://doi.org/10.1021/acs.jpcc.1c08222>.
- [15] M.L. Personick, B. Zugic, M.M. Biener, J. Biener, R.J. Madix, C.M. Friend, Ozone-activated nanoporous gold: a stable and storable material for catalytic oxidation, *ACS Catal.* 5 (2015) 4237–4241, <https://doi.org/10.1021/acscatal.5b00330>.

- [16] J. Kärger, D.M. Ruthven, D.N. Theodorou (Eds.), *Diffusion in Nanoporous Materials*, Wiley, 2012.
- [17] J.O. Hirschfelder, C.F. Curtiss, R.B. Bird, *Molecular Theory of Gases and Liquids*, Wiley & Sons Ltd, 1954.
- [18] J. Kärger, S. Vasenkov, Quantitation of diffusion in zeolite catalysts, *Micropor. Mesopor. Mater.* 85 (2005) 195–206, <https://doi.org/10.1016/j.micromeso.2005.06.020>.
- [19] S.J. Cooper, A. Bertei, P.R. Shearing, J.A. Kilner, N.P. Brandon, TauFactor: an open-source application for calculating tortuosity factors from tomographic data, *SoftwareX* 5 (2016) 203–210, <https://doi.org/10.1016/j.softx.2016.09.002>.
- [20] R. Mueller, S. Zhang, M. Klink, M. Bäumer, S. Vasenkov, The origin of a large apparent tortuosity factor for the Knudsen diffusion inside monoliths of a samaria-alumina aerogel catalyst: a diffusion NMR study, *Phys. Chem. Chem. Phys.* 17 (2015) 27481–27487, <https://doi.org/10.1039/c5cp04609b>.
- [21] J. Kärger, M. Avramovska, D. Freude, J. Haase, S. Hwang, R. Valiullin, Pulsed field gradient NMR diffusion measurement in nanoporous materials, *Adsorption* 27 (2021) 453–484, <https://doi.org/10.1007/s10450-020-00290-9>.
- [22] C. D'Agostino, R.D. Armstrong, G.J. Hutchings, L.F. Gladden, Product inhibition in glycerol oxidation over Au/TiO<sub>2</sub> catalysts quantified by NMR relaxation, *ACS Catal.* 8 (2018) 7334–7339, <https://doi.org/10.1021/acscatal.8b01516>.
- [23] C. D'Agostino, Y. Ryabenkova, P.J. Miedziak, S.H. Taylor, G.J. Hutchings, L.F. Gladden, M.D. Mantle, Deactivation studies of a carbon supported AuPt nanoparticulate catalyst in the liquid-phase aerobic oxidation of 1,2-propanediol, *Catal. Sci. Technol.* 4 (2014) 1313–1322, <https://doi.org/10.1039/c4cy00027g>.
- [24] M.D. Mantle, D.I. Enache, E. Nowicka, S.P. Davies, J.K. Edwards, C. Dagostino, D. P. Mascarenhas, L. Durham, M. Sankar, D.W. Knight, L.F. Gladden, S.H. Taylor, G.J. Hutchings, Pulsed-field gradient NMR spectroscopic studies of alcohols in supported gold catalysts, *J. Phys. Chem. C* 115 (2011) 1073–1079, <https://doi.org/10.1021/jp105946q>.
- [25] N. Lopez, J.K. Nørskov, Catalytic CO oxidation by a gold nanoparticle: a density functional study, *J. Am. Chem. Soc.* 124 (2002) 11262–11263, <https://doi.org/10.1021/ja026998a>.
- [26] S. Röhe, K. Frank, A. Schaefer, A. Wittstock, V. Zielasek, A. Rosenauer, M. Bäumer, CO oxidation on nanoporous gold: a combined TPD and XPS study of active catalysts, *Surf. Sci.* 609 (2013) 106–112, <https://doi.org/10.1016/j.susc.2012.11.011>.
- [27] M. Mavrikakis, P. Stoltze, J.K. Nørskov, Making gold less noble, *Catal. Letters* 64 (2000) 101–106.
- [28] A. Lackmann, C. Mahr, M. Schowalter, L. Fitzek, J. Weissmüller, A. Rosenauer, A. Wittstock, A comparative study of alcohol oxidation over nanoporous gold in gas and liquid phase, *J. Catal.* 353 (2017) 99–106, <https://doi.org/10.1016/j.jcat.2017.07.008>.
- [29] W.L. Yim, T. Nowitzki, M. Necke, H. Schnars, P. Nickut, J. Biener, M.M. Biener, V. Zielasek, K. Al-Shamery, T. Klüner, M. Bäumer, Universal phenomena of CO adsorption on gold surfaces with low-coordinated sites, *J. Phys. Chem. C* 111 (2007) 445–451, <https://doi.org/10.1021/jp0665729>.
- [30] A.P. Farkas, F. Solymosi, Activation and reactions of CO<sub>2</sub> on a K-promoted Au (111) surface, *J. Phys. Chem. C* 113 (2009) 19930–19936, <https://doi.org/10.1021/jp9061779>.
- [31] C. Xu, X. Xu, J. Su, Y. Ding, Research on unsupported nanoporous gold catalyst for CO oxidation, *J. Catal.* 252 (2007) 243–248, <https://doi.org/10.1016/j.jcat.2007.09.016>.
- [32] E.W. Thiele, Relation between catalytic activity and size of particle, *Ind. Eng. Chem.* 31 (1939) 916–920, <https://doi.org/10.1021/ie50355a027>.
- [33] D. Steinebrunner, G. Schnurpfeil, A. Wichmann, D. Wöhrle, A. Wittstock, Synergistic effect in zinc phthalocyanine–nanoporous gold hybrid materials for enhanced photocatalytic oxidations, *Catalysts* 9 (2019) 555, <https://doi.org/10.3390/catal9060555>.
- [34] M. Dvoyashkin, J. Zang, G.I. Yucelen, A. Katihar, S. Nair, D.S. Sholl, C.R. Bowers, S. Vasenkov, Diffusion of tetrafluoromethane in single-walled aluminosilicate nanotubes: pulsed field gradient NMR and molecular dynamics simulations, *J. Phys. Chem. C* 116 (2012) 21350–21355, <https://doi.org/10.1021/jp3054247>.
- [35] R.M. Corns, M.J.R. Hoch, T. Sun, J.T. Markert, Pulsed field gradient stimulated echo methods for improved NMR diffusion measurements in heterogeneous systems, *J. Magn. Reson.* 83 (1989) 252–266, [https://doi.org/10.1016/0022-2364\(89\)90189-3](https://doi.org/10.1016/0022-2364(89)90189-3).
- [36] S. Takahashi, H. Iwasaki, The diffusion of gases at high pressures. i. the self-diffusion coefficient of carbon dioxide, *Bull. Chem. Soc. Jpn.* 39 (1966) 2105–2109, <https://doi.org/10.1246/bcsj.39.2105>.
- [37] N.J. Trappeniers, P.H. Oosting, Selfdiffusion in gaseous and liquid methane, *Phys. Lett.* 23 (1966) 445–447, [https://doi.org/10.1016/0031-9163\(66\)91086-9](https://doi.org/10.1016/0031-9163(66)91086-9).
- [38] J. van Brakel, P.M. Heertjes, Analysis of diffusion in macroporous media in terms of a porosity, a tortuosity and a constrictivity factor, *Int. J. Heat Mass Transf.* 17 (1974) 1093–1103, [https://doi.org/10.1016/0017-9310\(74\)90190-2](https://doi.org/10.1016/0017-9310(74)90190-2).
- [39] E.E. Petersen, Diffusion in a pore of varying cross section, *AIChE J.* 4 (1958) 343–345, <https://doi.org/10.1002/aic.690040322>.
- [40] C. D'Agostino, J. Mitchell, L.F. Gladden, M.D. Mantle, Hydrogen bonding network disruption in mesoporous catalyst supports probed by PFG-NMR diffusometry and NMR relaxometry, *J. Phys. Chem. C* 116 (2012) 8975–8982, <https://doi.org/10.1021/jp2123295>.
- [41] M.J. Slaman, R.A. Aziz, Accurate transport properties and second virial coefficients for helium based on a state-of-the-art interatomic potential, *Int. J. Thermophys.* 16 (4) (1995) 1029.
- [42] A. Boushehri, J. Bzowski, J. Kestin, E.A. Mason, Equilibrium and transport properties of eleven polyatomic gases at low density, *J. Phys. Chem. Ref. Data* 16 (3) (1987) 445–466.
- [43] G. Emig, E. Klemm, *Technische Chemie*, in: *Tech. Chemie*, fifth ed., Springer, 2005, pp. 24–25.
- [44] M. Barrande, R. Bouchet, R. Denoyel, Tortuosity of porous particles, *Anal. Chem.* 79 (2007) 9115–9121, <https://doi.org/10.1021/ac071377r>.
- [45] Z. Sun, X. Tang, G. Cheng, Numerical simulation for tortuosity of porous media, *Micropor. Mesopor. Mater.* 173 (2013) 37–42, <https://doi.org/10.1016/j.micromeso.2013.01.035>.
- [46] Z. Qi, U. Vainio, A. Kornowski, M. Ritter, H. Weller, H. Jin, J. Weissmüller, Porous gold with a nested-network architecture and ultrafine structure, *Adv. Funct. Mater.* 25 (2015) 2530–2536, <https://doi.org/10.1002/adfm.201404544>.
- [47] H. Hui, R. Xia, J. Li, Q. Mei, Y. Ma, F. Chen, Y. Lei, Effects of cold rolling and annealing prior to dealloying on the microstructure of nanoporous gold, *Nanomaterials* 8 (2018) 540, <https://doi.org/10.3390/nano8070540>.
- [48] J.H. Cho, H.P. Ha, K.H. Oh, Recrystallization and grain growth of cold-rolled gold sheet, *Metall. Mater. Trans.* 36 (2005) 3415–3425, <https://doi.org/10.1007/s11661-005-0015-5>.

## Supporting Material

### 1. Evaluation of the PFG NMR measurements: basic principles

In the case of normal self-diffusion with a single diffusion coefficient ( $D$ ) PFG NMR attenuation curves can be presented as[1]:

$$\Psi = S_G/S_0 = e^{-D \cdot q^2 \cdot t} = e^{-D \cdot 4 \cdot \gamma^2 \cdot g^2 \cdot \delta^2 \cdot t} \text{ (eq. S1)}$$

$\Psi$ : PFG NMR signal attenuation,  $S_G$ ,  $S_0$ : NMR signal intensity with and without an applied field gradient, respectively,  $\gamma$ : Gyromagnetic ratio,  $\delta$ : effective gradient pulse length

where  $\Psi$  is the ratio of the NMR signal with ( $S_G$ ) and without ( $S_0$ ) applied field gradient,  $t$  is the time of observation of diffusion process (i.e., the diffusion time) and  $q = 2\gamma g\delta$ , where  $\gamma$  is the gyromagnetic ratio,  $g$  the gyromagnetic factor, and  $\delta$  is the effective gradient pulse length of a single gradient pulse in the 13-interval (bipolar) PFG NMR sequence. In the case of normal self-diffusion in three dimensional space, the mean square displacement (MSD) is related to the diffusivity and time by the Einstein relation[1]:

$$\langle r^2 \rangle = 6 \cdot D \cdot t \text{ (eq. S2)}$$

$\langle r^2 \rangle$ : Mean square displacement (MSD)

Within a porous material, each sorbate is expected to exhibit at least two diffusing ensembles at sufficiently short times (i.e., molecules diffusing inside, and molecules diffusing outside porous particles). In case of two molecule ensembles diffusing with different diffusivities, eq. S1 can be re-written as:

$$\Psi = S_G/S_0 = p_1 \cdot e^{-D_1 \cdot q^2 \cdot t} + p_2 \cdot e^{-D_2 \cdot q^2 \cdot t} \text{ (eq. S3)}$$

where constants  $p_1$  and  $p_2$  are the mole weighted phase fractions and  $D_1$  and  $D_2$  are the corresponding diffusivities of the respective ensembles. Due to the influence of longitudinal ( $T_1$ ) and transverse ( $T_2$ ) NMR relaxation, the phase fractions  $p_1$  and  $p_2$  can be different from the real fractions of the sorbate molecules diffusing inside and outside of the gold specimen at any given diffusion time. Specifically, the effect of the  $T_2$  NMR relaxation with relaxation times  $T_2^1$  and  $T_2^2$ , which occur inside (1) and outside (2) the gold discs, respectively, can be taken into account by replacing  $p_1$  and  $p_2$  with  $p_1 \cdot \exp(-t_{rel}/T_2^1)$  and  $p_2 \cdot \exp(-t_{rel}/T_2^2)$ . Here,  $p_1^*$  and  $p_2^*$  represent the  $T_2$ -corrected molecular fractions for diffusion inside and outside the porous material, respectively, and  $t_{rel}$  is the total time in the PFG NMR sequence during which the signal is reduced by the  $T_2$  NMR relaxation. Table S1 and Fig. S1 show the results of the NMR relaxation measurements.

**Table S1:**  $T_1$  and  $T_2$  NMR relaxation data measured for nanoporous gold samples with different sorbates at 15 bar.

Sorbate	Nuclei	$T_1$ /ms	$T_2^1$ /ms (inside npAu)	$T_2^2$ /ms (outside npAu)	Fraction 1 (inside npAu)	Fraction 2 (outside npAu)
CO	$^{13}\text{C}$	120	5.4	10.7	0.35	0.65
CH <sub>4</sub>	$^{13}\text{C}$	72	7.5	21.8	0.31	0.69
CH <sub>4</sub>	$^1\text{H}$	110	6.2	52.4	0.37	0.63
CO <sub>2</sub>	$^{13}\text{C}$	150	5.1	43	0.28	0.72

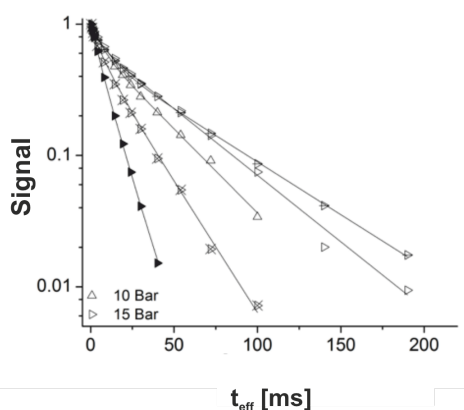


**Figure S1:** Transverse ( $T_2$ )  $^{13}\text{C}$  NMR relaxation data at  $23^\circ\text{C}$  (296 K) for the nanoporous gold samples loaded with CO (filled triangles),  $\text{CH}_4$  (triangles with two crosses), and  $\text{CO}_2$  (hollow triangles) at different loading pressures indicated in the figure by the triangle orientation. Also shown is  $T_2$   $^1\text{H}$  NMR relaxation data at 296 K for the nanoporous gold samples loaded with  $\text{CH}_4$  (triangles with a cross).

## 2. Analysis of the PFG NMR data: detailed description

Figure S2 shows examples of the measured  $^{13}\text{C}$  PFG NMR attenuation curves obtained at  $23^\circ\text{C}$  for the bulk gas (CO,  $\text{CH}_4$ , and  $\text{CO}_2$ ), i.e., in the *absence* of any porous material added. For methane diffusion, also  $^1\text{H}$  PFG NMR attenuation curves were measured in addition. As the proton PFG NMR attenuation curves coincided, within uncertainty, with the corresponding  $^{13}\text{C}$  PFG NMR attenuation curves, this finding confirms the absence of any measurement artefacts in our data. For the majority of the experiments, a bulk gas pressure of around 15 bar (in analogy to those carried out in the presence of the nanoporous gold samples) was applied. To check the dependence of the data on the gas loading, in case of  $\text{CO}_2$  additional measurements were carried out at a pressure of 10 bar (and  $23^\circ\text{C}$ ).

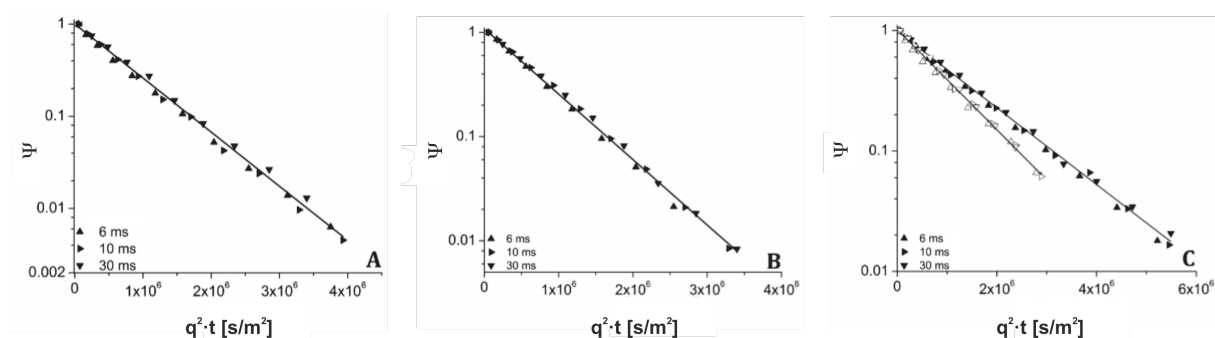


**Figure S2:**  $^{13}\text{C}$  PFG NMR attenuation curves measured for bulk CO gas at 15 bar (left), bulk  $\text{CH}_4$  gas at 15 bar (middle), and bulk  $\text{CO}_2$  gas at 10 bar (hollow symbols) and 15 bar (filled symbols) (right) for a range of diffusion times at  $23^\circ\text{C}$  (296 K).

As seen in Fig. S2, the  $^{13}\text{C}$  PFG NMR attenuation curves measured for each gas at different diffusion times show agreement with Eq. S1, i.e., are characterized by a mono-exponential decay behavior. Additionally, the slopes of all the attenuation curves at the different diffusion times coincide onto a single line, indicating that the corresponding diffusivities are independent of them. By fitting the data on basis of eq. S1, the self-diffusivities for CO,  $\text{CH}_4$ , and  $\text{CO}_2$  as given in Tab. 1 of the main text were derived. The self-diffusivity measured for  $\text{CO}_2$  at 10 bar was found to be  $(9.6 \pm 0.9) \times 10^{-7} \text{ m}^2/\text{s}$  and thus

within statistical uncertainty about a factor 1.5 (ratio of the pressures) larger, in agreement with the increase predicted by kinetic gas theory (see below).

The PFG NMR attenuation curves recorded under the same conditions (pressure of 15 bar, identical diffusion times) for CO, CH<sub>4</sub> and CO<sub>2</sub> in the *presence* of the npAu material are presented in Fig. 1 of the main text. Also, in this case reference measurements were performed for CO<sub>2</sub> at a lower pressure of 10 bar. The corresponding results are shown in Fig. S2 in comparison to the results for CO<sub>2</sub> and the other gases (CO and CH<sub>4</sub>) at 15 bar.

As the data acquired in the presence of the npAu samples clearly showed deviations from a mono-exponential behavior, the attenuation curves were fitted with eq. S3, i.e., assuming a bi-exponential decay (continuous lines in Fig. 1) due to two diffusing gas ensembles – one within and one outside of the porous material. The obtained ensemble fractions (see Tab. S1) derived from the  $T_2$  NMR measurements were in agreement, within uncertainty, with the ratio of the material filled and unfilled volume in the NMR tubes, taking the known porosity of the npAu specimen (70%) and their estimated particle bed volume into account. This correspondence provided evidence that that the obtained  $T_2$  fractions indeed were measured and assigned correctly.

For diffusion time of 6 ms and 10 ms, the root MSDs of molecules diffusing inside the discs were found to be smaller (6 ms) or in the range (10 ms) of the thickness of the discs (see Tab. 2 in the main text). Hence, effects resulting from the molecular exchange between the discs and the surrounding gas phase can be expected to be small here. For the largest investigated diffusion time of 30 ms, however, the root MSDs became significantly larger than the thickness of the discs. As a result, only a single diffusivity corresponding to a fast molecular exchange between porous material and the surrounding gas phase exchange was observed. As expected, the diffusivity derived in this case was larger than the diffusivities determined for 6 ms and 10 ms inside the discs but, at the same time, smaller than the diffusivities observed in the gas phase between the discs for the shorter diffusion times.

Since the tortuosity factors derived for all gases on the basis of the different diffusivities seen at 6 ms and 10 ms - including the measurements for CO<sub>2</sub> at 10 bar and those for CH<sub>4</sub> as an inert molecule – were, within statistical uncertainty, identical, it was concluded that they are gas and loading independent and that their mean value well describes the material's contribution to the decelerated diffusion within npAu's pore system.

### 3. Estimation of npAu's constrictivity

When dealing with the influence of the specific structural features of a porous material on gas diffusion within its pores, the resulting deceleration is typically accounted for by a single integral number, called tortuosity  $\tau$  which also constitutes that quantity which is directly accessible by PFG NMR measurements. As mentioned in the main text, other parts of the literature have proposed more sophisticated models according to which the material induced diffusion resistance can be split up in some respects into a contribution along the diffusive pathway and perpendicular to it (see eq. 1 and corresponding remarks in main text)[2,3].

As far as the latter, called constrictivity and describing the effect of varying pore cross sections or diameters, respectively, is concerned, Peterson showed that it can be approximated by[4]:

$$\delta \approx 1 - 0.21 \cdot \ln \left( \frac{A_{p,max}}{A_{p,min}} \right) = 1 - 0.21 \cdot \ln \left( \frac{d_{p,max}^2}{d_{p,min}^2} \right) = 1 - 0.42 \cdot \ln \left( \frac{d_{p,max}}{d_{p,min}} \right) \quad (eq. S4)$$

$A_{p,max}$ : maximum pore cross-sectional area,  $A_{p,min}$ : minimum pore cross-sectional area,  
 $d_{p,max}$ ,  $d_{p,min}$ : corresponding diameters



As pore and ligament sizes in npAu have been shown to be equal[5], instead of the pore diameters also the ligament diameters can be employed to derive  $\delta$ . Tomographic measurements revealed that the halfwidth of the (Gaussian) ligament size distribution is invariant for npAu samples exhibiting different mean ligament sizes  $\langle d_l \rangle$  when normalizing the distribution to this mean value. It comprises the range from  $0.5 \langle d_l \rangle$  to  $1.5 \langle d_l \rangle$ , meaning that the ratio equals 3. Entering this value in the above equation yields a constrictivity of  $\delta = 0.54$ .

#### 4. Determination of diffusion coefficients

In the following, it is described how the diffusion coefficients under the conditions of the catalytic experiments (1 bar) as given in Tab. 4 (main text) have been obtained. In case of CO and CO<sub>2</sub>, the molecular self-diffusion coefficients  $D_M$  at 1 bar – i.e. the pressure where the catalytic experiments were performed – were derived from the values determined by the PFG NMR at 15 bar. As far as the pressure dependence of  $D_M$  is concerned, kinetic gas theory predicts[6]:

$$D_M \sim \frac{1}{p} \Rightarrow \frac{D_{M,p_1}}{D_{M,p_2}} = \frac{p_2}{p_1} \quad (eq. S5)$$

Accordingly, the values at 1 bar are by a factor of 15 larger. For O<sub>2</sub> and He (carrier gas), not being part of the PFG NMR measurements, the values were calculated based on Chapman and Enskog's theory. In a gas mixture, as present under reaction conditions, the diffusing molecules influence each other, meaning that the diffusivities change. The effective coefficients can be calculated from the binary diffusion coefficients  $D_{M,i,j}$  of all constituents (including Helium and Oxygen) according to Wilke and Fairbanks[7]:

$$D_{M,mix,i} = \frac{1 - \chi_i}{\sum_{j \neq i} \frac{\chi_j}{D_{M,i,j}}} \quad (eq. S6)$$

$\chi_i$ : molar fraction of gas  $i$

With the binary diffusion coefficients  $D_{M,i,j}$ :

$$D_{M,i,j} = \left( \frac{1}{D_{M,i}} + \frac{1}{D_{M,j}} \right)^{-1} \quad (eq. S7)$$

Secondly, one has to take into account that at 1 bar the mean free path of the diffusing molecules in the bulk gas phase is larger or than the pore diameter ( $d_p \sim 20$  nm) so that a significant reduction of the diffusivity is expected, and Knudsen diffusion is expected to contribute significantly. The Knudsen diffusion coefficient  $D_{K,i}$  of a gas can be calculated on the basis of kinetic gas theory and from that the total diffusion coefficient  $D_{T,mix,i}$  of the specific gas in the mixture[6]:

$$D_{T,mix,i} = \left( \frac{1}{D_{M,mix,i}} + \frac{1}{D_{K,i}} \right)^{-1} \quad (eq. S8)$$

With  $D_{M,mix,i}$  according to eq. S6 and the Knudsen diffusion coefficient  $D_{K,i}$ :

$$D_{K,i} = \sqrt{\frac{8 \cdot d_p^2 \cdot R \cdot T}{9 \cdot \pi \cdot M_i}} \quad (eq. S9)$$

$M_i$ : molar mass of component  $i$ ,  $d_p$ : pore diameter

The values of the diffusion coefficients calculated on the basis of eq. S6 - S8 are given in Tab. 4 in the main text.

## 5. Calculation of characteristic lengths $\ell$

The characteristic length  $\ell$  of a catalyst particle can be understood as that dimension which, based on its macroscopic shape and size, effectively determines the diffusion profiles and corresponds to the ratio of the total volume of the catalyst and its outer surface (exposed to the reaction gases).[8] In a general form, it can be expressed by:

$$\ell = \frac{1}{2 \cdot \left( \frac{1}{x} + \frac{1}{y} + \frac{1}{z} \right)} \quad (\text{eq. S10})$$

(In this form, the analogy to the overall effect of parallel resistances - in an electrical circuit for example - becomes obvious.) In case of rectangular cuboids, the quantities  $x$ ,  $y$  and  $z$  represent the lateral extensions of the catalyst particle along the three Cartesian coordinates. For spheres,  $x = y = z = d$  ( $d$ : sphere diameter) applies so that a characteristic length of  $\ell = 1/6 d = 1/3 r$  ( $r$ : radius) results. In contrast, the characteristic length of cylinders is yielded for  $x = y = d$  and  $z = h$  with  $d$  and  $h$  being their diameter and height:

$$\ell = \frac{d \cdot h}{2 \cdot (d + 2h)} = \frac{r \cdot h}{2 \cdot (r + h)} \quad (\text{eq. S11})$$

In case of high aspect ratios (i.e., cylinders with a diameter being much larger than the height) as actually given in case of the npAu discs used in our catalytic experiments, it is evident that  $\ell$  approaches  $h/2$ . For the cylindrical platelets with diameters and heights being identical, the formula gives  $\ell = 1/6 h$  or, alternatively,  $\ell = 1/3 r$  (in agreement with spheres).

## 6. Determination of the rate constant $k$

The experimentally observed  $\text{CO}_2$  formation rate  $r_{\text{obs}}$  representing the macro kinetics is given by[9]:

$$\begin{aligned} r_{\text{obs}} &= \frac{1}{V} \frac{dn_{\text{CO}_2}}{dt} = \frac{1}{V} \cdot c_{\text{CO}_2} \cdot Q_T^o = \frac{1}{V} \cdot (X_{\text{CO}} \cdot c_{\text{CO}}) \cdot Q_T^o \\ &= \frac{1}{V} \cdot X_{\text{CO}} \cdot \frac{x_{\text{CO}} \cdot p^o}{R \cdot T^o} \cdot Q_T^o = \frac{p^o \cdot X_{\text{CO}} \cdot x_{\text{CO}} \cdot Q_T^o}{V \cdot R \cdot T^o} \quad (\text{eq. S12}) \end{aligned}$$

$X_{\text{CO}}$ : steady-state conversion ratio of carbon monoxide,  $x_{\text{CO}}$ ; molar fraction of carbon monoxide in the reaction mixture (0.01),  $Q_T^o$ : total volumetric flow at standard conditions (as adjusted by the mass flow controllers),  $R$ : ideal gas constant,  $T^o$ ,  $p^o$ : standard temperature and pressure. (Note that the gas flows adjusted by mass flow controllers refer to  $p^o = 1 \text{ bar}$  and  $T^o = 0^\circ\text{C}$  (273 K).

As far as the reaction volume  $V$  is concerned, the free (void) volume of the catalyst disc ( $r_{\text{disc}} = 1/2 d_{\text{disc}} = 2.5 \text{ mm}$ ,  $h = 200 \mu\text{m}$ ), where the reaction takes place, is relevant:

$$V_{\text{void}} = \phi \cdot \pi \cdot r_{\text{disc}}^2 \cdot h = \phi \cdot \frac{\pi}{4} \cdot d_{\text{disc}}^2 \cdot h \quad (\text{eq. S13})$$

which is given by the total volume of the disc-shaped npAu specimen multiplied with their porosity  $\phi$ . The micro kinetics, representing the kinetics of the actual surface reaction, can be described by a rate law of 1<sup>st</sup> order (see Introduction of the main text):

$$r_{int} = \frac{dc_{CO_2}}{dt} = k \cdot c_{CO} = k \cdot \frac{p_{CO}}{R \cdot T_R} = \frac{k \cdot x_{CO} \cdot p_R}{R \cdot T_R} \quad (eq.S14)$$

$k$ : micro kinetic rate constant,  $T_R$ ,  $p_R$ : temperature and pressure under reaction conditions

As explained in the main text, the catalyst effectiveness factor  $\eta$  – constituting the factor by which the catalytic conversion is diminished by diffusive mass transport limitations - corresponds to the ratio of  $r_{obs}$  and  $r_{int}$  and thus is given by:

$$\eta(\varphi) = \frac{r_{obs}}{r_{int}} = \left( \frac{4}{\phi \cdot \pi \cdot d_{disc}^2 \cdot h} \right) \cdot \left( \frac{p^o \cdot T_R \cdot Q_T^o}{p_R \cdot T^o} \right) \cdot \left( \frac{X_{CO}}{k} \right) \quad (eq.S15)$$

(For the sake of clarity, the expression has been grouped into a geometrical factor (1<sup>st</sup>), a factor representing the volume flow under reaction conditions (2<sup>nd</sup>) and the ratio between actual conversion and micro kinetic rate constant (3<sup>rd</sup>.) The catalyst effectiveness factor  $\eta$  is a direct function of the Thiele Modulus  $\varphi$ :

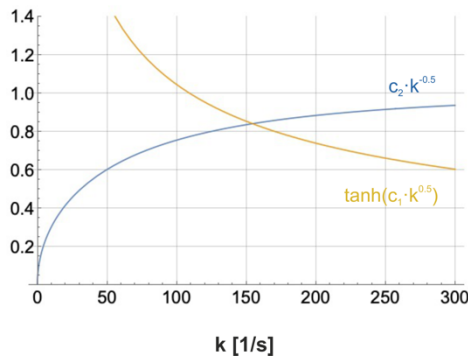
$$\eta = \frac{\tanh \varphi}{\varphi} \quad \text{with} \quad \varphi = \sqrt{\frac{k \cdot l^2}{D_E}} = \sqrt{\frac{k \cdot h^2}{4 \cdot D_E}} \quad (eq.S16)$$

(In eq. S16, it has been considered that for the disc-shaped samples the characteristic length  $l$  equals  $h/2$ .) Combining eq. S15 and S16 leads to the following expression, which – for a given set of experimental conditions and knowledge about the effective diffusivity  $D_E$  – allows evaluating the micro kinetics, i.e., the determination of  $k$ , from the observed macro kinetics:

$$\tanh(c_1 \cdot \sqrt{k}) = c_2 \cdot \frac{1}{\sqrt{k}}$$

$$\text{where: } c_1 = \frac{h}{2 \cdot \sqrt{D_E}} \quad \text{and} \quad c_2 = \left( \frac{2}{\phi \cdot \pi \cdot d_{disc}^2} \right) \cdot \frac{p^o \cdot T_R \cdot Q_T^o}{p_R \cdot T^o} \cdot \frac{X_{CO}}{\sqrt{D_E}} \quad (eq.S17)$$

At first sight, the approach is hampered by the lack of an analytic solution of eq. S17, but the problem can be readily tackled numerically. To this end both sides of the equation have been plotted as a function of  $k$  in Fig. S3 . Their crossing point reveals the value of the micro kinetical constant  $k$  where both sides of the equation are equal so that eq. S17 is fulfilled, in the present case for  $k = 155 \text{ s}^{-1}$ .



$\phi$	0.7
$d_{disc}$	$5 \cdot 10^{-3} \text{ m}$
$p^o$	$1 \cdot 10^5 \text{ Pa}$
$p_R$	$1 \cdot 10^5 \text{ Pa}$
$T^o$	$0^\circ\text{C}, 273.15 \text{ K}$
$T_R$	$30^\circ\text{C}, 303.15 \text{ K}$
$Q_T^o$	$8.3 \cdot 10^{-7} \text{ m}^3/\text{s}$
$X_{CO}$	0.4
$D_E$	$1.03 \cdot 10^{-6} \text{ m}^2/\text{s}$

**Figure S3:** Graphical solution of eq. S17 – right part (orange) and left part (blue) of the equation; the crossing point reveals the value of the rate constant  $k$  ( $155 \text{ s}^{-1}$ ) at  $30^\circ\text{C}$ . The table on the right-hand side shows all relevant experimental parameter used in the equation at a glance.

## 7. Determination of the catalyst area related rate constant and the turnover frequency (TOF)

The rate constant  $k$  as given above is related to the gas-filled void volume  $V_{void}$  of the catalyst (see eq. S13), which is a function of the porosity, of course. In contrast, for the rate constant  $k_A$  referred to the catalyst area  $A$  this is not the case – at least as long as the catalytic surface properties do not depend on the porosity (due to a different curvature of the ligaments, for instance) – and, thus, this quantity represents the more universal figure of merit for the catalytic activity. The catalyst area is obtainable from the specific surface area  $A_m$  of the material and the mass of the catalyst ( $m_{cat}$ ). As far as the former is concerned, one can revert to the following elegant formula, establishing a general relationship between specific surface areas of porous materials and their (mean) ligament diameter  $d_l$ [10]:

$$A_m = \frac{c}{\rho \cdot d_l} \quad (eq. S18)$$

Here,  $\rho$  represents the mass density of the material constituting the porous framework and  $c$  a dimensionless constant, characterizing the specific type of pore system under consideration, as given by the shape and connectivity of pores and ligaments. For npAu it was experimentally determined to be:  $c = 3,7$ . [10] On these grounds,  $k_A$  can be derived from  $k$  as follows:

$$k_A = k \cdot \frac{V_{void}}{A} = k \cdot \frac{V_{void}}{A_m \cdot m_{cat}} = k \cdot \frac{V_{void}}{m_{cat}} \cdot \frac{\rho_{Au} \cdot d_l}{c} \quad (eq. S19)$$

Since the void volume  $V_{void}$  and the material filled volume  $V_{ligaments}$  are related to each other by:

$$V_{void} = \frac{\phi}{1 - \phi} \cdot V_{ligaments} \quad (eq. S20)$$

eq. S19 can be rewritten as:

$$k_A = k \cdot \frac{\phi}{1 - \phi} \cdot \frac{V_{ligaments}}{m_{cat}} \cdot \frac{\rho_{Au} \cdot d_l}{c} \quad (eq. S21)$$

Taking into account that  $V_{ligaments}/m_{cat}$  equals the density of Au, eq. S21 can be further simplified to:

$$k_A = k \cdot \frac{\phi}{1 - \phi} \cdot \frac{d_l}{c} \quad (eq. S22)$$

Using for  $d_l$  the average value yielded by the FFT analysis of SEM micrographs (18 nm, see Experimental) and for  $\phi$  the value predetermined by the employed master alloy (0.7) a value of **1.76 10<sup>-6</sup> m/s** is then finally obtained for  $k_A$ .

Another quantity employed to characterize the catalytic activity of a catalyst is the turnover frequency (TOF), representing the (microkinetically) achievable number of catalytic conversions per time unit – in our case the number of CO molecules converted to CO<sub>2</sub> per second – related to number of catalytic surface sites. While the former is given by  $N_A \cdot V_{void} \cdot r_{int}$ , the latter equals to the area density of Au surface atoms  $\rho_{Au,surf}$  times the catalyst surface area  $A$ . Utilizing eq. S14 for  $r_{int}$ , leads to the following expression:

$$TOF = \frac{N_A \cdot V_{void} \cdot r_{int}}{A \cdot \rho_{Au,surf}} = \frac{N_A}{\rho_{Au,surf}} \cdot \frac{V_{void}}{A} \cdot k \cdot \frac{x_{CO} \cdot p_R}{R \cdot T_R} = \frac{N_A}{\rho_{Au,surf}} \cdot k_A \cdot \frac{x_{CO} \cdot p_R}{R \cdot T_R} \quad (eq. S23)$$

according to which the TOF can be directly derived from  $k_A$ . The density of Au surface atoms  $\rho_{Au,surf}$  needed to this end can be calculated on the basis of the lattice constant  $a_{Au}$  (409 pm = 4.09·10<sup>-10</sup> m, fcc crystal lattice) and assuming e.g. (111) planes[11]:

$$q_{Au,surf} = \frac{4}{\sqrt{3} \cdot a_{Au}^2} \quad (eq.S24)$$

In essence, the following equation for the TOF results:

$$TOF = N_A \cdot \frac{\sqrt{3}}{4} \cdot a_{Au}^2 \cdot k_A \frac{x_{CO} \cdot p_R}{R \cdot T_R} \quad (eq.S25)$$

On this basis a TOF of **0.03 s<sup>-1</sup>** can be calculated for the experimental conditions applied (0.01 vol% CO, p<sub>R</sub> = 1 bar, 30°C). Notably, this value represents a lower limit for two reasons. First of all, not all surface sites are necessarily catalytically active – most likely it is only a fraction. In case of CO, for instance, it has been shown that the molecule is primarily adsorbed at defect sites providing much higher binding energies than surface atoms on the ideal (111) surface (see Introduction of main text). Secondly, the assumed (111) surface constitutes the most densely packed plane in case of a fcc metal and, even though such surface orientations were indeed abundantly observed on the ligaments of npAu in certain areas, they overall were found to only constitute a fraction of their curved surfaces.

## 8. Literature overview for low temperature CO oxidation over npAu

CO oxidation over npAu at or around 30°C was quite intensively studied in the past so that it is apt to compare the catalytic activity determined in this study and disentangled from mass transport effects with other values previously reported. Table S2 shows a broad overview of corresponding work – including all relevant experimental parameters - that has appeared in the literature since 2006, when the very first results were published for this novel catalytic Au material. Only in some instances, diffusion limitations obscuring the micro kinetical potential can be excluded as very thin npAu samples were used (made out of white gold leaf). In all other cases, their unknown influence and a correspondingly reduced efficiency could be one reason for the lower activities observed. Furthermore, it remains unclear whether all npAu catalysts were catalytically fully activated. As pointed out in the Introduction of the main text, a reliable and reproducible standard activation protocol assuring the achievement of highest conversion levels was not established until recently so that various and differing approaches were tried. Thus, varying degrees of activation might also be responsible for the scatter that becomes obvious in the synopsis of the data in Tab. S2.

**Table S2:** Overview over kinetic data reported in the literature regarding low-temperature CO oxidation over npAu

Publication		Sample characteristics <sup>1)</sup>					Reaction conditions							Catalytic results			
Ref.	Year	Type	h / $\mu\text{m}$	d <sub>l</sub> / $\text{nm}^2$	A <sub>m</sub> <sup>3)</sup> / $\text{g m}^{-2}$	x <sub>Ag</sub> <sup>4)</sup> / %	m <sub>cat</sub> <sup>5)</sup> / mg	T <sub>R</sub> / °C	p <sub>R</sub> / mbar	Q <sub>T</sub> <sup>°</sup> / $\text{Nml/min}$	x(CO) / vol%	x(O <sub>2</sub> ) / vol%	Carrier gas	X <sup>6)</sup> / %	r <sub>m</sub> <sup>7)</sup> / $\text{mol g}^{-1} \text{s}^{-1}$	r <sub>A</sub> <sup>8)</sup> / $\text{mol m}^{-2} \text{s}^{-1}$	TOF <sup>9)</sup> / $\text{s}^{-1}$
[12]	1975	-	-	10	1	-	-	22	333	-	15	15	He	2	1.4·10 <sup>-7*</sup>	1.7·10 <sup>-7*</sup>	0.01
[13]	2006	m	300	40	4	1	80	23	1000	15	4	77	N <sub>2</sub>	73	4.0·10 <sup>-6*</sup>	1.1·10 <sup>-6*</sup>	0.07
[14]	2007	p	25	6	30	-	20	25	1000	67	1	10	N <sub>2</sub>	99	2.4·10 <sup>-5*</sup>	8.1·10 <sup>-7*</sup>	0.05
[9]	2009	m	200 - 300	30 - 50	4	1	22	30	1000	50	4	20	He	28	1.9·10 <sup>-5*</sup>	5.2·10 <sup>-6*</sup>	0.32
[15]	2011	p	25	30 - 35	12*	1	20	25	1000	37	1	10	N <sub>2</sub>	5	6.7·10 <sup>-7*</sup>	5.8·10 <sup>-8*</sup>	0.004
[16]	2011	p	100	4	75	15	1	30	1000	60	1	1	N <sub>2</sub>	14	6.2·10 <sup>-5</sup>	5.8·10 <sup>-8*</sup>	0.05
[17]	2012	p	20 - 100	4-21	10 - 75	5-15	1 - 22*	30	1000	60	1	1	N <sub>2</sub>	15	3.0·10 <sup>-6</sup> - 9.2·10 <sup>-5</sup>	3.0·10 <sup>-7</sup> - 1.5·10 <sup>-6*</sup>	0.02 - 0.09
[18]	2013	p	25	8	30	1 - 5	20	20	1000	40	1	10	N <sub>2</sub>	44 - 93	6.5·10 <sup>-6</sup> - 1.4·10 <sup>-5*</sup>	2.2·10 <sup>-7</sup> - 4.6·10 <sup>-7*</sup>	0.01 - 0.03
[19]	2013	m	200 - 300	30 - 40	10	1	28**	50	1000	50	1	20	N <sub>2</sub>	77	1.0·10 <sup>-5*</sup>	1.0·10 <sup>-6*</sup>	0.06
[20]	2014	m	0.1	8	24*	-	15	30	1000	40	10	1	N <sub>2</sub>	90	1.8·10 <sup>-5*</sup>	7.4·10 <sup>-7*</sup>	0.05
[21]	2014	p	1 - 200	12 - 16	14	5	50	20-30	1000	50	2	2	He	100*	1.5·10 <sup>-5</sup> - 1.7·10 <sup>-5*</sup>	1.1·10 <sup>-6</sup> - 1.3·10 <sup>-6</sup>	0.07-0.08-
[22]	2017	m	250	64 - 78	10	-	-	40	1000	50	5	10	N <sub>2</sub>	-	2.0·10 <sup>-5</sup> - 4.5·10 <sup>-5</sup>	2.0·10 <sup>-6</sup> - 4.5·10 <sup>-6*</sup>	0.11 - 0.28
[23]	2018	m	100	15	12	4	455**	30	1000	910	1	10	N <sub>2</sub>	85	1.2·10 <sup>-5*</sup>	1.1·10 <sup>-6*</sup>	0.07

1) Typically, disc-shaped monolithic samples (type: m) with high aspect ratios were employed the diameter d<sub>disc</sub> of which was much larger than their thickness h. Where powders (type: p) were employed, h denotes the particle size.

2) Mean ligament diameter as specified in the publication.

3) Specific surface area as given in the ref. or calculated (\*) based on eq. S18.

4) Residual (bulk) silver content (at%) as specified in the publication.

5) Mass of nanoporous Gold used in the experiment as detailed in the ref. or calculated from reaction conditions and steady-state rate per mass (\*) or the geometry of the specimen (\*\*).

6) Conversion of carbon monoxide as detailed in the ref. or calculated from reaction conditions and rate per mass (\*).

7) Rate per mass as stated in the ref. or calculated from reaction conditions (\*).

8) Rate per area as stated in the ref. or calculated from the specific surface area and the rate per mass (\*).

9) TOF as stated in the ref. or calculated from eq S25 (\*).

## References

- [1] J. Kärger, D.M. Ruthven, D.N. Theodorou, *Diffusion in Nanoporous Materials*, 2012. <https://doi.org/10.1002/9783527651276>.
- [2] J. van Brakel, P.M. Heertjes, Analysis of diffusion in macroporous media in terms of a porosity, a tortuosity and a constrictivity factor, *Int. J. Heat Mass Transf.* 17 (1974) 1093–1103. [https://doi.org/10.1016/0017-9310\(74\)90190-2](https://doi.org/10.1016/0017-9310(74)90190-2).
- [3] A. Ledesma-Durán, S.I. Hernández, I. Santamaría-Holek, Relation between the porosity and tortuosity of a membrane formed by disconnected irregular pores and the spatial diffusion coefficient of the Fick-Jacobs model, *Phys. Rev. E.* 95 (2017) 1–10. <https://doi.org/10.1103/PhysRevE.95.052804>.
- [4] E.E. Petersen, Diffusion in a pore of varying cross section, *AIChE J.* 4 (1958) 343–345. <https://doi.org/10.1002/aic.690040322>.
- [5] R.N. Viswanath, V.A. Chirayath, R. Rajaraman, G. Amarendra, C.S. Sundar, Ligament coarsening in nanoporous gold: Insights from positron annihilation study, *Appl. Phys. Lett.* 102 (2013). <https://doi.org/10.1063/1.4812290>.
- [6] J.O. Hirschfelder, C.F. Curtiss, R.B. Bird, *Molecular Theory of Gases and Liquids*, Wiley & Sons Ltd, 1954.
- [7] D.F. Fairbanks, C.R. Wilke, Diffusion Coefficients in Multicomponent Gas Mixtures, *Ind. Eng. Chem.* 42 (1950) 471–475. <https://doi.org/10.1021/ie50483a022>.
- [8] M. Baerns, *Technische Chemie*, 2005. <https://doi.org/10.1007/3-540-28887-2>.
- [9] A. Wittstock, B. Neumann, A. Schaefer, K. Dumbuya, C. Kübel, M.M. Biener, V. Zielasek, H.P. Steinrück, J.M. Gottfried, J. Biener, A. Hamza, M. Bäumer, Nanoporous Au: An unsupported pure gold catalyst?, *J. Phys. Chem. C.* 113 (2009) 5593–5600. <https://doi.org/10.1021/jp808185v>.
- [10] E. Detsi, E. De Jong, A. Zinchenko, Z. Vuković, I. Vuković, S. Punzhin, K. Loos, G. Ten Brinke, H.A. De Raedt, P.R. Onck, J.T.M. De Hosson, On the specific surface area of nanoporous materials, *Acta Mater.* 59 (2011) 7488–7497. <https://doi.org/10.1016/j.actamat.2011.08.025>.
- [11] J.W. Anthony, R.A. Bideaux, K.W. Bladh, M.C. Nichols, eds., *Handbook of Mineralogy*, Mineralogical Society of America, Chantilly, 2003.
- [12] N.W. Cant, P.W. Fredrickson, Silver and gold catalyzed reactions of carbon monoxide with nitric oxide and with oxygen, *J. Catal.* 37 (1975) 531–539. [https://doi.org/10.1016/0021-9517\(75\)90188-8](https://doi.org/10.1016/0021-9517(75)90188-8).
- [13] V. Zielasek, B. Jürgens, C. Schulz, J. Biener, M.M. Biener, A. V. Hamza, M. Bäumer, Gold catalysts: Nanoporous gold foams, *Angew. Chemie - Int. Ed.* 45 (2006) 8241–8244. <https://doi.org/10.1002/anie.200602484>.
- [14] C. Xu, X. Xu, J. Su, Y. Ding, Research on unsupported nanoporous gold catalyst for CO oxidation, *J. Catal.* 252 (2007) 243–248. <https://doi.org/10.1016/j.jcat.2007.09.016>.
- [15] D.Q. Han, C.Q. Zhou, H.M. Yin, D.J. Zhang, X.H. Xu, Reactivity of the alkaline pretreated nanoporous gold for the CO oxidation, *Catal. Letters.* 141 (2011) 1026–1031. <https://doi.org/10.1007/s10562-011-0619-x>.
- [16] L.C. Wang, H.J. Jin, D. Widmann, J. Weissmüller, R.J. Behm, Dynamic studies of CO oxidation on nanoporous Au using a TAP reactor, *J. Catal.* 278 (2011) 219–227. <https://doi.org/10.1016/j.jcat.2010.12.007>.
- [17] L.C. Wang, Y. Zhong, D. Widmann, J. Weissmüller, R.J. Behm, On the Role of Residual Ag in Nanoporous Au Catalysts for CO Oxidation: A Combined Microreactor and TAP Reactor Study, *ChemCatChem.* 4 (2012) 251–259. <https://doi.org/10.1002/cctc.201100297>.
- [18] D. Li, Y. Zhu, H. Wang, Y. Ding, Nanoporous gold as an active low temperature catalyst toward CO oxidation in hydrogen-rich stream., *Sci. Rep.* 3 (2013) 3015. <https://doi.org/10.1038/srep03015>.
- [19] A. Wichmann, A. Wittstock, K. Frank, M.M. Biener, B. Neumann, L. Mädler, J. Biener, A. Rosenauer, M. Bäumer, Maximizing activity and stability by turning gold catalysis upside

- down: Oxide particles on nanoporous gold, *ChemCatChem*. 5 (2013) 2037–2043. <https://doi.org/10.1002/cctc.201200759>.
- [20] T. Fujita, T. Tokunaga, L. Zhang, D. Li, L. Chen, S. Arai, Y. Yamamoto, A. Hirata, N. Tanaka, Y. Ding, M. Chen, Atomic observation of catalysis-induced nanopore coarsening of nanoporous gold, *Nano Lett.* 14 (2014) 1172–1177. <https://doi.org/10.1021/nl403895s>.
- [21] T. Déronzier, F. Morfin, M. Lomello, J.L. Rousset, Catalysis on nanoporous gold-silver systems: Synergistic effects toward oxidation reactions and influence of the surface composition, *J. Catal.* 311 (2014) 221–229. <https://doi.org/10.1016/j.jcat.2013.12.001>.
- [22] C. Mahr, P. Kundu, A. Lackmann, D. Zanaga, K. Thiel, M. Schowalter, M. Schwan, S. Bals, A. Wittstock, A. Rosenauer, Quantitative determination of residual silver distribution in nanoporous gold and its influence on structure and catalytic performance, *J. Catal.* 352 (2017) 52–58. <https://doi.org/10.1016/j.jcat.2017.05.002>.
- [23] G. Pia, E. Sogne, A. Falqui, F. Delogu, Ag surface segregation in nanoporous Au catalysts during CO oxidation, *Sci. Rep.* 8 (2018) 1–9. <https://doi.org/10.1038/s41598-018-33631-4>.



## Publication III

**New perspectives for evaluating the mass transport in porous catalysts and  
unfolding macro- and microkinetics**

**Stefan Wild**, Christoph Mahr, Andreas Rosenauer, Thomas Risse,  
Sergey Vasenkov and Marcus Bäumer

*Catalysis Letters* **2022**.

<https://doi.org/10.1007/s10562-022-04218-6>



# New Perspectives for Evaluating the Mass Transport in Porous Catalysts and Unfolding Macro- and Microkinetics

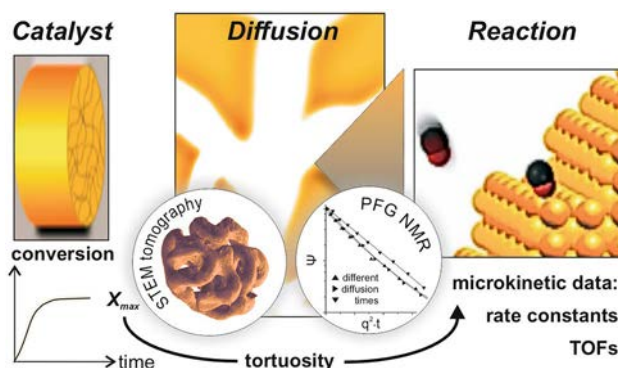
Stefan Wild<sup>1,2</sup> · Christoph Mahr<sup>2,3</sup> · Andreas Rosenauer<sup>2,3</sup> · Thomas Risse<sup>4</sup> · Sergey Vasenkov<sup>5</sup> · Marcus Bäumer<sup>1,2</sup>

Received: 27 October 2022 / Accepted: 11 November 2022  
© The Author(s) 2022

## Abstract

In this article we shed light on newly emerging perspectives to characterize and understand the interplay of diffusive mass transport and surface catalytic processes in pores of gas phase metal catalysts. As a case study, nanoporous gold, as an interesting example exhibiting a well-defined pore structure and a high activity for total and partial oxidation reactions is considered. PFG NMR (pulsed field gradient nuclear magnetic resonance) measurements allowed here for a quantitative evaluation of gas diffusivities within the material. STEM (scanning transmission electron microscopy) tomography furthermore provided additional insight into the structural details of the pore system, helping to judge which of its features are most decisive for slowing down mass transport. Based on the quantitative knowledge about the diffusion coefficients inside a porous catalyst, it becomes possible to disentangle mass transport contributions from the measured reaction kinetics and to determine the kinetic rate constant of the underlying catalytic surface reaction. In addition, predictions can be made for an improved effectiveness of the catalyst, i.e., optimized conversion rates. This approach will be discussed at the example of low-temperature CO oxidation, efficiently catalysed by npAu at 30 °C. The case study shall reveal that novel porous materials exhibiting well-defined micro- and mesoscopic features and sufficient catalytic activity, in combination with modern techniques to evaluate diffusive transport, offer interesting new opportunities for an integral understanding of catalytic processes.

## Graphical Abstract



**Keywords** Porous heterogeneous catalysts · Tortuosity factor · Diffusive mass transport · Catalyst effectiveness factors · Pulsed field gradient NMR · TEM tomography · Nanoporous gold

## 1 Introduction

In heterogeneous catalysis, a general problem arises from two conflicting demands. On the one hand, large surface areas are necessary to achieve sufficient conversion levels.

✉ Marcus Bäumer  
mbaumer@uni-bremen.de

Extended author information available on the last page of the article

Therefore, porous materials are used—typically as supports for finely-dispersed nanoparticulate catalysts but also in form of porous bulk catalysts [1]. On the other hand, however, high specific surface areas are affiliated with small pore diameters which, in turn, can cause mass transport limitations [2]. These can severely reduce the overall catalyst performance, when the diffusion of reactants and products to/from the catalytically active areas or sites on the catalyst's surface is slower than the actual surface reaction. A catalytic process, as operated in industry, for instance, is schematically sketched in Fig. 1. While on the reactor scale convection dominates and can be adjusted and optimized, at small scales diffusion is the only transport mechanism for reactants to access the surfaces of micropores and small mesopores [2]. In contrast to convection, the diffusive mass transport in such pores cannot be easily quantified even if the process conditions are well known. The diffusive mass transport depends on structural factors of the catalyst, pore wall-gas interactions, and the resulting diffusivities of the involved gases [2].

Apart from film diffusion at the outer surface of a catalyst particle, diffusion within the pore system is a major factor that affects mass transport and can limit the productivity [1]. On the one hand, Knudsen diffusion which is slower than diffusion in the bulk gas phase can contribute to this effect. It occurs when the pore diameters are smaller than the mean free path of the molecules so that collisions of gas molecules with the pore walls prevail over intermolecular collisions. On the other hand, the structural constitution of the pore system, being characteristic for a specific catalyst

material, can elongate the diffusive pathways and slow down the mass transport depending on the shape of the pores, their connectivity and pore size distribution [2].

Typically, the majority of porous catalysts exhibit mesopores in a range of a few 10 nm (see, Fig. 1). They ascertain a sufficiently large specific surface area while, at the same time, usually not posing too high diffusion resistances for the reaction gases. In cases where the catalyst preparation method allows deliberately introducing a certain number of additional macropores, hierarchically organized pore systems may be created, in which the latter take the role of “gateways” and act as distributors for the mesopore ensemble [3]. Micropores, hampering diffusion most but increasing the specific surface area substantially, occur material specific [4]. Zeolites, for instance, comprise them due to their crystallography [4], while in case of activated carbon [5] they are the result of the preparation process.

Yet, such a classification is not sufficient to estimate how severely diffusion limitations will degrade a catalyst's performance. To assess such impediments, as given by the specific type and the structural characteristics of a pore system, a quantity, called tortuosity  $\tau$ , was introduced which integrally quantifies to which degree diffusion in porous solids is slowed down in comparison to the bulk gas phase ( $\tau > 1$ ) [2]. A structurally more differentiated perspective takes into account that pathway elongations (due to non-straight, but tortuous pores) as well as strongly varying pore diameters or pore cross sections, respectively, can play a role. The latter aspect comes into play when locations in the pore system, where the pore diameters are minimal, represent “bottle

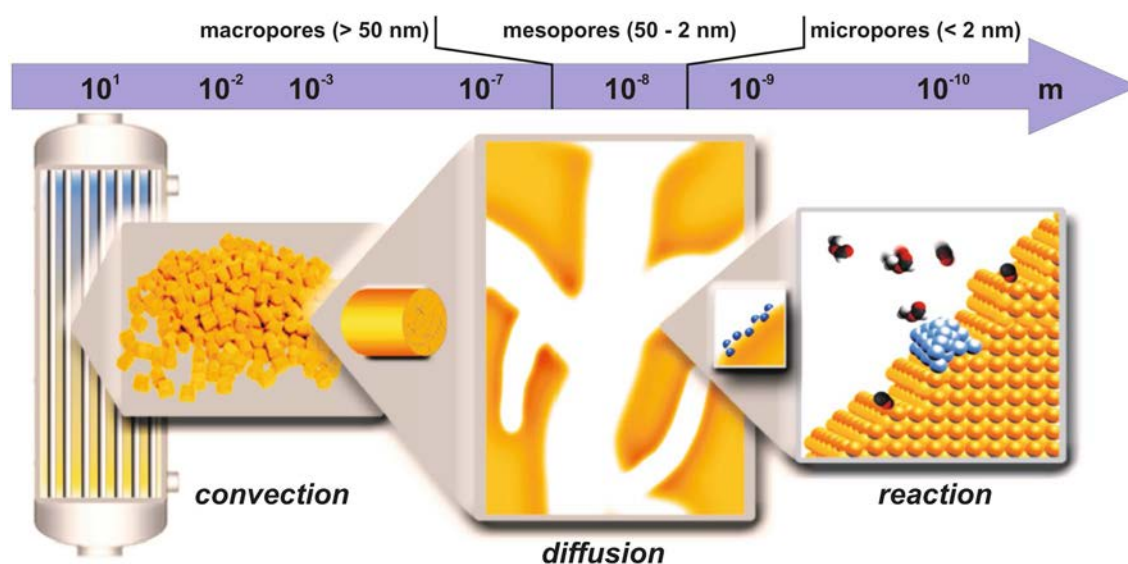


**Fig. 1** Schematic sketch of the various length scales which are important for catalytic processes; diffusive transport can be of relevance in the range between a few 100 nm and a few nm. In particular, within the pore network of porous catalysts mass transport is only accom-

plished in this way. Pores are classified into micropores (single molecule or confined diffusion), mesopores (Knudsen and molecular diffusion) and macropores (typically dominated by molecular diffusion), according to their diameter

necks” for the diffusing molecules which they have to overcome. On this basis, two parameters are needed to characterize the pore system: one, also called tortuosity in the literature, and another one, called constrictivity ( $\delta < 1$ ) [2].

Understanding and modelling transport processes in porous catalysts is an important topic under several perspectives, but not as much in the focus of fundamental research of the catalytic community as compared to questions regarding the catalytic surface reactions, i.e., the catalytic properties of a material. In practical applications, however, lower product yields caused by transport limitations will cut profits [6]. Accordingly, in corporate R&D (research and development) significant effort is undertaken to develop catalyst formulations that guarantee facile accessibility of the catalytically active areas or sites for the reactants and an optimized removal of the products.

But also in scientific studies, a quantitative consideration of mass transport contributions to the results of catalytic experiments is inevitable when, for instance, evaluating the catalytic properties of a novel material. Unless transport limitations can be avoided experimentally [7–9], measured conversions do not necessarily reflect the intrinsic catalytic activity, i.e., the maximum number of chemical turnovers which could (in principle) take place on a catalyst’s surface. In case the supply of reactants by diffusion is not fast enough, the apparent (observable) kinetics, also dubbed macrokinetics, will not represent the kinetics of the underlying catalytic surface reactions, called microkinetics in the following [10]. Aiming at characterizing and quantifying the latter, data about the diffusion within the catalyst is needed to be able to extract this information from the experimental results [11].

In 1939, Ernest W. Thiele proposed a concept which allows quantitatively assessing the influence of mass transport limitations on heterogeneously catalyzed reactions [12]. To this end, he introduced a dimensionless number, later called Thiele modulus, which unites all relevant quantities. Apart from a length characterizing the macroscopic geometry of the catalyst particles used and reflecting the relevant dimension for the diffusion profiles, it contains the ratio of the microkinetic rate constant and the effective diffusion coefficient within the porous material [1]. Using this well-established concept, it is possible not only to calculate the reduction of the catalyst’s effectiveness due to mass transport limitations in a straightforward and elegant fashion, but also to optimize transport properties and, in turn, the yield of products based on predictions or simulations, respectively [13].

A problem, however, often existing in this context relates to missing knowledge about those porosity-related features of a material, which determine gas diffusivities within its pore system. Basically, two experimental options are available to get such information: (i) STEM (scanning

transmission electron microscopy) tomography [14–17] as well as related techniques and, (ii) techniques capable of microscopic diffusion measurements, such as pulsed field gradient nuclear magnetic resonance (PFG-NMR [2, 18]). While (i) is based on 3D reconstructions of the mesoscopic pore structure, from which these quantities can be numerically derived or estimated, (ii) allows to measure the diffusion of gas molecules within the pores directly. Over the last years, both methodologies have revealed an outstanding potential and helped to lay the foundation for a quantitative understanding of mass transport processes in porous matter, as will become obvious in this perspective article.

Particularly interesting in this context are materials with well-defined and homogeneous pore structures, guaranteeing identical or similar diffusion throughout a catalyst particle. Since modern materials science, and especially the realm of nanotechnological structuring options has borne a wealth of novel approaches to prepare porous catalysts with tailored properties, such materials become increasingly available [19]. In addition, if the catalytic surface properties do not change at different locations within the pore system, fascinating new opportunities result that allow maximizing catalytic activity and minimizing transport limitations, i.e., optimizing the productivity of a catalyst.

To illustrate this aspect, we will revert in this article to nanoporous gold (npAu) as a case study [20]. This novel skeletal metal catalyst has attracted considerable attention over the last years [21–25], after its high catalytic activity for total as well as partial oxidation reactions at low temperatures was discovered in 2006 and 2010, respectively [26–28]. Exhibiting a well-defined and tunable mesoporosity, npAu is particularly well-suited to disentangle the microkinetics and the mass transport properties if reactivity measurements are combined with techniques to quantify diffusion properties, i.e., PFG NMR and (S) TEM tomography.

After briefly introducing npAu and its structural characteristics, we will shed light on the following topics—each presented in an own section of this article:

- Dependence of the specific surface area on the mean ligament size in case of well-ordered pore structures
- Diffusion of gases and gas mixtures in porous matter
- Direct measurement of gas diffusivities in porous materials by PFG NMR
- Determination of tortuosities by STEM tomography
- Relationship between macro- and microkinetics
- Optimization of a catalyst’s performance by reducing mass transport limitations

## 2 Nanoporous Gold as a Prototype of a Well-Defined Porous Metal Catalyst

Although in heterogeneous catalysis the main class of porous materials applied are oxides (used as supports for noble metal catalysts e.g.), also porous metals belong to the portfolio of industrially employed catalysts [1]. A prominent example of that kind is Raney nickel, which is synthesized by leaching Al out of a NiAl alloy under alkaline conditions [29]. As a result, a powder is obtained consisting of porous Ni particles. Nanoporous gold is actually prepared in a similar way, namely by leaching a less noble metal out of an Au containing alloy, such as AuAg. In contrast to Raney nickel, however, the process is carried out in an acid. The corrosion process, often called dealloying, can be performed with or without control of the electrochemical potential, utilizing a potenti- or galvanostatic setup [30, 31]. Under purely chemical conditions, the process is referred to as free corrosion and is particularly easy to carry out practically. Upon submersing an AuAg alloy specimen containing between 60 and 80 at% Ag—for instance in form of a thin disc (several mm in diameter and a few 100 microns in thickness)—in conc.  $\text{HNO}_3$ , almost all Ag is leached out of the material

over a time period of 12–24 h (resulting in residual Ag bulk contents of typically  $\leq 1$  at% [30]).

During the process, where Ag is continuously removed from the solid and dissolved as  $\text{Ag}^+(\text{aq})$ , Au surface atoms become mobile and diffuse from and to step edges [32, 33]. In this way, large structural rearrangements are evoked which are accompanied by the concomitant formation of void spaces, gradually resulting in extended pores [32, 33]. When the dealloying process finally comes to an end, a highly porous bi-continuous nanostructure is formed, comprising ligaments and pores in the mesoporous regime (5–50 nm). In contrast to Raney nickel, the material does not break up into small particles during the synthesis so that monoliths are obtained, exhibiting the shape and grain structure of the original alloy specimen [34]. The pore systems found in these monoliths are structurally homogenous, as can be inferred from Fig. 2, showing an exemplary SEM micrograph acquired at the outer surface of a disc-shaped sample. Typically, the same porosity is observed throughout the material, i.e., also in the interior of such a npAu disc [35].

The ring-shaped feature in the 2D Fourier transformation of the SEM picture (see also ref. [36] in this context), which is also depicted in Fig. 2 (2D FFT, bottom left), indicates that

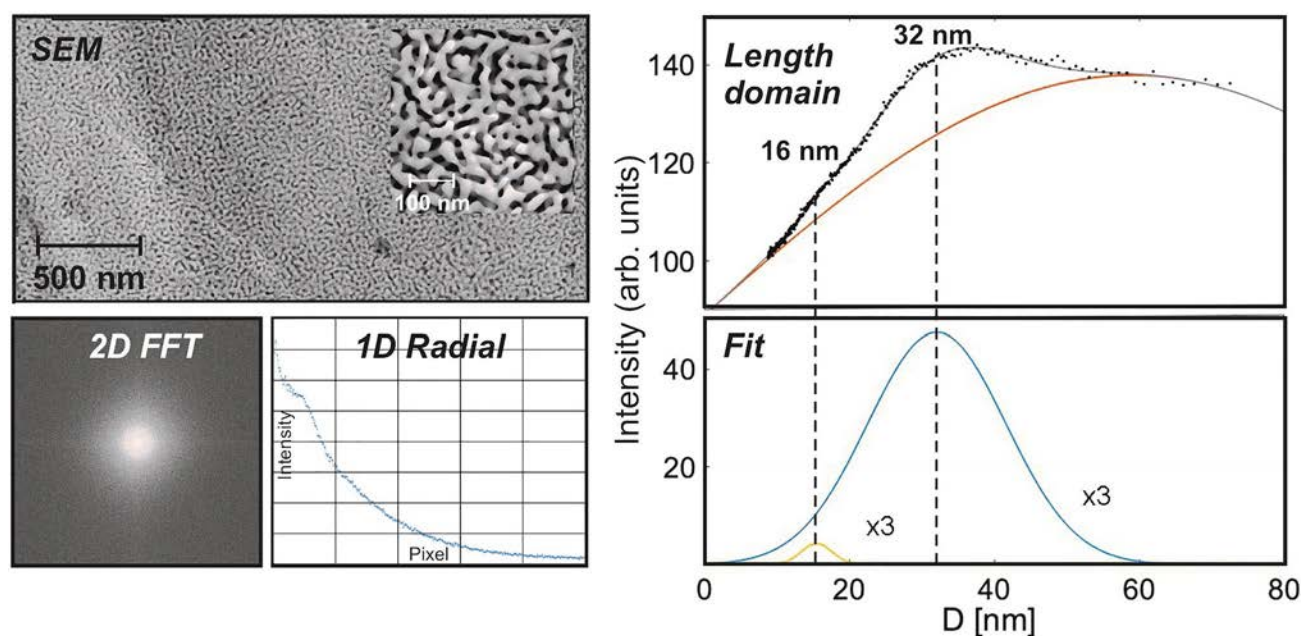


**Fig. 2** Structural characterization of npAu (prepared by free corrosion) and evaluation of mean pore and ligament sizes: To this end, the SEM micrograph (top left) is Fourier transformed. The 2D (spatial) frequency domain reveals the isotropy of the pore structure (bottom left) and can be radially integrated (bottom middle). Converted back into the length domain (top right) and fitted (bottom right), two maxima can be discerned—in addition to a broad background. These can be assigned to the mean value of the distance from ligament to

ligament (i.e., the sum of ligament and pore diameter) in case of the pronounced maximum (at 32 nm) and to the individual values of pore and ligament size, respectively, in case of the small maximum (at 16 nm), indicating that the latter are identical. (In contrast, the broad background, exhibiting a maximum around 60 nm, is likely to originate from periodicities perpendicular to the pore/ligament diameters, i.e., is related to the ligament lengths.)

the structure is spatially isotropic. After radially integrating the 2D FFT image (Fig. 2, bottom middle) and converting the x-axis from reciprocal values to distances in real space again (Fig. 2, top right), the resulting curve reveals periodically occurring lengths. In case of the example presented in Fig. 2, two maxima are discernible. The more pronounced one at 32 nm is ascribable to the mean value of ligament plus pore sizes, which is the prominent distance occurring in the pore structure. The less intense maximum corresponds to half of this value (16 nm). Based on the observation that the average ligament and pore diameters are typically identical for npAu [37, 38], it can be assigned to the individual values, i.e., the mean pore and ligament size.

For as-prepared samples (free corrosion), typically ligament sizes between 20 and 50 nm are obtained [30, 31]. It is worth noting, however, that the initial ligament diameter can also be increased (up to several 100 nm) by subsequently annealing the material in a controlled fashion [39]. Interestingly and characteristic of npAu, the thermally induced coarsening takes place without a change of the shape and the connectivity of ligaments and pores [39]. In this way, npAu samples with differing mean pore sizes but self-similar pore systems can be generated [37, 40–42], illustrating what has been alluded to already in the Introduction—namely options to tailor catalytic materials based on knowledge from materials science.

As will be shown in the following sections, catalysts, such as npAu, which can be prepared with a well-defined and spatially homogeneous pore structure ensure predictable surface areas and conditions for diffusive transport. Furthermore, identical or similar surface and thus catalytic properties can be expected under these circumstances throughout the material. This perspective article aims at elucidating that and how such features lay the foundation for a meaningful disentanglement of macro- and microkinetics as well as for an understanding and description of the catalytic process as a whole [43].

NpAu has been chosen as a case study in this context because of its ability to efficiently catalyze total oxidations as well as partial oxidations under aerobic conditions. The first studies reporting high activity for CO oxidation at room temperature and even below attracted attention as this observation was unexpected—taking into account that supported Au nanoparticles, which have been studied already since the 1980's [44], show activity only in a very narrow range of sizes (a few nm), being an order of magnitude smaller than npAu's ligaments. Without going into details here—the interested reader is referred to a number of extensive and excellent reviews on this topic [20, 22, 23, 25]—npAu's

catalytic potential arises from a combination of different features. On one hand, it comprises a high density of low-coordinated surface atoms making up as much as a fifth (20%) of all surface atoms [45]. For CO as an adsorbate, for instance, it has been shown that it can bind there much more strongly than on regular Au sites [46, 47]. Adsorption energies between 0.4 and 0.6 eV were experimentally determined and theoretically predicted [46], as compared to a value of 0.3 eV which was calculated for an ideal Au (111) surface [48]. On the other hand, residual silver remaining in the material after dealloying is found at the surface in concentrations which are up to an order of magnitude larger than in the bulk of the ligaments [49, 50]. Various theoretical studies provided ample evidence that Ag plays an important part for the oxidation reactions taking place on the surface of npAu (see e.g. ref. [51]). Since binding of molecular oxygen on Au is too weak to allow for its dissociative adsorption, it was concluded that Ag incurs the role of an oxygen activating species. Even though it has not been finally clarified whether metallic silver areas, bimetallic ensembles or oxidic Ag species are responsible, it seems clear that the two metals interact synergistically in the catalytic cycles on the surface.

Within this perspective article, we will focus on low-temperature CO oxidation, since former studies revealed a comparatively simple reaction kinetics in this case which facilitates the following discussion. Specifically, a reaction order of  $\sim 1$  was found for CO and one close to zero for oxygen [24, 52], suggesting that the supply of oxygen on the surface is distinctly faster than the supply of CO so that the former is kinetically not relevant. Since the Thiele formalism predicts that a reaction order of 1 does not change under mass transport limiting conditions (for other reaction orders this is not the case), for both, the macro- ( $r_{macro}$ ) and the microkinetics ( $r_{micro}$ ), a rate law of 1st order can be assumed which just depends on the partial pressure of CO ( $p(CO)$ ):

$$r_{micro} = k_V \cdot p(CO) = k_A \cdot A_V \cdot p(CO) \quad (1)$$

$k_V$ : rate constant related to volume,  $k_A$ : rate constant related to catalytic surface area  $A$ ,  
 $A_V$ : specific surface area per volume,  $p(CO)$ : CO partial pressure

In the context of heterogeneously catalyzed reactions, it has to be taken into account that, while in standard kinetics rate laws are typically based on volume-related rate constants  $k_V$  ( $\text{mol}/(\text{m}^3 \cdot \text{s})$ ), the use of rate constants related to the surface area of the catalyst  $A$  is more appropriate in the former case ( $k_A$  ( $\text{mol}/(\text{m}^2 \cdot \text{s})$ ), see Eq. 1). Both are connected by the specific surface area  $A_V$  per volume catalyst ( $\text{m}^2/\text{m}^3 = 1/m$ ; see also next section).

### 3 Dependence of the Specific Surface Area on the Ligament Size in Case of Well-Ordered Pore Structures

The specific surface area  $A_m$  per mass ( $\text{m}^2/\text{g}$ ) is an important characteristic feature of a porous catalyst. Experimental techniques to determine it are physisorption measurements (with  $\text{N}_2$  or Ar) or cyclic voltammetry (CV). Both of them, however, are associated with certain limitations. In the first case, rather large amounts of the material are needed, since the minimum total surface area required for meaningful results lies in the range of  $1 \text{ m}^2$ . For npAu exhibiting specific surface areas of  $3\text{--}10 \text{ m}^2/\text{g}$ , for example, several 100 mg of the material are needed. Accordingly, such measurements were seldom done. In the second case, the electrochemically determined surface area in liquid phase does not necessarily reflect the one which is relevant for gas phase reactions. Ref. [53] summarizes results obtained for npAu with both techniques.

An attractive alternative for ordered and homogeneous pore systems, which spares regular experimental characterizations, was recently proposed in the literature [54]. It is based on the derivation of specific surface areas from structural parameters, specifically from the mean diameter  $d_L$  of the ligaments, constituting the pore system. As this novel approach allows for an elegant and unified analysis of the interplay of mass transport and catalysis in case of such materials, we briefly discuss the underlying considerations in the following.

The specific surface area  $A_m$  is defined as the ratio of the assessable surface area  $A$  and the mass  $m$  of a specimen and is related to  $A_V$ , i.e., the surface area per volume  $V$  in the following way:

$$A_m = A/m = A/V \cdot \rho_p = A_V/\rho_p \quad (2)$$

Here,  $\rho_p$  denotes the mass density of the porous material which is equivalent to the mass density  $\rho$  of the bulk material (in case of npAu: the mass density of Au) multiplied with the material filled fraction. This fraction equals to 1 minus the void fraction, which, in turn, is given by the porosity  $\phi$ :

$$\rho_p = (1 - \phi) \cdot \rho \quad (3)$$

If pore systems are comprised of recurring structural motifs, they can be described as a periodic arrangement of identical elementary cells. Strictly speaking, this requirement, of course, is only fulfilled for crystalline porous materials, such as zeolites e.g., but principally also met by homogeneous self-similar structures, as given for npAu, where small partial volumes already reflect the pore system in total as far as pore diameters, pore shapes and the pore connectivity are concerned. In this case, the material can also be envisioned to consist of periodic cells exhibiting

identical surface areas and the same specific surface area than the whole pore system. In other words, it is sufficient to consider such a unit cell to assess  $A_m$  and  $A_V$  instead of a macroscopic specimen [54].

To this end, let us assume that such cells are cubic and have an edge length  $a$ . In this case, their volume is given by  $a^3$ . When furthermore assuming cylindrical ligaments making up the material-filled fraction within the cell, their surface area must be proportional to  $r_L \cdot L_L$  or  $d_L \cdot L_L$ , respectively, with  $r_L$  and  $d_L$  denoting their radius and diameter, respectively, and  $L_L$  their total length. As the ligaments of all cells need to be connected to jointly constitute the pore system of the material,  $L_L$  needs to be correlated with  $a$  (i.e.:  $L_L \sim a$ ). In turn, for  $A_V$  the following proportionality can be derived:

$$A_V \sim \frac{d_L \cdot L_L}{a^3} \sim \frac{d_L \cdot a}{a^3} = d_L/a^2. \quad (4)$$

This expression can be simplified further: since the material-filled volume of an elementary cell is given by  $(1 - \phi) \cdot V = (1 - \phi) \cdot a^3$  and, at the same time, is proportional to the volume of the cylindrical ligaments i.e.  $d_L^2 \cdot L_L \sim d_L^2 \cdot a$ , it follows:

$$(1 - \phi) \cdot a^3 \sim d_L^2 \cdot a \Leftrightarrow a \sim 1/\sqrt{1 - \phi} \cdot d_L \quad (5)$$

meaning that, for a given porosity,  $a$  and  $d_L$  are actually related to each other. Accordingly, Eq. 4 can be rewritten as:

$$A_V \sim \frac{1 - \phi}{d_L} \text{ or } : A_V = \zeta \cdot \frac{1 - \phi}{d_L} \quad (6)$$

showing that the (assumed) size of the unit cell  $a$  finally drops out of the equation. To convert the relation into an equation, a proportionality constant  $\zeta$  was introduced in Eq. 6. Using furthermore Eqs. 2 and 3, for the specific surface area  $A_m$  the following formula finally results:

$$A_m = \frac{A_V}{\rho_p} = \frac{\zeta \cdot (1 - \phi)}{d_L \cdot \rho_p} = \frac{\zeta \cdot (1 - \phi)}{d_L \cdot (1 - \phi) \cdot \rho} = \frac{\zeta}{d_L \cdot \rho} \sim \frac{1}{d_L} \quad (7)$$

Accordingly,  $A_m$  is directly proportional to the inverse (mean) ligament diameter. The constant  $\zeta$  is material specific and depends on the type of pore structure under consideration. Examples and associated values of  $\zeta$  are given in ref. [54] and can range between  $\sim 0.5$  and  $\sim 6$ .

In case of npAu, it can be taken advantage of the fact that ligament ( $d_L$ ) and the pore diameters ( $d_p$ ) are typically equal (see section above) so that also the latter can be used for the calculation instead of the former [38]. The constant  $\zeta$  of npAu was determined on the basis of experimentally measured values for  $A_m$  by Detsi et al. Their obtained value of 3.7 indicates that npAu's porosity is similar to a so-called

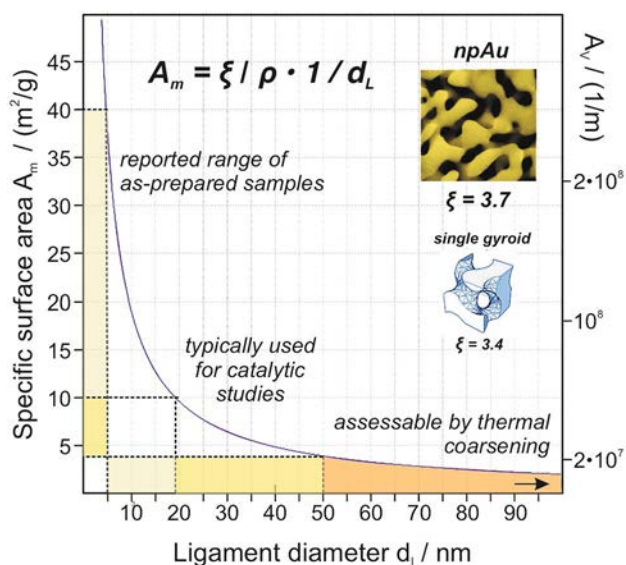


**Fig. 3** Dependence of the specific surface areas  $A_m$  and  $A_v$  on the mean ligament diameter, according to Eq. 7. For the majority of catalytic studies published in literature, npAu catalysts were used which exhibited ligament diameters between ~20 and 50 nm. For this size range surface areas between ~4 and 10  $\text{m}^2/\text{g}$  are expected. Larger ligament sizes can be obtained by subsequent thermal coarsening; in this case, however, the surface areas are typically too small for catalytic applications. The constant  $\zeta$  determined for npAu resembles that of a single gyroid structure, suggesting a certain comparability of the pore arrangements

(single) gyroid pore structure (see, Fig. 3 and Ref. [54]). Figure 3 shows  $A_m$  as a function of the ligament diameter as derived from Eq. 7. The plot reveals that catalytically interesting surface areas between 4 and 10  $\text{m}^2/\text{g}$  are achievable for ligament sizes of npAu lying between 5 and 50 nm, i.e., for values which can be obtained with established preparation protocols in a controllable fashion [55].

#### 4 Diffusion of Gases and Gas Mixtures in Porous Matter

As pointed out in the Introduction, the porosity of a heterogeneous catalyst does not only determine its specific surface area but also the mass transport within the material. Since the supply of reactants needs to take place via diffusion, which is restricted as compared to the bulk gas phase, the structural confinements posed by the porous system will play a role. These take effect in two different ways. On the one hand, collisions with the pore walls prevail over molecule–molecule interactions when the pore diameters fall below the mean free path of the molecules in the bulk phase. Around atmospheric pressure, this transition typically occurs in the mesoporous range and leads to Knudsen diffusion. On the other hand, the tortuous pore system only allows certain

pathways for the diffusing gas molecules, resulting in longer distances to be overcome [2].

The first aspect can be dealt with comparatively easily. As the Knudsen diffusion coefficient only depends on the confining dimensions of the medium (and the molecular mass of the gas) and not on the gas environment (and its composition), it can be calculated based on kinetic gas theory [2]:

$$D_K = \sqrt{\frac{8 \cdot d_p^2 \cdot R \cdot T}{9 \cdot \pi \cdot M}} \quad (8)$$

$T$ : temperature,  $M$ : molecular weight of the gas,  $d_p$ : (mean) pore diameter.

In case molecular diffusion—characterized by the molecular diffusion coefficient  $D_M$ —is also contributing, the resulting total diffusion coefficient  $D_T$ , influenced by both mechanisms, is assessable by reverting to the so-called Bosanquet equation [2, 56]:

$$D_T = \left( \frac{1}{D_M} + \frac{1}{D_K} \right)^{-1} \quad (9)$$

Figure 4 shows  $D_T$  of CO—taken as an example in view of the case study discussed in this article (low-temperature CO oxidation over npAu)—as a function of the pore diameter  $d_p$  at 25 °C and a pressure of 1 bar, i.e., for conditions under which most of the catalytic studies published in literature so far [43] were carried out. For pore sizes of 20–50 nm, representing typical values for npAu samples used in such experiments, the plot reveals that Knudsen rather than molecular diffusion dominates. Since the latter inversely depends on the pressure (according to simple kinetic gas theory), the molecular diffusion coefficient decreases at higher pressures. If it becomes significantly smaller than  $D_K$ ,  $D_T$  approaches  $D_M$ . At 15 bar, for example, where the PFG NMR measurements discussed in the next section were performed, this is the case as  $D_M$  is only about half as large as  $D_K$ .

Under catalytic reaction conditions, of course, not only one gas species but also other molecules are present in the gas phase. In contrast to  $D_K$ , the resulting molecular diffusion coefficient  $D_{M,mix}$  is then dependent on the composition of the gas phase, according to [57]:

$$D_{M,mix,i} = \frac{1 - \chi_i}{\sum_{j \neq i} \frac{\chi_j}{D_{M,i,j}}} \quad (10)$$

$\chi_i$ : molar fraction of gas  $i$

Here,  $D_{M,i,j}$  represent the binary diffusion coefficients which, in turn, can be calculated on the basis of the individual ones via [2]:



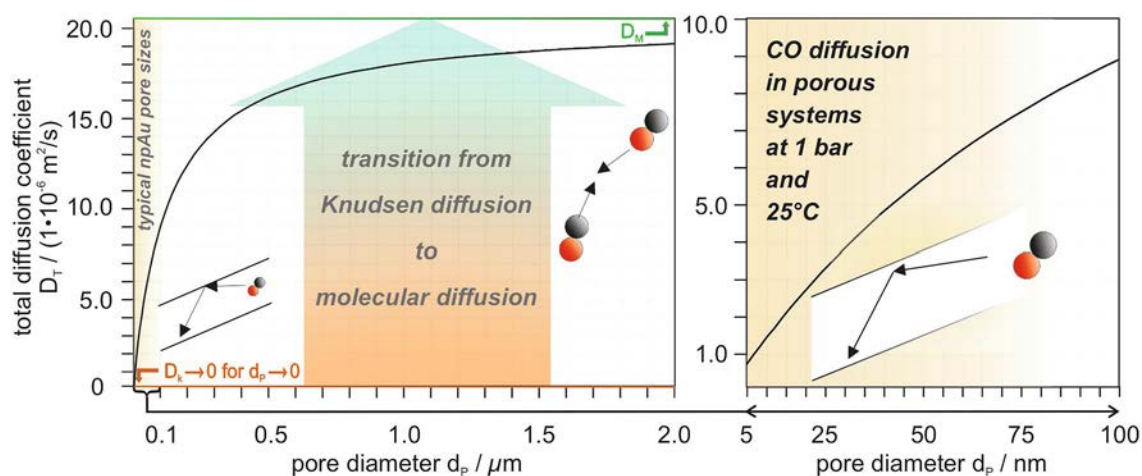


**Fig. 4** Dependence of the total diffusion coefficient  $D_T$  (Eq. 9) of CO on the pore diameter  $d_p$  when diffusing in a porous material at 1 bar and 25 °C. For large pore diameters (see left panel),  $D_T$  approaches  $D_M$ , i.e., the molecular diffusion coefficient ( $20.4 \cdot 10^{-6} \text{ m}^2/\text{s}$ , green line), determined by intermolecular collisions. For pore diameters

being significantly smaller than the mean free pathway in the bulk gas phase (see right panel),  $D_T$  can be up to an order of magnitude smaller and is mostly determined by Knudsen diffusion. For 1 bar and 25 °C, this situation is given in case of the pore diameters typically occurring for as-prepared npAu samples

$$D_{M,i,j} = \left( \frac{1}{D_{M,i}} + \frac{1}{D_{M,j}} \right)^{-1} \quad (11)$$

Equations 10 and 11 predict that in the presence of a gas component in large excess the molecular diffusion coefficients of all other components will approach the value of this species, in particular if its molecular weight is distinctly smaller. Such a situation is often given in catalytic lab experiments, where a carrier gas, such as He (see below) makes up the major part of the gas feed.

While for Knudsen diffusion basically only the (mean) pore diameter is decisive, more material-specific impediments result from the structural details of the pore system. To characterize this contribution, a quantity, called tortuosity  $\tau$  was introduced in the literature as the factor by which diffusion of a gas molecule is slowed down as compared to straight pores [2]:

$$D_E = \frac{1}{\tau} \cdot D_T \Leftrightarrow \tau = \frac{D_T}{D_E} \quad (12)$$

Accordingly,  $\tau$  represents the ratio of  $D_T$ —comprising already the influence of Knudsen diffusion—and the effective, i.e., actual diffusion coefficient  $D_E$  within the porous material. In this way, it is a means allowing to quantify the impact of the pore shapes, their spatial arrangement and their connectivity in an integral fashion. To this end, it is important that the diffusing molecules do not “stick” to the pore surfaces, meaning that molecule-pore wall interactions can essentially be described as hard-core repulsive interactions.

Aiming, however, at a more physical and more structure-specific interpretation, two factors slowing down the mass

transport should be differentiated between: the effect of longer diffusive pathways within the porous material and the effect of pore size variations [58]. The importance of the latter aspect becomes apparent when taking into account that locations where the pore diameters become significantly smaller than their average may act as “bottle necks” for the diffusing molecules which are difficult to pass. A quantity introduced to consider this impact is the so-called constrictivity  $\delta$  ( $0 < \delta < 1$  [59]), while contributions resulting from pathway elongations are subsumed in a separate number, unfortunately also called tortuosity in the literature, but denoted  $\tau'$  in the following. On these grounds, the relation between  $D_E$  and  $D_T$  can alternatively expressed by [60, 61]:

$$D_E = \frac{\delta}{\tau'^2} \cdot D_T \quad (13)$$

In line with this more physical approach,  $\tau'$  enters Eq. 13 squared. It is easily comprehensible that a molecule can take different (porous) pathways, when diffusing along a pore and reaching a pore node. The larger the angle  $\theta$ , by which the molecule is redirected when moving forward along one of them, the larger the additional diffusion length to be overcome as compared to a straight trajectory. Quantitatively, the elongation increases by  $1/\cos(\theta)$ . In addition, their statistical probability plays a role which also scales with  $1/\cos(\theta)$ , finally resulting in a  $1/\cos^2(\theta) \sim \tau'^2$  dependence.

In contrast, the constrictivity bears on the diffusive flux only in a linear fashion. As shown by Peterson [59],  $\delta$  depends on the ratio of the maximum and minimum pore cross section and can be estimated, using the following equation:

$$\begin{aligned} \delta &\approx 1 - 0.21 \cdot \ln \left( \frac{A_{p,max}}{A_{p,min}} \right) = 1 - 0.21 \cdot \ln \left( \frac{d_{p,max}^2}{d_{p,min}^2} \right) \\ &= 1 - 0.42 \cdot \ln \left( \frac{d_{p,max}}{d_{p,min}} \right) \end{aligned} \quad (14)$$

$A_{p,max}$ : maximum pore cross-sectional area,  $A_{p,min}$ : minimum pore cross-sectional area,  $d_{p,max}$ ,  $d_{p,min}$ : corresponding diameters

Due to the logarithmic dependence, the area ratio can be substituted by the ratio of the corresponding pore diameters or alternatively ligament diameters, when taking into account that the former and latter are typically identical for npAu. The analysis is simplified further by the invariance of the (Gaussian) ligament size distribution when normalizing it to the average ligament size  $d_L$  [39]. To assess  $d_{L,max}/d_{L,min}$  its halfwidth, ranging from 0.5 to 1.5 of the mean value, may be used. On this basis, a value of 3 can be derived for the ratio for which, in turn, Eq. 14 yields a constrictivity of  $\delta \sim 0.5$  for npAu.

Even though the differentiation between  $\delta$  and  $\tau'$  may be expedient to judge impediments for the mass transport along and perpendicular to the diffusive pathways, it is important to note that both quantities are not necessarily independent from each other. In case of low constrictivities, the probability of “bottle necks”, the molecules need to pass on their pathway through the pore system, statistically increases with the length, thus diminishing the share of longer pores to the diffusive flux. We will come back to this point later.

## 5 Direct Measurement of Gas Diffusivities by PFG NMR

Over the last decades, PFG NMR has demonstrated an unprecedented potential to directly study the self-diffusion of molecules in porous materials [2, 18]. While in the liquid phase, such kind of studies are comparatively easy to conduct, measurements in the gas phase are distinctly more difficult due to the much lower ( $10^{-3}$ ) density of molecules, and only became possible with the advent of NMR instruments working at high magnetic field. The applicability of this technique was clearly demonstrated not only for measurements of self-diffusion in bulk gases, but also within porous matter, such as zeolites and oxides [2, 18]. In contrast, nanostructured metal materials have not been studied until very recently at the example of npAu [43], possibly because they have been considered not to be accessible by PFG-NMR. Specifically, the induction of eddy currents has to be expected for metallic specimen which can potentially lead to measurement artefacts.

Briefly, PFG-NMR is based on labelling and, after a controlled diffusion time  $t$ , unlabelling positions of diffusing molecules by applying magnetic field gradient pulses. For

more details and an in-depth discussion, the interested reader is referred to the excellent book of J. Kärger et al. on this topic [2]. The property directly measured in PFG NMR is the mean square displacement (MSD), which is related to the self-diffusion coefficient and to the (known) diffusion time  $t$ , according to the Einstein relation for 3-dimensional diffusion:

$$\langle r^2 \rangle = 6 \cdot D \cdot t \quad (15)$$

$\langle r^2 \rangle$ : mean square displacement (MSD);  $D$ : self-diffusion coefficient.

The MSD and the corresponding self-diffusion coefficient are obtained from the attenuation  $\Psi$  of the PFG NMR signal, viz. the ratio of the PFG NMR signal magnitude with ( $S_G$ ) and without ( $S_0$ ) the field gradient pulses. In a typical PFG NMR experiment the attenuation is measured as a function of the magnetic field gradient amplitude ( $g$ ), while keeping all other parameters fixed. Such dependencies of  $\Psi$  on  $g$  are referred to as PFG NMR attenuation curves. For normal, 3-dimensional diffusion, the following equation applies:

$$\Psi = S_G/S_0 = e^{-D \cdot q^2 \cdot t} \quad (16)$$

$q = \gamma g \delta$ , where  $\gamma$  is the gyromagnetic ratio, and  $\delta$  is the total effective gradient pulse duration for labelling or unlabelling gradient pulses.

Provided, however, that two ensembles of diffusing molecules exist, as given when, in the presence of a porous material, a part of the gas molecules diffuses inside and a part outside of the pore system, a bi-exponential decay behavior is expected:

$$\Psi = S_G/S_0 = p_1 \cdot e^{-D_1 \cdot q^2 \cdot t} + p_2 \cdot e^{-D_2 \cdot q^2 \cdot t} \quad (17)$$

Here,  $p_1$  and  $D_1$  denote the fraction and diffusion coefficient of the first ensemble (inside) and  $p_2$  and  $D_2$  the corresponding values of the second one (outside). The condition for being able to distinguish between both ensembles in the PFG NMR measurements is that the intra-particle MSD for a given diffusion time  $t$  is distinctly smaller than the physical dimension of a typical porous particle. Otherwise, the diffusing molecules can leave the pore system within the diffusion time and become part of the ensemble outside the material (or vice versa) so that both ensembles are mixed and become identical in the limit of large diffusion times, resulting in a mono-exponential decay.

Figure 5 and Table 1 summarize some of the results obtained for npAu and CO at 15 bar and room temperature. For diffusion times of 6 and 10 ms the measured PFG NMR attenuation curves clearly reveal deviations from a mono-exponential decay behavior as observed for the bulk gas phase (see Fig. 5, left panel). Rather, they can be fitted biexponentially according to Eq. 17, resulting in two

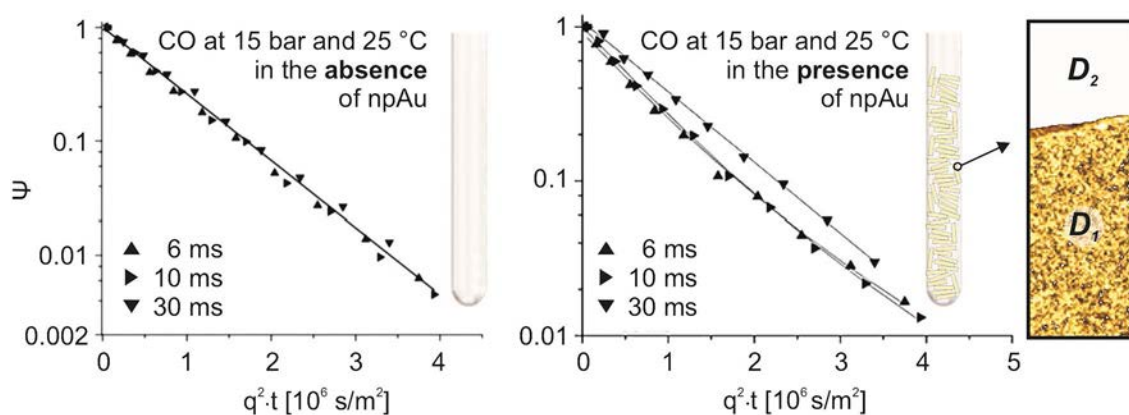


**Fig. 5**  $^{13}\text{C}$  PFG NMR diffusion measurements for  $^{13}\text{CO}$  at 15 bar and 25 °C in the absence (bulk gas phase, left panel) and presence of npAu (right panel). In the latter case an NMR tube was filled with npAu discs (diameter: 3 mm, thickness: 200 microns). The signal attenuation  $\Psi$  was measured for 3 different diffusion times  $t$  in both

cases: 6, 10 and 30 ms. In the presence of npAu, the curves show a biexponential behavior for 6 and 10 ms. By fitting both regimes, the diffusion coefficients  $D_1$  and  $D_2$  inside and outside npAu's pore system could be determined (see Table 1)

**Table 1** Results of the least-square fitting of the data shown in Fig. 5, summarizing the diffusion coefficients of CO determined by PFG NMR at 15 bar and 25 °C for 3 different diffusion times  $t$  in the absence ( $D_{bulk}$ ) and presence of npAu ( $D_1$ ,  $D_2$ )

$t$ [ms]	$D_{bulk}$ ( $10^{-7}$ ) [ $\text{m}^2/\text{s}$ ]	$RMSD_1$ [ $\mu\text{m}$ ]	$RMSD_2$ [ $\mu\text{m}$ ]	$D_1$ ( $10^{-7}$ ) [ $\text{m}^2/\text{s}$ ]	$D_2$ ( $10^{-7}$ ) [ $\text{m}^2/\text{s}$ ]	$D_2/D_1$
6	$14 \pm 1$	$149 \pm 15$	$218 \pm 15$	$7.0 \pm 1.4$	$15 \pm 2$	$2.1 \pm 0.5$
10	$14 \pm 1$	$201 \pm 20$	$290 \pm 20$	$7.2 \pm 1.4$	$15 \pm 2$	$2.1 \pm 0.4$
30	$13 \pm 1$	$430 \pm 20$	$430 \pm 20$	$10.5 \pm 1$	$10.5 \pm 1$	–

In the presence of npAu and for diffusion times of 6 ms and 10 ms two gas ensembles can be distinguished between: one diffusing inside (subscript: 1) and one outside (subscript: 2) of npAu. In addition to the corresponding diffusion coefficients, the root mean square displacements (RMSD) are given. The last column shows the ratio  $D_2/D_1$ , corresponding to the tortuosity factor  $\tau$ , according to Eq. 12

distinctly different diffusion coefficients (Table 1). The larger one ( $D_2$ ) was found to match the value for the bulk gas phase ( $D_{bulk}$ ), hence belonging to CO molecules diffusing outside the pore system of npAu, whereas the smaller one ( $D_1$ ) can be assigned to the molecules diffusing inside the pore system. For  $t=30$  ms, however, where the mean square displacement already exceeds the smallest dimension of the npAu specimen studied (3 mm discs with a thickness of around 200 microns), only a mono-exponential decay can be discerned, indicating that this diffusion time is too long for distinguishing between both ensembles.

As already mentioned in the previous section, at 15 bar the contribution of Knudsen diffusion is minor and molecular diffusion governs the movement of CO inside the pores as it does in the surrounding bulk gas phase. Accordingly, this aspect cannot play a decisive role for  $D_1$  which is only half as large than  $D_2$ , revealing that diffusion inside npAu is slowed down by a factor of 2 as compared to the bulk gas phase. Measurements with  $\text{CH}_4$ , interacting very weakly with Au surfaces and included in the study for reference purposes, showed the same behavior. This similarity proves that the transient adsorption of CO on the surface of npAu—being

a prerequisite for a catalytic conversion, of course—is not of importance either. Therefore, the decelerated mass transport can be fully ascribed to the structural impediments, subsumed in the tortuosity factor  $\tau$ , which was introduced above. With  $D_1$  corresponding to  $D_E$  and  $D_2 = D_M = D_T$ , the ratio  $D_2/D_1$  then directly reflects  $\tau$  according to Eq. 12 ( $\tau = D_2/D_1 = 2$ ).

## 6 Determination of Tortuosities by STEM Tomography

An alternative to assessing tortuosities of porous materials by PFG NMR diffusion measurements are microscopy-based methods. A technique which, in this respect, underwent a steep development in the recent years and proved its capability to provide such information and to furthermore give detailed insight into the mesoscopic structure of porous materials is STEM tomography [14–16]. To this end, thin electron transparent specimen in the range of a few 10 nm need to be prepared. These are then successively tilted with the sample holder in the microscope, covering typically an

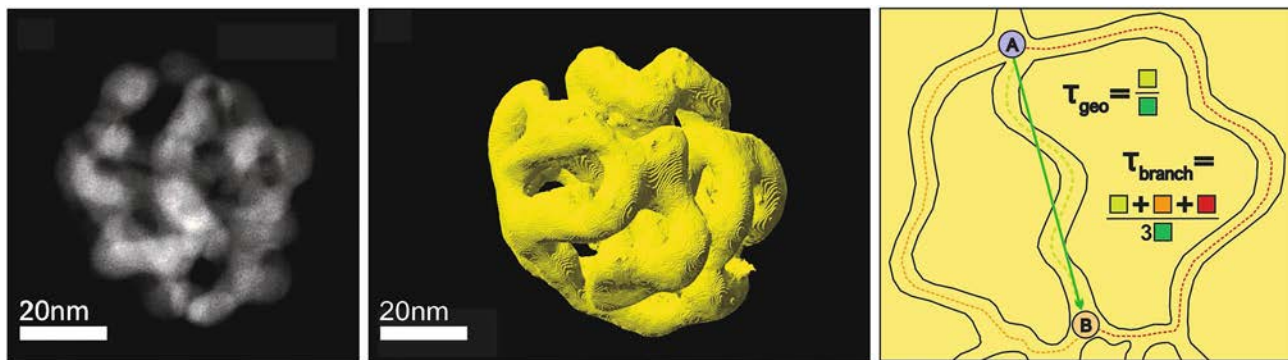


**Fig. 6** TEM micrograph of a npAu nanoparticle (left) and its 3D reconstruction (middle) based on STEM tomography. The picture on the right hand-side schematically illustrates the difference between the geometric and the branch tortuosity of a porous structure. (It shall

be mentioned that  $\tau_{geo}$  often is calculated not on the basis of curved pathways (such as the green dotted one) but on the basis of trajectories consisting of straight segments being somewhat shorter than the curved ones.)

angle range between  $-70^\circ$  and  $70^\circ$ . For all tilting angles STEM images (around 100) are acquired, corresponding to 2D projections in the corresponding direction.

Using appropriate algorithms [17, 62, 63], such a data set then allows for a 3D reconstruction of the specimen investigated. (For more details, the interested reader is referred to Refs. [14–16]). By applying a further numerical analysis, also tortuosity factors characterizing the pore system can be determined [64, 65]. Such methods, however, are based on specific geometric models [66]. The most straightforward one results in the so-called geometric tortuosity  $\tau_{geo}$ . It quantifies the ratio of the shortest average pathway for diffusing molecules, when moving from one point to another one within a given pore system, and the straight geometrical distance between these points (irrespective of the solid phase). If, alternatively, all possible pathways, the molecules may take within a structure of interconnected pores, are considered, the so-called branch tortuosity  $\tau_{branch}$  is obtained, which is defined as the average length of this multitude as compared to the straight distance (see Fig. 6). (Accordingly,  $\tau_{branch}$  is always larger than  $\tau_{geo}$ .)

In case of npAu, Mahr et al. recently published a STEM tomography study, using in this case nanoparticles, which were small enough for the measurements [67]. These can be prepared in analogy to macroscopic npAu samples (namely by dealloying AuAg nanoparticles instead [68]). Figure 6 shows the 3D reconstruction of such a sample, providing a clear visual impression of its pore system. The quantitative evaluation of the structure revealed a geometrical tortuosity of  $\tau_{geo} = 1.2$ , whereas a branch tortuosity of  $\tau_{branch} = 1.9$  was derived. In addition to the statistical uncertainty associated with the tomographic data (20–25%), the limited volume and number of particles that can be studied in this way of course limits the numerical accuracy of such data further. Nevertheless, the insight into the structural details of a porous system provided by (S)TEM tomography can still

be of substantial help to judge which of its characteristics predominately influence the diffusive transport.

When comparing the values obtained for  $\tau_{geo}$  and  $\tau_{branch}$  with  $\tau$  derived from the PFG NMR measurements for npAu, a good agreement of the latter with  $\tau_{branch}$  can be noticed at first sight. Yet, such an assessment does not take the influence of the constrictivity into account. As mentioned above,  $\delta$  lies in the range of  $\sim 0.5$  in case of npAu. On these grounds, a tortuosity factor  $\tau'$  close to 1 results from Eq. 13, which rather reflects  $\tau_{geo}$  than  $\tau_{branch}$ . This finding is in line with the consideration that low constrictivities lead to a preference for the shortest pathways through a pore system, i.e., lead to a decreasing contribution of longer alternatives to the diffusive transport. Hence, for npAu overall pore size variations seem to be more important than pathway elongations.

## 7 Relationship Between Macro- and Micro-kinetics

The productivity of a catalyst depends on the interplay of its intrinsic activity, i.e., the rate of the underlying surface reaction, and its transport properties [11]. If the rate by which reactants are delivered to the inner, catalytically active surface areas (and/or by which products are transported back into the surrounding bulk gas phase) is significantly slower than the rate of the surface reaction, the former and not the latter determines the achievable conversion. The net effectiveness of a catalyst can be characterized by the so-called effectiveness factor  $\eta$ , which is defined as the ratio of the observed rate ( $r_{macro}$ ) and the rate of the surface reaction(s) ( $r_{micro}$ ) under steady state conditions:

$$\eta = \frac{r_{macro}}{r_{micro}} \quad (18)$$

This factor, representing a figure of merit for a given catalytic process, approaches 1 when transport limitations are negligible and decreases as such contributions become increasingly influential.

The macrokinetics, on the one hand, can be calculated in case of a continuous process on the basis of the conversion  $X_i$  which is observed at a pressure  $p$  and a temperature  $T$  for the reactant  $i$  added to the feed with an initial concentration  $c_i^0$  (corresponding to the mole fraction  $x_i$ ):

$$r_{macro} = -\frac{1}{V} \frac{dn_i}{dt} = \frac{\dot{V}}{V} \cdot (X_i \cdot c_i^0) = \frac{\dot{V}}{V} \cdot X_i \cdot \frac{x_i \cdot p}{R \cdot T} \quad (19)$$

$\dot{V}$  here denotes the space velocity and  $V$  the reaction volume. In case of a porous catalyst, the latter equals the void volume  $V_{void}$  (non-material filled volume in the reactor, neglecting areas not filled with catalyst particles). The microkinetics  $r_{micro}$ , on the other hand, is describable by the kinetic rate law which applies for the underlying catalytic surface reaction. For low-temperature CO oxidation over npAu (30 °C), which will be considered here, it is given by Eq. 1. For such a first order kinetics,  $\eta$  can be expressed in the following way [11]:

$$\eta = \frac{\tanh(\varphi)}{\varphi} \text{ with } \varphi = \sqrt{\frac{k_V \cdot \ell^2}{D_E}} \quad (20)$$

Here,  $\varphi$  represents the Thiele modulus already alluded to in the Introduction. Apart from the microkinetic rate constant  $k_V$  and the effective diffusion coefficient  $D_E$  (of CO as the rate determining species in this case) within the porous catalyst (cf. Eqs. 12 or 13), it is dependent on a geometrical constant ( $\ell$ ), representing a characteristic length of the catalyst particles practically employed. It is given by the ratio of their volume and their outer surface area and can be calculated for various geometries by the following general formula:

$$\ell = \frac{1}{2 \cdot \left( \frac{1}{x} + \frac{1}{y} + \frac{1}{z} \right)} \quad (21)$$

The quantities  $x$ ,  $y$  and  $z$  here represent the lateral extensions of the catalyst particle along the three Cartesian coordinates. For spheres and cubes, for example,  $x$ ,  $y$  and  $z$  are equal and correspond to the sphere diameter  $d$  or edge length  $a$ , respectively. For cylinders,  $x$  and  $y$  correspond to the diameter  $d$  while  $z$  to their height  $h$ .

As mentioned before, a central problem—when using the Thiele modulus formalism to determine achievable conversion rates on the basis of known microkinetics or to extract the microkinetics from observed macrokinetics—is missing knowledge about the effective diffusivity of the gases ( $D_E$ ) within the porous catalyst. While there is sufficient data in the literature regarding molecular diffusion coefficients in

the bulk gas phase on the basis of which, in turn, total diffusion coefficients  $D_T$  (for pure gases and gas mixtures, see above) can be derived [2, 57, 69, 70], the material-related factors, i.e., tortuosities and constrictivities needed to determine  $D_E$  (Eqs. 12 or 13), are often unknown. In the literature, these were frequently guessed on the basis of assumptions or analogies to similarly structured pore systems. It can be easily shown for a random angle distribution of pore directions that  $\tau' = \sqrt{2}$  (corresponding to the mean value of  $1/\cos^2(\theta)$ , see section 4.) results [71]. As demonstrated by theoretical studies on this topic [58, 72, 73], however, tortuosities can vary substantially for pore systems for which this condition is not (strictly) met. Accordingly, experimental values are inevitable when aiming at a quantitatively precise assessment of gas diffusivities in a porous catalyst material.

In the following, we illustrate the possibilities given to disentangle macro- and microkinetics provided that such data are available. To this end, we revert to experiments carried out for low-temperature CO oxidation over npAu, summarized in Fig. 7. Using monolithic npAu discs with a thickness of 200  $\mu\text{m}$  and a diameter of 5 mm (orange trace in the middle panel of Fig. 7), a steady state conversion of 40% ( $X = 0.4$ ) could be achieved under the chosen reaction conditions (1 vol% CO, 20 vol% O<sub>2</sub>, carrier gas: He, 30 °C, atmospheric pressure, total gas flow: 40 sscm). It is worth noting that an activation procedure was applied which had been proven before to reproducibly lead to the same high conversion level for samples identically prepared by established dealloying protocols for free corrosion [74]. As depicted in the left panel of Fig. 7, it consists of several rapid heating steps to 300 °C (see left part of Fig. 7), which can be assumed to remove potential impurities on the surface (left, e.g., as remainders of the preparation) so that a defined and optimal surface state for the catalytic turnover can be reliably created.

To determine its kinetics, i.e., the microkinetics of the surface reaction, first the molecular diffusion coefficient ( $D_{M,mix}$ ) for CO under reaction conditions and its Knudsen diffusion ( $D_K$ ) coefficient for the given pore size (20 nm) need to be determined, utilizing Eqs. 8, 10 and 11. On basis of Eq. 8 (considering that, in the gas mixture, instead of  $D_M$   $D_{M,mix}$  enters the equation), then the total diffusion coefficient  $D_T$ , comprising contributions of both diffusion mechanisms, can be calculated. Since at 1 bar the mean pore diameter is distinctly smaller than the mean free path of CO molecules in the bulk gas phase (see Fig. 4),  $D_T$  basically reflects  $D_K$ . Notably, this circumstance reflects a situation, for which self-diffusion and transport diffusion become equivalent so that data for the former may be used even under reaction conditions. On contrary, in case of dominating molecular diffusion and noticeable local concentration gradients originating from the catalytic turnover at the pore walls, the corresponding coefficients will differ

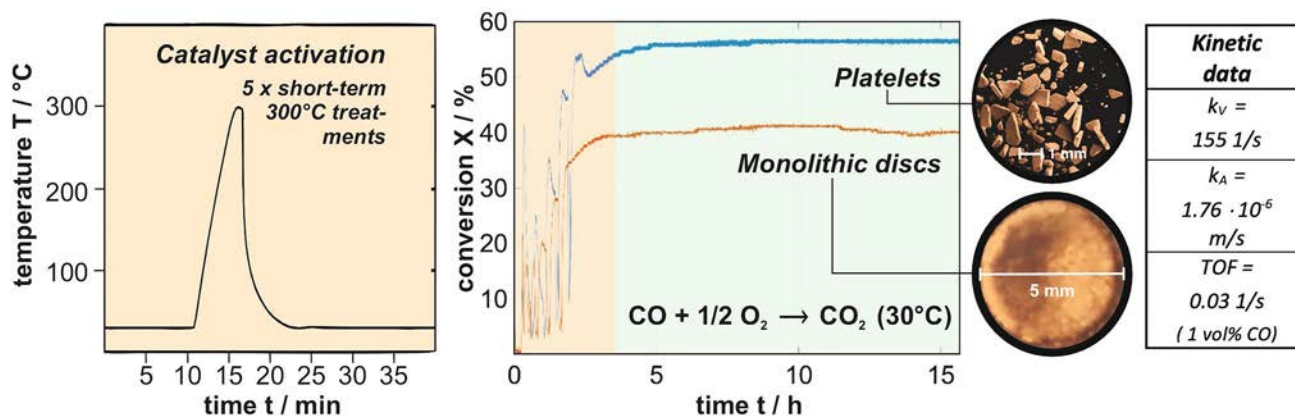


**Fig. 7** CO oxidation over npAu at 30 °C: Using a recently published activation procedure (left) [74]—consisting of several short 300 °C annealing steps—as-prepared npAu catalysts can be reliably activated for CO oxidation within a couple of hours. Monolithic npAu discs (diameter: 5 mm, thickness: 200 microns) activated in this way showed under the applied reaction conditions ( $p_{\text{Total}}=1$  bar,  $p(\text{CO})=10$  mbar,  $p(\text{O}_2)=100$  mbar, balanced with He as carrier

gas) a conversion of ~40%. Taking advantage of the effective diffusion coefficient of CO determined by PFG NMR, the microkinetic data compiled on the right hand-side could be extracted. In addition to the monolithic samples, also npAu platelets (diameter: a few 100 microns, thickness: 200 microns) were investigated which were obtained by mechanical breakup of the 5 mm monoliths. In this way, the conversion could be increased to ~60% (see next section)

of course (unless a carrier gas, for example, is present in large excess ensuring a basically constant  $D_{M,\text{mix}}$  within the catalyst particle, i.e., a homogeneous molecular environment for the diffusing molecules).

One important difference between self- and transport-diffusion has to be taken into account in any event, however, when finally deriving  $D_E$  from  $D_T$  and tortuosities, determined by PFG NMR, for instance. When, in case of a working catalyst, reactants are consumed, the diffusive flux per area (according to the 1st Fick law) is relevant which can only take place in the void volume and not in the material-filled volume of the porous material. Accordingly, it is reduced by the porosity so that  $D_E$  not only scales with  $l/\tau$  (see Eqs. 12), but is also proportional to  $\phi$  [60]:

$$D_E = \frac{\phi}{\tau} \cdot D_T \quad (22)$$

In Table 2, all diffusion coefficients for CO relevant for the evaluation of the experiments in Fig. 7 are compiled [43].

To eventually determine the microkinetics, i.e., the rate constant  $k_V$  (Eq. 1), furthermore the characteristic length  $\ell$  of the applied catalyst particles is needed. In case of the thin disc-shaped npAu monoliths used for the experiments presented in Fig. 7 (diameter  $d$ : 5 mm, thickness  $h$ : 200  $\mu\text{m}$ ), Eq. 21 predicts that  $\ell$  approaches  $h/2$ , i.e., 100  $\mu\text{m}$ .

Although Eq. 20 allows no analytical solution for  $k_V$ , such an evaluation can be done numerically or graphically [43]. Based on the value for  $k_V$  obtained this way and given in Fig. 7, also the rate constant  $k_A$  (see Eq. 1) referred to the catalytic surface area is assessable. Taking advantage of Eq. 7, the following relationship can be derived:

$$k_A = k_V \cdot \frac{\phi}{1 - \phi} \cdot \frac{d_l}{c} \quad (23)$$

**Table 2** Overview of the relevant diffusion coefficients of CO needed to derive its effective diffusion coefficient  $D_E$  within npAu under the reaction conditions of Fig. 7

$D_M$ [ $10^{-6}$ m <sup>2</sup> /s]	$D_{M,\text{mix}}$ [ $10^{-6}$ m <sup>2</sup> /s]	$D_K$ [ $10^{-6}$ m <sup>2</sup> /s]	$D_T$ [ $10^{-6}$ m <sup>2</sup> /s]	$D_E$ [ $10^{-6}$ m <sup>2</sup> /s]
1 bar 30 °C	1 vol% CO (10 vol% O <sub>2</sub> , 89 vol% He)	Pore diameter: $d_p=20$ nm	$\left(\frac{1}{D_{M,\text{mix}}} + \frac{1}{D_K}\right)^{-1}$	$\tau=2.1$ and $\phi=0.7$
20.4	83.4	3.2	3.1	1.0

While  $D_M$  represents the molecular diffusion coefficient measured by PFG NMR for the bulk gas and rescaled to 1 bar,  $D_{M,\text{mix}}$  refers to the gas mixture, used for the actual catalytic experiments.  $D_K$  is the Knudsen diffusion coefficient of CO in pores with a diameter of 20 nm, being typical for npAu. The total diffusion coefficient  $D_T$  taking contributions from molecular (in the reaction mixture) and Knudsen diffusion into account basically reflects  $D_K$ .  $D_E$  results from  $D_T$  when considering also the tortuosity  $\tau$  and porosity  $\phi$  of npAu

In addition, the turnover frequency  $TOF$  (number of catalytic revolutions per surface atom and second) may be obtained for the given reaction conditions (in case of the experiments shown in Fig. 7:  $x_{CO} = 0.01$ ,  $p = 1$  bar,  $T = 30$  °C) on these grounds:

$$TOF = N_A \cdot \frac{\sqrt{3}}{4} \cdot a_{Au}^2 \cdot k_A \frac{x_{CO} \cdot P}{R \cdot T} \quad (24)$$

Regarding the  $TOF$  as a measure often used to characterize the catalytic activity, two aspects have to be taken into account. First of all, and in contrast to  $k$  and  $k_A$ , this quantity represents a rate and, as such, depends on the CO concentration or, as in Eq. 24, on  $x_{CO}$ . Since it was found that the  $CO_2$  formation rate scales linearly with  $x_{CO}$  up to values of  $\sim 0.3$  (30 vol%) [52],  $TOFs$  up to  $1$  s<sup>-1</sup> can be achieved, when increasing the CO partial pressure in the feed. Secondly, a specific number density of surface atoms must be chosen as a basis for the calculation. In case of Eq. 24, a closed packed Au (111) was considered. Neither Au NPs nor npAu are expected to expose only (111) surfaces. Moreover, it is unlikely that all surface atoms contribute to the catalytic turnovers equally. Accordingly, the value, given in Fig. 7 for the  $TOF$ , represents only a lower limit. Nevertheless, the kinetic data compiled in the table on the right hand-side of Fig. 7 ( $k_v$ ,  $k_A$ ,  $TOF$ ) represent the first results characterizing the genuine catalytic activity of npAu for low-temperature CO oxidation without ambiguities arising from unknown contributions of mass transport limitations [43].

## 8 Optimization of a Catalysts' Performance by Reducing Mass Transport Limitations

The CO oxidation experiments discussed above revealed a catalyst effectiveness  $\eta$  of about 70%, meaning that mass transport limitations played a non-negligible role, as reflected by a Thiele modulus  $\varphi$  larger than 1 [43]. The latter has to be below  $\sim 0.3$  for  $\eta$  reaching values close to 1 [11].

Taking Eq. 20 into account, in principle different strategies are possible to decrease the Thiele modulus and thus to increase the catalytic productivity. On the one hand, pore diameters can be increased to reduce the contribution of Knudsen diffusion and thus to increase  $D_E$ —an option principally existing for npAu by controlled thermal coarsening of the porosity. Yet, in this way also the specific surface inversely declines as inferable from Fig. 3. This loss must then be compensated by applying a larger amount of the catalyst. In cases where the catalyst material is expensive, as in case of npAu, such an option is unattractive. On the other hand, catalyst particles with a smaller characteristic length  $\ell$  may be employed. Such an approach is often easier to realize and not connected with disadvantageous side effects.

Other options, as reducing the tortuosity or optimizing the constrictivity of a porous catalyst, are typically beyond the realm of possibilities, since such parameters are material specific and cannot be changed readily.

Having knowledge about the microkinetics (i.e.,  $k_v$ ) and the diffusive transport (i.e.,  $D_E$ ) allows predicting how  $\eta$  varies with the characteristic length  $\ell$  i.e., with the dimensions of the catalyst particles used. Figure 8 shows the results in case of low-temperature CO oxidation over npAu, indicating that catalytic yields close to the microkinetic limit ( $> 95\%$ ), can be achieved when  $\ell$  is smaller than  $\sim 30$   $\mu\text{m}$  (under the given experimental conditions). Taking into account that the data discussed so far were obtained with disc-shaped monolithic npAu samples exhibiting a characteristic length of 100  $\mu\text{m}$ , it can be predicted that a reduction to a third of this value should lead to an increase of  $\eta$  from 70 to almost 100%. Reverting to Eq. 20, such a gain is expected when downsizing the disc diameters from the mm regime into the range of a few 100  $\mu\text{m}$ . Experimentally, this can be realized by crushing the original npAu discs into smaller platelets. Applying a suitable procedure for this process (which does not deteriorate the fragile porous structure) provided conversions being 50% higher than those achieved with the larger discs, in accord with the predictions (see Fig. 7, blue trace) [43]. Figure 8 also reveals that for samples of the latter kind, the thickness sensitively influences the productivity. An increase by just 50%, i.e., to values above 300  $\mu\text{m}$ , already shifts  $\eta$  into the range below 50%.

Overall, these results demonstrate the potential which is offered by techniques allowing to quantitatively characterize diffusion processes in porous catalysts. In combination with catalytic studies, novel perspectives emerge to quantitatively assess the degree to which catalytic processes are influenced by mass transport effects (under given reaction conditions) and indicate what measures must be taken to optimize conversions.

## 9 Summary and Conclusions

The performance of a gas-phase porous heterogeneous catalyst depends on the kinetics of the underlying surface reactions and its surface area, on the one hand, and on the diffusion rates of the involved gas molecules in its pore system, on the other hand. It is the interplay of both aspects which finally determines the observed rates and achievable conversion levels. In this article, we aimed at elucidating new perspectives for quantitatively assessing and optimizing the overall process, resulting from the availability of novel catalytic materials with well-defined pore structures and the advent of elaborated experimental methods, allowing to characterize diffusive transport in porous matter.

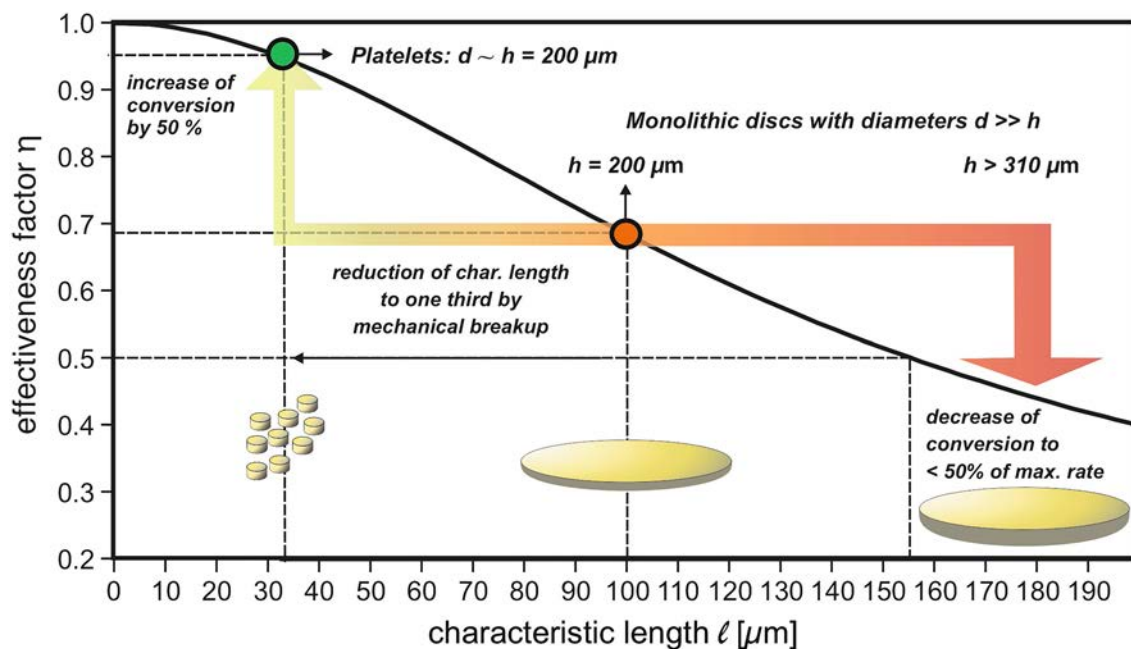


**Fig. 8** Effectiveness factor, corresponding to the ratio of observed rate (macrokinetics) and microkinetic rate, in case of CO oxidation over npAu at 30 °C as a function of the characteristic length of the catalyst particle actually used. When breaking up monolithic disc-shaped npAu samples exhibiting diameters (several mm), which are much larger than their thickness (a few 100 microns), – a sample type

often employed in catalytic studies on npAu—into smaller platelets with diameters and thicknesses in the range of a few 200 microns, the conversion can be pushed to almost 100% of the maximum rate, reflecting the genuine catalytic potential of the material in the absence of mass transport limitations

Nanoporous gold, used in this article to illustrate these topics, can be considered as a good example in this respect. The fabrication of this novel porous metal catalyst by chemical or electrochemical dealloying is comparatively easy and leads to a homogeneous mesoporosity that can reproducibly be obtained. Its high catalytic potential for total as well as partial oxidation reactions at low temperatures does not rank behind (oxide) supported Au nanoparticles. While such traditionally prepared heterogeneous catalysts typically lack options to control porosity and surface properties, npAu illustrates the promising realm of novel strategies to synthesize catalytic materials with well-defined properties regarding catalytic turnover and mass transport. As a porous metal, npAu offers the additional advantage of a good thermal conductivity preventing the development of temperature gradients or hot spots under catalytic conditions.

In parallel, powerful experimental methods evolved in the last years, allowing to precisely characterize the transport properties. The seminal work of J. Kärger and coworkers demonstrated that, in particular, PFG NMR offers unrivaled possibilities in this respect. Taking advantage of the ongoing instrumental developments in this field, diffusivities of molecules in porous matter are measurable not only in the liquid but also in the gas phase. While oxides have been in the focus of research for a longer time, recent experiments with npAu indicated that also porous metals are assessable by this

technique. On these grounds, the tortuosity  $\tau$  of a pore system can be determined, which, in conjunction with knowledge about molecular and Knudsen diffusion coefficients of considered reaction gases, allows to get quantitative insight into their diffusivities being relevant for the mass transport therein. Besides, STEM tomography, as an additional or alternative characterization method, offers the opportunity to obtain local microscopic information about the structural details on the meso-scale. Such data can then help to evaluate which of them—pathway elongations or pore size variations—are mainly responsible for potential mass transport limitations, reducing the catalyst's productivity.

On the basis of such quantitative knowledge about the transport properties of a porous catalyst, the underlying microkinetics, in terms of rate constants or TOFs, can be extracted from observed macrokinetics. For npAu, this approach led to kinetic data which, for the first time, enabled a reliable comparison with other gold catalysts regarding low-temperature CO oxidation—without ambiguities arising from unknown and interfering mass transport limitations. In this context, the spatially homogeneous and self-similar pore structure of npAu and the availability of a reliable activation protocol ensured that the data characterize the material and not just single samples. Under such circumstances, catalytic surface conditions are expected which do not vary



locally and result in reproducibly achievable steady state conversions.

As illustrated at this example, in this way also the basis is laid for systematically improving the catalytic productivity. Here, different strategies are principally conceivable. One option, also existing for npAu to eliminate mass transport limitations, is given by increasing the (mean) pore diameter so that the contribution of Knudsen diffusion is reduced. Yet, it has to be taken into account in this context that also the specific surface area is likewise diminished. Alternatively, the tortuosity or constrictivity of the material may be optimized. As synthetic approaches for selectively varying these parameters do typically not exist, the most straightforward way is an adjustment of the catalytic particle size (i.e., their characteristic length). In case of CO oxidation over npAu, for example, a reduction of the dimensions of the npAu monoliths used led to an increase of the conversion close to the microkinetic limit, in line with the theoretical predictions.

**Acknowledgements** M.B., A.R. and T.R. gratefully acknowledge funding of the work provided by the *German Research Foundation (DFG)* within the framework of the *Research Unit 2213 “Nanoporous Gold”* (Grand nos.: BA 1710/29-2, RO2057/12-2 and RI 1025/3-2). A portion of this work was carried out in the McKnight Brain Institute at the National High Magnetic Field Laboratory’s AMRIS Facility, which is supported by National Science Foundation Cooperative Agreement No. DMR-1157490 and the State of Florida. This work was supported in part by an NIH award, S10RR031637, for magnetic resonance instrumentation.

**Funding** Open Access funding enabled and organized by Projekt DEAL.

## Declarations

**Conflict of interest** All authors declare no conflict of interest.

**Open Access** This article is licensed under a Creative Commons Attribution 4.0 International License, which permits use, sharing, adaptation, distribution and reproduction in any medium or format, as long as you give appropriate credit to the original author(s) and the source, provide a link to the Creative Commons licence, and indicate if changes were made. The images or other third party material in this article are included in the article’s Creative Commons licence, unless indicated otherwise in a credit line to the material. If material is not included in the article’s Creative Commons licence and your intended use is not permitted by statutory regulation or exceeds the permitted use, you will need to obtain permission directly from the copyright holder. To view a copy of this licence, visit <http://creativecommons.org/licenses/by/4.0/>.

## References






1. Deutschmann O, Knözinger H, Kochloeff K, Turek T (2007). In: Belluss G, Bohnet M et al (eds) *Ullmann’s Encyclopedia of Industrial Chemistry, Heterogeneous Catalysis and Solid Catalysts*. Wiley-VCH Verlag GmbH & Co. KGaA, Weinheim
2. Kärger J, Ruthven DM, Theodorou DN (2012) *Diffusion in nanoporous materials*. Wiley-VCH Verlag GmbH & Co. KGaA, Weinheim
3. Wu L, Li Y, Fu Z, Su BL (2020) Hierarchically structured porous materials: synthesis strategies and applications in energy storage. *Natl Sci Rev* 7:1667–1701. <https://doi.org/10.1093/nsr/nwaa183>
4. Attfield MP (2002) Microporous materials. *Sci Prog* 85(319):345. <https://doi.org/10.3184/003685002783238771>
5. Rodríguez-Reinoso F (2001) Activated carbon and adsorption. *Encycl Mater Sci Technol* 22:34. <https://doi.org/10.1016/b0-08-043152-6/00005-x>
6. Heaton CA (1991) *An introduction to Industrial Chemistry*. Chapman & Hall, Bishopbriggs, Glasgow
7. Perego C, Peratello S (1999) Experimental methods in catalytic kinetics. *Catal Today* 52:133–145. [https://doi.org/10.1016/S0920-5861\(99\)00071-1](https://doi.org/10.1016/S0920-5861(99)00071-1)
8. Mears DE (1971) Tests for transport limitations in experimental catalytic reactors. *Ind Eng Chem Process Des Dev* 10:541–547. <https://doi.org/10.1021/i260040a020>
9. Chmelik C, Liebau M, Al-Naji M, Möllmer J, Enke D, Gläser R, Kärger J (2018) One-shot measurement of effectiveness factors of chemical conversion in porous catalysts. *ChemCatChem* 10:5602–5609. <https://doi.org/10.1002/cctc.201801530>
10. Campbell CT (1994) Future directions and industrial perspectives micro- and macro-kinetics: their relationship in heterogeneous catalysis. *Top Catal* 1:353–366. <https://doi.org/10.1007/BF01492288>
11. Fogler HS (2016) *Elements of Chemical reaction engineering*. Prentice Hall, Boston, pp 719–766
12. Thiele EW (1939) Relation between catalytic activity and size of particle. *Ind Eng Chem* 31:916–920. <https://doi.org/10.1021/ie50355a027>
13. Lommerts BJ, Graaf GH, Beenackers AACM (2000) Mathematical modeling of internal mass transport limitations in methanol synthesis. *Chem Eng Sci* 55:5589–5598. [https://doi.org/10.1016/S0009-2509\(00\)00194-9](https://doi.org/10.1016/S0009-2509(00)00194-9)
14. Weyland M, Midgley PA (2004) Electron tomography. *Mater Today* 7:32–40. [https://doi.org/10.1016/S1369-7021\(04\)00569-3](https://doi.org/10.1016/S1369-7021(04)00569-3)
15. Santos AJ, Lacroix B, Maudet F, Paumier F, Hurand S, Dupeyrat C, Gómez VJ, Huffaker DL, Girardeau T, García R, Morales FM (2022) Application of advanced (S)TEM methods for the study of nanostructured porous functional surfaces: a few working examples. *Mater Charact* 185:1–15. <https://doi.org/10.1016/j.matchar.2022.111741>
16. Midgley PA, Weyland M (2003) 3D electron microscopy in the physical sciences: the development of Z-contrast and EFTEM tomography. *Ultramicroscopy* 96:413–431. [https://doi.org/10.1016/S0304-3991\(03\)00105-0](https://doi.org/10.1016/S0304-3991(03)00105-0)
17. Hawkes PW (2007). In: Frank J (ed) *Electron tomography methods for three-dimensional visualization of structures in the cell, the electron microscope as a structure projector*. Springer, New York, pp 83–111
18. Kärger J, Avramovska M, Freude D, Haase J, Hwang S, Valiullin R (2021) Pulsed field gradient NMR diffusion measurement in nanoporous materials. *Adsorption* 27:453–484. <https://doi.org/10.1007/s10450-020-00290-9>
19. Chowdhury AH, Salam N, Debnath R, Islam SM, Saha T (2019) Fggh. In: Pottathara YB, Thomas S et al (eds) *Nanomaterials synthesis: design, fabrication and applications, design and fabrication of porous nanostructures and their applications*. Elsevier, Amsterdam, pp 265–294
20. Wittstock A, Biener J, Erlebacher J (2012) Bäumer M (2012) nanoporous gold: from an ancient technology to a high-tech material. *Royal Society of Chemistry, Cambridge*
21. Wittstock A, Wichmann A, Biener J, Bäumer M (2011) Nanoporous gold: a new gold catalyst with tunable properties. *Faraday Discuss* 152:87–98. <https://doi.org/10.1039/c1fd00022e>

22. Wittstock A, Biener J, Bäumer M (2010) Nanoporous gold: a new material for catalytic and sensor applications. *Phys Chem Chem Phys* 12:12919–12930. <https://doi.org/10.1039/c0cp00757a>
23. Lee JD, Miller JB, Shneidman A, Sun L, Weaver JF, Aizenberg J, Biener J, Boscoboinik JA, Foucher AC, Frenkel AI, Van Der Hoeven JES, Kozinsky B, Marcella N, Montemore MM, Ngan HT, O'Connor CR, Owen CJ, Stacchiola DJ, Stach EA, Madix RJ, Sautet P, Friend CM (2021) Dilute alloys based on Au, Ag, or Cu for efficient catalysis: from synthesis to active sites. *Chem Rev* 122:8758–8808. <https://doi.org/10.1021/acs.chemrev.1c00967>
24. Xu C, Xu X, Su J, Ding Y (2007) Research on unsupported nanoporous gold catalyst for CO oxidation. *J Catal* 252:243–248. <https://doi.org/10.1016/j.jcat.2007.09.016>
25. Biener J, Biener MM, Madix RJ, Friend CM (2015) Nanoporous gold: understanding the origin of the reactivity of a 21st century catalyst made by pre-columbian technology. *ACS Catal* 5:6263–6270. <https://doi.org/10.1021/acs.catal.5b01586>
26. Xu C, Su J, Xu X, Liu P, Zhao H, Tian F, Ding Y (2007) Low temperature CO oxidation over unsupported nanoporous gold. *J Am Chem Soc* 129:42–43. <https://doi.org/10.1021/ja0675503>
27. Zielasek V, Jürgens B, Schulz C, Biener J, Biener MM, Hamza AV, Bäumer M (2006) Gold catalysts: nanoporous gold foams. *Angew Chemie - Int Ed* 45:8241–8244. <https://doi.org/10.1002/anie.200602484>
28. Wittstock A, Zielasek V, Biener J, Friend CM, Bäumer M (2010) Nanoporous gold catalysts for selective gas-phase oxidative coupling of methanol at low temperature. *Science* 327:319–322. <https://doi.org/10.1126/science.1183591>
29. Adkins H, Billica HR (1948) The preparation of raney nickel catalysts and their use under conditions comparable with those for platinum and palladium catalysts. *J Am Chem Soc* 70:695–698. <https://doi.org/10.1021/ja01182a080>
30. Graf M, Roschning B, Weissmüller J (2017) Nanoporous gold by alloy corrosion: method-structure-property relationships. *J Electrochem Soc* 164:C194–C200. <https://doi.org/10.1149/2.1681704jes>
31. Lackmann A, Bäumer M, Wittstock G, Wittstock A (2018) Independent control over residual silver content of nanoporous gold by galvanodynamically controlled dealloying. *Nanoscale* 10:17166–17173. <https://doi.org/10.1039/c8nr03699c>
32. Erlebacher J, Aziz MJ, Karma A, Dimitrov N, Sieradzki K (2001) Evolution of nanoporosity in dealloying. *Nature* 410:450–453. <https://doi.org/10.1038/35068529>
33. Zinchenko O, De Raedt HA, Detsi E, Onck PR, De Hosson JTM (2013) Nanoporous gold formation by dealloying: a Metropolis Monte Carlo study. *Comput Phys Commun* 184:1562–1569. <https://doi.org/10.1016/j.cpc.2013.02.004>
34. Kertis F, Snyder J, Govada L, Khurshid S, Chayen N, Erlebacher J (2010) Structure/processing relationships in the fabrication of nanoporous gold. *Jom* 62:50–56. <https://doi.org/10.1007/s11837-010-0087-6>
35. Seker E, Reed ML, Begley MR (2009) Nanoporous gold: fabrication, characterization, and applications. *Materials* 2:2188–2215. <https://doi.org/10.3390/ma2042188>
36. Fujita T, Chen MW (2008) Characteristic length scale of bicontinuous nanoporous structure by fast fourier transform. *Jpn J Appl Phys* 47:1161–1163. <https://doi.org/10.1143/JJAP.47.1161>
37. Viswanath RN, Chirayath VA, Rajaraman R, Amarendra G, Sundar CS (2013) Ligament coarsening in nanoporous gold: insights from positron annihilation study. *Appl Phys Lett* 102:253101-1–253101-4. <https://doi.org/10.1063/1.4812290>
38. Fujita T, Qian LH, Inoke K, Erlebacher J, Chen M (2008) Three-dimensional morphology of nanoporous gold. *Appl Phys Lett* 92:10–13. <https://doi.org/10.1063/1.2948902>
39. Jeon H, Kang NR, Gwak EJ, Jang J, Han HN, Hwang JY, Lee S, Kim J (2017) Self-similarity in the structure of coarsened nanoporous gold. *Scr Mater* 137:46–49. <https://doi.org/10.1016/j.scripamat.2017.05.009>
40. Chen AY, Shi SS, Liu F, Wang Y, Li X, Gu JF, Xie XF (2015) Effect of annealing atmosphere on the thermal coarsening of nanoporous gold films. *Appl Surf Sci* 355:133–138. <https://doi.org/10.1016/j.apsusc.2015.07.065>
41. Sun Y, Burger SA, Balk TJ (2014) Controlled ligament coarsening in nanoporous gold by annealing in vacuum versus nitrogen. *Philos Mag* 94:1001–1011. <https://doi.org/10.1080/14786435.2013.876113>
42. Kuwano-Nakatani S, Fujita T, Uchisawa K, Umetsu D, Kase Y, Kowata Y, Chiba K, Tokunaga T, Arai S, Yamamoto Y, Tanaka N, Chen M (2015) Environment-sensitive thermal coarsening of nanoporous gold. *Mater Trans* 56:468–472. <https://doi.org/10.2320/matertrans.MF201403>
43. Baniani A, Wild S, Forman EM, Risse T, Vasenkov S, Bäumer M (2022) Disentangling catalysis and mass transport: using diffusion measurements by pulsed field gradient NMR to reveal the microkinetics of CO oxidation over nanoporous gold. *J Catal* 413:1123–1131. <https://doi.org/10.1016/j.jcat.2022.08.020>
44. Haruta M (2002) Novel catalysis of gold deposited on metal oxides. *CATTECH* 6(102):115. <https://doi.org/10.1023/A:1020181423055>
45. Lackmann A, Mahr C, Schowalter M, Fitzek L, Weissmüller J, Rosenauer A, Wittstock A (2017) A comparative study of alcohol oxidation over nanoporous gold in gas and liquid phase. *J Catal* 353:99–106. <https://doi.org/10.1016/j.jcat.2017.07.008>
46. Yim WL, Nowitzki T, Necke M, Schnars H, Nickut P, Biener J, Biener MM, Zielasek V, Al-Shamery K, Klüner T, Bäumer M (2007) Universal phenomena of CO adsorption on gold surfaces with low-coordinated sites. *J Phys Chem C* 111:445–451. <https://doi.org/10.1021/jp0665729>
47. Ruggiero C, Hollins P (1997) Interaction of CO molecules with the Au(332) surface. *Surf Sci* 377–379:583–586. [https://doi.org/10.1016/S0039-6028\(96\)01451-3](https://doi.org/10.1016/S0039-6028(96)01451-3)
48. Mavrikakis M, Stoltze P, Nørskov JK (2000) Making gold less noble. *Catal Letters* 64:101–106. <https://doi.org/10.1023/A:1019028229377>
49. Schaefer A, Ragazzon D, Wittstock A, Walle LE, Borg A, Bäumer M, Sandell A (2012) Toward controlled modification of nanoporous gold. A detailed surface science study on cleaning and oxidation. *J Phys Chem C* 116:4564–4571. <https://doi.org/10.1021/jp207638t>
50. Li Y, Dononelli W, Moreira R, Risse T, Bäumer M, Klüner T, Moskaleva LV (2018) Oxygen-driven surface evolution of nanoporous gold: insights from ab initio molecular dynamics and Auger electron spectroscopy. *J Phys Chem C* 122:5349–5357. <https://doi.org/10.1021/acs.jpcc.7b08873>
51. Moskaleva LV, Röhe S, Wittstock A, Zielasek V, Klüner T, Neyman KM, Bäumer M (2011) Silver residues as a possible key to a remarkable oxidative catalytic activity of nanoporous gold. *Phys Chem Chem Phys* 13:4529–4539. <https://doi.org/10.1039/c0cp02372h>
52. Wittstock A, Neumann B, Schaefer A, Dumbuya K, Kübel C, Biener MM, Zielasek V, Steinrück H, Gottfried JM, Biener J, Hamza A, Bäumer M (2009) Nanoporous Au: an unsupported pure gold catalyst? *J Phys Chem C* 113:5593–5600. <https://doi.org/10.1021/jp808185v>
53. Tan YH, Davis JA, Fujikawa K, Ganesh NV, Demchenko AV, Stine KJ (2012) Surface area and pore size characteristics of nanoporous gold subjected to thermal, mechanical, or surface modification studied using gas adsorption isotherms, cyclic voltammetry, thermogravimetric analysis, and scanning electron microscopy. *J Mater Chem* 22:6733–6745. <https://doi.org/10.1039/C2JM16633J>

54. Detsi E, De Jong E, Zinchenko A, Vuković Z, Vuković I, Punzhin S, Loos K, ten Brinke G, De Raed HA, Onck PR, De Hosson JTM (2011) On the specific surface area of nanoporous materials. *Acta Mater* 59:7488–7497. <https://doi.org/10.1016/j.actamat.2011.08.025>
55. McCue I, Stuckner J, Murayama M, Demkowicz MJ (2018) Gaining new insights into nanoporous gold by mining and analysis of published images. *Sci Rep* 8:1–11. <https://doi.org/10.1038/s41598-018-25122-3>
56. Bosanquet CH (1944) Wall effects in gas-temperature measurements. *Br TA Rep BR-507 BR-507*
57. Fairbanks DF, Wilke CR (1950) Diffusion coefficients in multi-component gas mixtures. *Ind Eng Chem* 42:471–475. <https://doi.org/10.1021/ie50483a022>
58. Ledesma-Durán A, Hernández SI, Santamaría-Holek I (2017) Relation between the porosity and tortuosity of a membrane formed by disconnected irregular pores and the spatial diffusion coefficient of the Fick-Jacobs model. *Phys Rev E* 95:1–10. <https://doi.org/10.1103/PhysRevE.95.052804>
59. Petersen EE (1958) Diffusion in a pore of varying cross section. *AIChE J* 4:343–345. <https://doi.org/10.1002/aic.690040322>
60. van Brakel J, Heertjes PM (1974) Analysis of diffusion in macroporous media in terms of a porosity, a tortuosity and a constrictivity factor. *Int J Heat Mass Transf* 17:1093–1103. [https://doi.org/10.1016/0017-9310\(74\)90190-2](https://doi.org/10.1016/0017-9310(74)90190-2)
61. Epstein N (1989) On tortuosity and the tortuosity factor in flow and diffusion through porous media. *Chem Eng Sci* 44:777–779. [https://doi.org/10.1016/0009-2509\(89\)85053-5](https://doi.org/10.1016/0009-2509(89)85053-5)
62. Gilbert P (1972) Iterative methods for the three-dimensional reconstruction of an object from projections. *J Theor Biol* 36:105–117. [https://doi.org/10.1016/0022-5193\(72\)90180-4](https://doi.org/10.1016/0022-5193(72)90180-4)
63. Goris B, Van den Broek W, Batenburg KJ, Mezerji HH, Bals S (2012) Electron tomography based on a total variation minimization reconstruction technique. *Ultramicroscopy* 113:120–130. <https://doi.org/10.1016/j.ultramic.2011.11.004>
64. Lee TC, Kashyap RL, Chu CN (1994) Building skeleton models via 3-D medial surface axis thinning algorithms. *CVGIP Graph Model Image Process* 56:462–478. <https://doi.org/10.1006/cgip.1994.1042>
65. Kerschnitzki M, Kollmannsberger P, Burghammer M, Duda GN, Weinkamer R, Wagermaier W, Fratzl P (2013) Architecture of the osteocyte network correlates with bone material quality. *J Bone Miner Res* 28:1837–1845. <https://doi.org/10.1002/jbmr.1927>
66. Reich SJ, Svidrytski A, Hlushkou D, Stoeckel D, Kübel C, Höltzel A, Tallarek U (2018) Hindrance factor expression for diffusion in random mesoporous adsorbents obtained from pore-scale simulations in physical reconstructions. *Ind Eng Chem Res* 57:3031–3042. <https://doi.org/10.1021/acs.iecr.7b04840>
67. Mahr C, Dworzak A, Schowalter M, Oezaslan M, Rosenauer A (2021) Quantitative 3D characterization of nanoporous gold nanoparticles by transmission electron microscopy. *Microsc Microanal* 27:678–686. <https://doi.org/10.1017/S1431927621000519>
68. Oezaslan M, Heggen M, Strasser P (2012) Size-dependent morphology of dealloyed bimetallic catalysts: linking the nano to the macro scale. *J Am Chem Soc* 134:514–524. <https://doi.org/10.1021/ja2088162>
69. Hirschfelder JO, Curtiss CF, Bird RB (1954) *Molecular theory of gases and liquids*. Wiley & Sons Ltd, Hoboken
70. Mason EA, Keestin J, Bzowski J, Boushehri A (1987) Equilibrium and transport properties of eleven polyatomic gases at low density. *J Phys Chem Ref Data* 16:445–466
71. Wheeler A (1951) Reaction rates and selectivity in catalyst pores. *Adv Catal* 3:249–327. [https://doi.org/10.1016/S0360-0564\(08\)60109-1](https://doi.org/10.1016/S0360-0564(08)60109-1)
72. Pisani L (2011) Simple expression for the tortuosity of porous media. *Transp Porous Media* 88:193–203. <https://doi.org/10.1007/s11242-011-9734-9>
73. Zalc JM, Reyes SC, Iglesia E (2004) The effects of diffusion mechanism and void structure on transport rates and tortuosity factors in complex porous structures. *Chem Eng Sci* 59:2947–2960. <https://doi.org/10.1016/j.ces.2004.04.028>
74. Wild S, Bäumer M, Risse T (2022) Thermal activation of nanoporous gold for carbon monoxide oxidation. *J Phys Chem C* 126:1770–1777. <https://doi.org/10.1021/acs.jpcc.1c08222>

**Publisher's Note** Springer Nature remains neutral with regard to jurisdictional claims in published maps and institutional affiliations.

## Authors and Affiliations

Stefan Wild<sup>1,2</sup> · Christoph Mahr<sup>2,3</sup>  · Andreas Rosenauer<sup>2,3</sup>  · Thomas Risse<sup>4</sup>  · Sergey Vasenkov<sup>5</sup>  · Marcus Bäumer<sup>1,2</sup> 

<sup>1</sup> Institute for Applied and Physical Chemistry, University of Bremen, 28359 Bremen, Germany

<sup>2</sup> MAPEX Center of Materials and Processes, University of Bremen, 28359 Bremen, Germany

<sup>3</sup> Institute of Solid State Physics, University of Bremen, Otto-Hahn-Allee 1, 28359 Bremen, Germany

<sup>4</sup> Institute of Chemistry and Biochemistry, Free University Berlin, 14195 Berlin, Germany

<sup>5</sup> Department of Chemical Engineering, University of Florida, Gainesville, FL 32611, USA